

# LOAN DOCUMENT

	PHOTOGRAPH THIS SHEET	INVENTORY <b>0</b>																												
DTIC ACCESSION NUMBER	LEVEL																													
<p><b><i>BFRL-ML-TV-TR-2008-4512</i></b></p> <p>DOCUMENT IDENTIFICATION <b><i>1 Dec 96</i></b></p>																														
<p><b>DISTRIBUTION STATEMENT A</b> Approved for Public Release Distribution Unlimited</p>																														
DISTRIBUTION STATEMENT																														
<table border="1" style="width: 100%; border-collapse: collapse;"> <tr> <td colspan="2">ACCESSION FOR</td> </tr> <tr> <td>NTIS</td> <td>ORAS</td> </tr> <tr> <td>DTIC</td> <td>TRAC</td> </tr> <tr> <td>UNANNOUNCED</td> <td></td> </tr> <tr> <td>JUSTIFICATION</td> <td></td> </tr> <tr><td colspan="2"> </td></tr> <tr><td colspan="2"> </td></tr> <tr><td colspan="2"> </td></tr> <tr><td colspan="2"> </td></tr> <tr><td colspan="2">BY</td></tr> <tr><td colspan="2">DISTRIBUTION/</td></tr> <tr><td colspan="2">AVAILABILITY CODES</td></tr> <tr> <td>DISTRIBUTION</td> <td>AVAILABILITY AND/OR SPECIAL</td> </tr> <tr> <td style="height: 40px; vertical-align: bottom;"><b>A-1</b></td> <td></td> </tr> </table> <p style="text-align: center;">DISTRIBUTION STAMP</p>	ACCESSION FOR		NTIS	ORAS	DTIC	TRAC	UNANNOUNCED		JUSTIFICATION										BY		DISTRIBUTION/		AVAILABILITY CODES		DISTRIBUTION	AVAILABILITY AND/OR SPECIAL	<b>A-1</b>		<div style="border: 1px solid black; height: 150px; margin-bottom: 10px;"></div> <p style="text-align: center;">DATE ACCESSIONED</p> <div style="border: 1px solid black; height: 100px; margin-bottom: 10px;"></div> <p style="text-align: center;">DATE RETURNED</p> <div style="border: 1px solid black; height: 100px;"></div> <p style="text-align: center;">REGISTERED OR CERTIFIED NUMBER</p>	
ACCESSION FOR																														
NTIS	ORAS																													
DTIC	TRAC																													
UNANNOUNCED																														
JUSTIFICATION																														
BY																														
DISTRIBUTION/																														
AVAILABILITY CODES																														
DISTRIBUTION	AVAILABILITY AND/OR SPECIAL																													
<b>A-1</b>																														
<div style="border: 1px solid black; padding: 10px; font-size: 2em; font-weight: bold;">20000310 036</div> <p style="text-align: center;">DATE RECEIVED IN DTIC</p>																														
<p>PHOTOGRAPH THIS SHEET AND RETURN TO DTIC-FDAC</p>																														

HANDLE WITH CARE

**AFRL-ML-TY-TR-2000-4512**



## **PULSED STREAMER CORONA REACTOR CHARACTERIZATION - PHASE II**

**DR. BRUCE R. LOCKE  
KALYANA SWAMINATHAN  
WRIGHT C. FINNEY  
DR. RONALD J. CLARK**

**DEPARTMENT OF CHEMICAL ENGINEERING  
FAMU-FSU COLLEGE OF ENGINEERING  
FLORIDA STATE UNIVERSITY  
TALLAHASSEE FL 32310-6046**

**Approved for Public Release; Distribution Unlimited**

**AIR FORCE RESEARCH LABORATORY  
MATERIALS & MANUFACTURING DIRECTORATE  
AIRBASE & ENVIRONMENTAL TECHNOLOGY DIVISION  
TYNDALL AFB FL 32403-5323**

## NOTICES

USING GOVERNMENT DRAWINGS, SPECIFICATIONS, OR OTHER DATA INCLUDED IN THIS DOCUMENT FOR ANY PURPOSE OTHER THAN GOVERNMENT PROCUREMENT DOES NOT IN ANY WAY OBLIGATE THE US GOVERNMENT. THE FACT THAT THE GOVERNMENT FORMULATED OR SUPPLIED THE DRAWINGS, SPECIFICATIONS, OR OTHER DATA DOES NOT LICENSE THE HOLDER OR ANY OTHER PERSON OR CORPORATION; OR CONVEY ANY RIGHTS OR PERMISSION TO MANUFACTURE, USE, OR SELL ANY PATENTED INVENTION THAT MAY RELATE TO THEM.

THIS REPORT IS RELEASABLE TO THE NATIONAL TECHNICAL INFORMATION SERVICE (NTIS). AT NTIS, IT WILL BE AVAILABLE TO THE GENERAL PUBLIC, INCLUDING FOREIGN NATIONS.

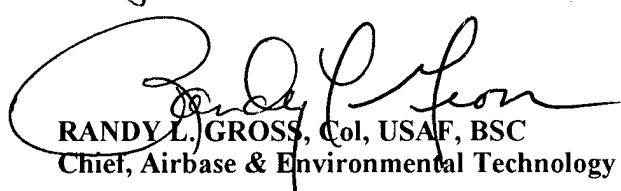
THIS TECHNICAL REPORT HAS BEEN REVIEWED AND IS APPROVED FOR PUBLICATION.



**JOSEPH D. WANDER, Ph.D**  
Program Manager



**CHRISTINE WAGENER-HULME, Lt Col, USAF, BSC**  
Chief, Environmental Technology Development Branch



**RANDY L. GROSS, Col, USAF, BSC**  
Chief, Airbase & Environmental Technology Division

REPORT DOCUMENTATION PAGE			Form Approved OMB No. 0704-0188	
Public reporting burden for this collection of information is estimated to average 1 hour per response, including the time for reviewing instructions, searching existing data sources, gathering and maintaining the data needed, and completing and reviewing the collection of information. Send comments regarding this burden estimate or any other aspect of this collection of information, including suggestions for reducing this burden, to Washington Headquarters Services, Directorate for Information Operations and Reports, 1215 Jefferson Davis Highway, Suite 1204, Arlington, VA 22202-4302, and to the Office of Management and Budget, Paperwork Reduction Project (0704-0188), Washington, DC 20503.				
1. AGENCY USE ONLY (Leave blank)		2. REPORT DATE 1 Dec 1996		3. REPORT TYPE AND DATES COVERED Interim Report 25 Jun 1996 - 1 Dec 1996
4. TITLE AND SUBTITLE Pulsed Streamer Corona Reactor Characterization - Phase II			5. FUNDING NUMBERS Contract F08635-95-C-0020 Supplemental Support Group (SSG) Task 9.03	
6. AUTHOR(S) Locke, Bruce R., Dr.; Swaminathan, Kalyana; Finney, Wright C.; Clark, Ronald J., Dr.				
7. PERFORMING ORGANIZATION NAME(S) AND ADDRESS(ES) Department of Chemical Engineering FAMU-FSU College of Engineering Florida State University Tallahassee, Florida 32310-6046			8. PERFORMING ORGANIZATION REPORT NUMBER	
9. SPONSORING/MONITORING AGENCY NAME(S) AND ADDRESS(ES) US Air Force Armstrong Laboratory Environics Directorate 139 Barnes Drive, Suite 2 Tyndall AFB FL 32403-5323			10. SPONSORING/MONITORING AGENCY REPORT NUMBER  AFRL-ML-TY-TR-2000-4512	
11. SUPPLEMENTARY NOTES				
12a. DISTRIBUTION AVAILABILITY STATEMENT Approved for public release; distribution unlimited			12b. DISTRIBUTION CODE  A	
13. ABSTRACT (Maximum 200 words) The performance of a pulsed streamer corona reactor has been studied to determine the effects of gas composition on nitrogen oxide removal. Experimental studies with a range of gas compositions indicate that additives such as ethylene and water vapor have large effects on nitrogen oxide removal, however, carbon monoxide has no effect. Analysis of byproducts indicate the formation of carbon dioxide and formic acid. Reactor kinetic modeling shows reasonable agreement with experiments and predicts that the reaction rate constants for electron collisions with nitrogen and oxygen are linear functions of the applied electric field.				
14. SUBJECT TERMS NOx, pulsed streamer corona			15. NUMBER OF PAGES 130	
			16. PRICE CODE	
17. SECURITY CLASSIFICATION OF REPORT Unclassified	18. SECURITY CLASSIFICATION OF THIS PAGE Unclassified	19. SECURITY CLASSIFICATION OF ABSTRACT Unclassified	20. LIMITATION OF ABSTRACT UL	

## **PREFACE**

This report details the work performed during the project "Phase II, Pulsed Streamer Reactor Characterization", through contract with the United States Air Force and on subcontract with Applied Research Associates, Inc. Some of the work given in this report was performed as part of the master's thesis of Mr. Swaminathan Kalyana. Assistance from Dr. William Landing, Florida State University Department of Oceanography, for sample analysis by ion chromatography is gratefully acknowledged. David Grymonpre', Steven White, Howie Hanson, and Shawn Goldstein assisted in the conduction of laboratory experiments.

## EXECUTIVE SUMMARY

The removal of nitric oxide (NO) from air streams using pulsed streamer corona discharge, a type of non-thermal plasma, is considered in the present study. Pulsed streamer corona technology is based upon the application of an electric discharge to produce highly reactive free radicals in a gaseous medium. In this study, a pulsed streamer corona discharge reactor was operated to study the removal of NO-containing gases. The reactor was designed, constructed, and preliminary analysis and experiments performed during previously funded phases of this project. Most of the details concerning these aspects were reported in the final report documents for those phases. In the present study physical and chemical characterization of the pulsed corona reactor were performed. The physical characteristics of the discharge, such as the rise time, peak voltage, current, power, and pulse width of the voltage pulse were measured. NO removal from feed gases of various compositions including pure nitrogen, and dry and humid air, with and without added ethylene and carbon monoxide, was studied. In an atmosphere of nitrogen, the main reaction mechanism for the removal of NO was found to be through reduction of NO to molecular nitrogen, while in the case of dry air, NO was oxidized to NO<sub>2</sub>. In humid air, NO<sub>2</sub> removal occurs through oxidation pathways to nitric acid. The addition of hydrocarbons, namely ethylene, significantly affected NO removal.

A kinetic reactor model was also developed to characterize the chemical reactions taking place in the pulsed streamer corona reactor. The kinetic rate constants for the production of highly reactive free radicals such as O, N, and OH were obtained by fitting the model to the NO removal experimental data. The model was then used to predict the output concentrations of various other species, including O<sub>3</sub>, N<sub>2</sub>O, and a number of organic compounds, in order to test the model and to guide the experimental analysis of byproduct characterization.

The major findings of the present work include:

### 1) **Task 1** (Section 7.1.4 RFP) - Gas Phase Pulsed Corona Experiments.

An extensive series of experiments to consider the effect of the feed gas composition on the pulsed corona reactor performance for a range of reactor residence times and applied pulsed voltages was conducted. Experiments with NO in dry nitrogen, NO in dry air, NO in humid air,

NO and ethylene in dry and humid air, and NO, ethylene, and CO in dry and humid air were performed with reactor residence times varying from approximately 5 seconds to 60 seconds and applied pulsed voltages ranging from 30 kV to 50 kV. A minimum of two repeat runs for each set of conditions were performed. Specific results from these runs indicate:

a) In pure nitrogen gas, NO was chemically reduced to  $N_2$ . About 99% removal of  $NO_x$  was observed at 50 kV pulsed voltage for a gas residence time of 44 seconds in pure nitrogen. NO removal in pure nitrogen occurred at a lower energy density than that reported in the literature for dielectric barrier discharge reactors and some corona discharge reactors (Penetrante et al., 1996). In addition, the pure nitrogen experiments tend to support the hypothesis that the NO removal is dependent not only on the power density to the reactor, but also upon the absolute value of the applied electric field. Wolf et al. (1996), Mizuno et al. (1995), and Masuda et al. (1990) also found that the field strength affects the NO removal in pulsed corona discharge and dielectric barrier reactors independent of the power density, in contradiction to the theoretical predictions and claims of Penetrante et al. (1996). Our data for NO removal in nitrogen matches quite closely with that reported by Wolf et al. (1996) for their work at high electric fields with dielectric barrier discharge reactors.

b) All NO removal rates were monotonic functions of the reactor residence time, and showed increasing amounts of NO removal with higher voltages. NO removal from dry air in the presence of ethylene as a function of reactor residence time showed the fastest removal rate of all the conditions studied. The addition of water vapor to the feed gas (saturated at room temperature) did not enhance the NO removal. The concentration profiles of NO versus residence time for the various applied voltages in humid air, in the presence of 500 ppm CO in humid air, and in the presence of 500 ppm of ethylene in humid air were almost the same.

c) The oxidation of NO leads to the formation of  $NO_2$ , and therefore many of the experiments showed an increase in  $NO_2$  concentration with residence time followed by a decrease at very long residence time, as expected for a sequence of chemical reactions occurring in series. In addition, generally more  $NO_2$  was formed at the higher voltages in the presence of

oxygen but not in pure nitrogen. The addition of oxygen in the form of dry air increased the rate of NO removal, however, it also increased the rate of formation of NO<sub>2</sub> as expected by the chemical kinetics. In dry air, NO was oxidized to form NO<sub>2</sub> and N<sub>2</sub>O. NO<sub>2</sub> formation was significantly reduced in the presence of water vapor. The addition of ethylene to the dry air feed gas enhanced NO<sub>2</sub> removal. In humid air, however, the addition of 500 ppm CO and 500 ppm ethylene had almost no effect on NO<sub>2</sub> removal compared to the case of humid air alone.

**2) Task 2** (Section 7.1.2 RFP) and **Task 4** (Section 7.1.6 RFP) - Reactor and Kinetic Modeling.

Chemical reaction modeling was performed using the CHEMKIN software package with details described in the Modeling section of this report. The specific results from the model and model/data comparison include:

a) In general, the model profiles of NO and NO<sub>2</sub> matched the experimental data fairly well, and the model indicated a small amount of N<sub>2</sub>O formation which was also observed experimentally. The overall reaction rate constant for nitrogen dissociation was determined by fitting the model with the NO experimental data. The experiments, as well as the modeling results, follow the general trends indicated in the literature on non-thermal plasma treatment methods.

b) The rate constants for nitrogen and oxygen dissociation were determined from the NO removal and the NO<sub>2</sub> formation data. The reaction rate constant for nitrogen dissociation was different from the value obtained in pure nitrogen; this is also expected based upon observations reported in the literature that electronegative gases affect the electron energy distribution and thus the chemical reaction rate constants. The pseudo first-order rate constant for nitrogen dissociation was 0.0475 s<sup>-1</sup> in an atmosphere of nitrogen at 50 kV, but in dry air the rate constant was lowered to 0.03 s<sup>-1</sup>. Hence, as expected from the literature, the rate constant depends upon the composition of the gas. The differences in the rate constants for nitrogen and oxygen dissociation in dry air were functions of the applied voltage. At low voltage (30 kV) the rate constants were almost equal (approximately .01 s<sup>-1</sup>) and at the high voltage (50 kV) the rate constants were 0.025 s<sup>-1</sup> for nitrogen dissociation and 0.25 s<sup>-1</sup> for oxygen dissociation. This



factor of ten difference is significantly smaller than theoretical studies (Penetrante et al., 1995) where it was predicted that the G-values for oxygen and nitrogen dissociation would differ by about 600 times. It should also be noted that these theoretical studies also do not predict a field dependence as seen in our work.

c) The measured  $\text{N}_2\text{O}$  matched well with the predictions of the model. This result is significant since this is an independent check of the model. The amount of ozone produced from dry air, as measured using a KI titration method, was about a factor of three higher than that predicted by the model. Further refinement of the model and additional experiments to measure ozone concentration is continuing.

### 3) **Task 3** (Section 7.1.5 RFP) - Byproduct Identification.

a) Complete removal of ethylene was observed for the case of humid air with NO. The exhaust gas from the reactor was sparged through a liquid solution and this liquid was analyzed by HPLC. Byproduct analysis by HPLC indicated that less than 1% of the carbon from 500 ppm ethylene leads to the formation of formic acid. Two additional peaks of similar magnitude to the formic acid peak were observed on the HPLC. Through a process of elimination, it was shown that these peaks were not due to acetic acid, formaldehyde, ethylene glycol, glycolaldehyde, ethanol, or methanol. Exact identification of these peaks was not successful; however, based on the magnitude of the formic acid peak, it is expected that these peaks represent at most a few percent of the initial total carbon from the ethylene degradation. Work is continuing to make further identification of these peaks.

b) The liquid samples were also analyzed by ion chromatography where nitrate and nitrite could be quantified. This analytical method, which is very accurate and has a detection limit in the ppb range, showed no nitrite and a small amount of nitrate. The amount of nitrate measured by this technique corresponds to about 5% of the nitrogen from the feed NO converted to nitric acid. It thus appears that a balance on nitrogen was not obtained. Of about 100 ppm NO in the initial feed gas of a humidified gas stream, only a few percent of the nitrogen was detected as nitric acid. It is possible that some of the acid formed could have been deposited on the walls of

the reactor, however it was difficult to assess this quantitatively. Recommendations for future work include the analysis of aerosol formation.

c) In dry air, over 95% of the 500 ppm ethylene fed into the reactor was decomposed at 50 kV pulsed voltage and 44 seconds residence time. Approximately 130 ppm of CO<sub>2</sub> was produced during these conditions as measured by the GC/MS. This would imply that approximately 13% of the carbon fed to the reactor left the reactor as carbon dioxide. Measurements by HPLC found no formic acid under these conditions. Further work is needed to determine the fate of the remaining carbon.

#### 4) **Task 5** (Section 7.1.3 RFP) - Liquid Reactor System Specification.

A liquid phase reactor has been designed and constructed. This reactor consists of a 1 liter jacketed glass vessel equipped with ports to allow the pulsed voltage electrode assembly to be inserted. Modification of the high voltage electrode will allow rapid changes in the discharge tips. The top of the reactor will allow for the introduction and removal of samples as well as for electrical connections to the ground electrode. The basic features of this reactor are similar to those used in previous work by our group (Sharma et al., 1993; Joshi et al., 1995), but the reactor is somewhat larger and more easily operated and modified than previous designs.

## TABLE OF CONTENTS

<u>section</u>	<u>page</u>
I. INTRODUCTION .....	1
A. RESEARCH OBJECTIVES .....	3
B. BACKGROUND .....	4
Electron Beams .....	4
Dielectric Barrier Discharge .....	6
Corona Discharge .....	7
Physical Characteristics of the Pulsed Corona Discharge .....	11
II. EXPERIMENTAL APPARATUS AND PROCEDURES .....	16
A. POWER SUPPLY .....	16
B. REACTOR SPECIFICATIONS .....	18
C. ANALYTICAL INSTRUMENTATION .....	18
D. FEED GAS SYSTEM .....	18
E. EXPERIMENTAL PROCEDURES .....	20
F. LIQUID PHASE REACTOR SPECIFICATIONS .....	22
III. REACTION MODELING .....	25
IV. EXPERIMENTAL RESULTS & DISCUSSION .....	33
A. PHYSICAL DISCHARGE CHARACTERISTICS .....	33
B. NO REMOVAL IN NITROGEN .....	39
C. NO REMOVAL IN DRY AIR .....	46
D. OZONE FORMATION IN DRY AIR .....	52
E. NO REMOVAL IN HUMID AIR .....	53
F. THE EFFECT OF CO ON NO REMOVAL IN HUMID AIR .....	57
G. NO REMOVAL FROM AIR IN THE PRESENCE OF ETHYLENE .....	62
DRY AIR .....	64
HUMID AIR .....	67
V. CONCLUSIONS .....	78
VI. RECOMMENDATIONS .....	83
VII. REFERENCES .....	85
APPENDICES .....	86

## LIST OF TABLES

<u>Number</u>		<u>Page</u>
1	List of Chemical Reactions Considered for Modeling .....	29
2	Voltage Characteristics of the Pulse in Dry Air.....	34
3	Current & Power Characteristics of the Pulse in Dry Air.....	38
4	Byproducts Predicted by the Model Due to Ethylene Breakdown .....	71
5	Additional List of Chemical Reactions Considered for Modeling NO Removal in the Presence of Ethylene .....	75

## LIST OF FIGURES

1.	Summary of Energy Efficiency of NO Removal at High Concentrations .....	9
2.	Summary of Energy Efficiency of NO Removal at Low Concentrations.....	10
3.	Pulsed Power Supply Diagram .....	17
4a.	Gas Phase Experimental Setup .....	19
4b.	Liquid Reactor Design .....	23
5.	Ozone Concentration Profile to Illustrate the Modeling .....	26
6.	Power Supply Calibration.....	33
7.	Voltage Waveform in an Atmosphere of Dry Air at 40 kV .....	35
8.	Current Waveform in an Atmosphere of Dry Air at 40 kV .....	36
9.	Power Waveform in an Atmosphere of Dry Air at 40 kV .....	37
10a.	NO Concentration Profile in an Atmosphere of Nitrogen .....	40
10b.	NO <sub>2</sub> Concentration Profile in an Atmosphere of Nitrogen .....	40
11.	NO/NO <sub>2</sub> Removal from Nitrogen versus Energy Density .....	42
12.	Model Profile of Different Species in an Atmosphere of Nitrogen .....	43
13.	Model Fit for NO Concentration Profile in an Atmosphere of Nitrogen.....	43
14.	Rate Constants for Nitrogen Dissociation in Pure Nitrogen.....	45

15.	NO Concentration Profile in an Atmosphere of Dry Air .....	47
16.	NO <sub>2</sub> Concentration Profile in an Atmosphere of Dry Air .....	47
17.	Model Profile of Different Species in an Atmosphere of Dry Air .....	49
18.	Model Fit for NO Concentration Profile in an Atmosphere of Dry Air .....	49
19.	Rate Constants of Nitrogen and Oxygen Dissociation as a Function of Applied Voltage in an Atmosphere of Dry Air .....	51
20.	Ozone Concentration Profile Predicted by the Model .....	51
21.	NO Concentration Profile in an Atmosphere of Humid Air .....	54
22.	NO <sub>2</sub> Concentration Profile in an Atmosphere of Humid Air .....	54
23.	Model Profile of Different Species in an Atmosphere of Humid Air .....	56
24.	Model Fit for NO Removal in an Atmosphere of Humid Air .....	56
25.	NO <sub>2</sub> Model Profile in an Atmosphere of Humid Air .....	58
26.	Rate Constants of Water Dissociation as a Function of Applied Voltage in an Atmosphere of Humid Air .....	58
27.	NO Concentration Profile in an Atmosphere of Humid Air and CO .....	60
28.	NO <sub>2</sub> Concentration Profile in an Atmosphere of Humid Air and CO .....	60
29.	Model Profile of Different Species in the presence of 500 ppm of CO in Humid Air .....	61
30.	Comparison of the Model Prediction of NO and NO <sub>2</sub> Profile with Experimental Data in Case of NO Removal in the presence of 500 ppm of CO in Humid Air .....	61
31.	NO Concentration Profile in an Atmosphere of Dry Air and 500 ppm of Ethylene .....	66
32.	NO <sub>2</sub> Concentration Profile in an Atmosphere of Dry Air and 500 ppm of Ethylene .....	66
33.	Concentration Profile of Different Species Predicted by the Model for NO Removal in the Presence of 500 ppm Ethylene in Dry Air With the Experimental Data .....	68
34.	Concentration Profile of Breakdown Products Predicted by the Model for NO Removal in Dry Air with 500 ppm Ethylene .....	68
35.	Ethylene Model Profile With and Without the Presence of Water in Case of NO Removal from Air .....	70
36.	NO Concentration Profile in an Atmosphere of Humid Air and 500 ppm of Ethylene .....	70

37.	NO <sub>2</sub> Concentration Profile of Breakdown Products Predicted by the Model in Case of NO Removal in Humid Air with 500 ppm of Ethylene.....	71
38.	NO <sub>2</sub> Concentration Profiles in an Atmosphere of Humid Air and 500 ppm Ethylene .....	73
39.	Concentration Profile of Different Species Predicted by the Model in Case of NO Removal in the Presence of 500 ppm of Ethylene in Humid Air.....	73
40.	Chromatogram from HPLC Analysis of Gas Sample from Corona Experiment at 50 kV with NO, Ethylene, and Humid Air .....	74
41.	Summary of NO Removal in Different Atmospheres.....	82
42.	Summary of NO <sub>2</sub> removal in Different Atmospheres.....	82

## SECTION I

### INTRODUCTION

Nitrogen oxides released into the atmosphere arise primarily from the combustion of fossil fuels from both stationary and mobile sources. In 1992, U.S. emissions of anthropogenic nitrogen oxides were estimated to be 23 million tons. Of this, 45% was from mobile sources and the remainder came from stationary sources (Ozkan et al., 1995). The seven oxides of nitrogen that may be present in ambient air are NO, NO<sub>2</sub>, N<sub>2</sub>O, NO<sub>3</sub>, N<sub>2</sub>O<sub>3</sub>, N<sub>2</sub>O<sub>4</sub> and N<sub>2</sub>O<sub>5</sub>. Of these nitrogen oxides, the only ones subject to regulatory control are NO and NO<sub>2</sub>, and these are together referred to as NO<sub>x</sub>. Although N<sub>2</sub>O is not considered to be an air pollutant, it contributes to stratospheric ozone destruction and it is a greenhouse gas (U.S. EPA, 1993).

Nitric oxide (NO) is an odorless gas that is only slightly soluble in water (0.006 g/100 g of water at 24 °C and 1 atm pressure). It is toxic and makes up 90-95% of the NO<sub>x</sub> emissions from fossil fuel combustion. Nitrogen dioxide (NO<sub>2</sub>) is a reddish brown gas with a characteristic pungent odor. It is corrosive and highly oxidizing. It is formed rapidly in the atmosphere from the oxidation of NO, and it is a toxic agent which can negatively affect human health. Nitrous oxide (N<sub>2</sub>O), or laughing gas, is a colorless gas with a slight odor at high concentrations (U.S. EPA, 1993).

NO and NO<sub>2</sub> are highly toxic if inhaled in high concentrations. NO entering the body forms nitrite which oxidizes the iron in hemoglobin, rendering it ineffective as an oxygen carrier. In 1986, the World Health Organization recommended that the exposure of humans to NO<sub>2</sub> should not exceed 200 ppbv for more than one hour a month. Long-term exposure at 50 ppbv can cause pulmonary damage and increased airway resistance in healthy individuals (U.S. EPA, 1993).

NO<sub>x</sub> gases are one of the main contributors to the formation of photochemical smog. This smog is primarily due to the reaction of NO<sub>x</sub> and hydrocarbons which, at high concentrations, contribute to a reduction in visibility. Under the influence of UV light these compounds produce a variety of harmful compounds such as peroxyacetyl nitrate (PAN) and ozone. Ozone is a highly toxic substance which leads to breathing problems above concentrations of 500 ppbv. NO<sub>x</sub> emissions are one of the primary contributors to acid rain, which is associated with a number of effects including acidification of lakes and streams, and accelerated corrosion of buildings and

monuments (Leslie et al., 1992).

The two main mechanisms that are primarily responsible for  $\text{NO}_x$  formation during combustion process are thermal  $\text{NO}_x$  and fuel  $\text{NO}_x$ . Thermal  $\text{NO}_x$  results from the oxidation of  $\text{N}_2$  contained in combustion air, whereas fuel  $\text{NO}_x$  originates from the oxidation of chemically bound nitrogen in the fuel. Abatement of  $\text{NO}_x$  emissions can be achieved by (1) modifying the combustion process, such as using low- $\text{NO}_x$  burners, gas recirculation, and staged combustion, and (2) using post-combustion removal methods (Chang et al., 1992).

Among the post-combustion control methods, selective catalytic reduction (SCR) is the most advanced technology currently used to remove  $\text{NO}_x$  from gas streams. One disadvantage with the SCR process is that the particulate matter commonly found in flue gas streams generated by the combustion of fossil fuels tends to "poison" catalysts, and therefore lower SCR performance. Another post-combustion removal method for  $\text{NO}_x$  is selective non-catalytic reduction (SNCR). SNCR relies on the injection of ammonia into the gas stream to chemically reduce NO to  $\text{N}_2$  and  $\text{H}_2\text{O}$  in the presence of  $\text{O}_2$ . However, SNCR is effective only between 900 and 1100 °C (Kokkinos et al., 1991).

One alternative to SCR and SNCR processes that has been studied since the 1970's is the gas phase plasma oxidation of  $\text{NO}_x$  using an electric discharge. Electric discharges initiate electron-gas reactions that in turn produce highly reactive radicals. The application of an electric discharge to a gas can lead to the creation of a thermal or a non-thermal plasma.

A thermal plasma is a "hot" or "equilibrium" plasma, which is characterized by a high gas temperature and approximately equal gas and electron temperatures. Typical examples are those produced in arcs and plasma torches. A "non-thermal plasma", as the name implies, is a plasma in which the electron temperature is considerably higher than that of the components of the ambient gas. The electrons produced are short-lived and rarely collide with a pollutant molecule, but they undergo many collisions with the predominant gas molecules, producing radicals that in turn lead to the removal of the toxic molecules (Penetrante, 1993). Hence, the essence of the non-thermal plasma technique is the efficient use of electrical energy to generate gas phase radicals by electron impact excitation, ionization, and dissociation.

The different types of non-thermal plasmas that have been investigated are:



1. Electron Beam
2. Dielectric Barrier Discharge
3. Corona Discharge.

The electron beam process involves the direct irradiation of gases by an external source beam of highly energetic electrons to produce active radicals and atoms, which react with  $\text{NO}_x$  to form nitric acid as well as other products. The use of electron beams to prevent pollution was initiated in the 1970's in Japan by the Japan Atomic Energy Research Institute and the Ebara Corporation, and pilot scale studies are currently being conducted in several countries such as the U.S., Germany, and Poland (Frank et al., 1993).

In a dielectric barrier discharge, the plasma is sustained between one or more dielectric surfaces backed by a conductor. A repetitively pulsed or AC voltage is applied to the electrodes, resulting in a filamentary periodic pulsed plasma (Chang et al., 1992). The dielectric barrier discharge is currently used in industry for ozone synthesis (Dhali et al., 1991; Kogelschatz and Eliasson, 1995).

Corona discharges such as pulsed streamer corona, AC corona, and DC corona, have been studied for the treatment of flue gas, VOC's, and for the synthesis of gases such as ozone. In the present study, the removal of NO from dry and humid air streams is investigated using positive pulsed streamer corona. The effect on NO removal of additives such as carbon monoxide and ethylene is also considered. The exhaust gases coming out of jet engines (F101 engine with JP4 fuel) have four compounds (ethylene, acetylene, propene, and formaldehyde) accounting for 27% of volatile organic emissions at idle power (Spicer et al., 1992). Ethylene is used in the present study as a model hydrocarbon to consider the effect of hydrocarbons on  $\text{NO}_x$  chemistry.

## **A. RESEARCH OBJECTIVES**

The specific goals of this research, as outlined in the statement of work for this contract, include:

### *Gas-Phase Pulsed Corona Experiments.*

1) **Task 1.** Investigation of the intermediate and final by-products formed in the destruction of combustion source exhausts. Use of digital storage oscilloscope or high speed computer data

acquisition system to measure gas phase pulsed corona discharge characteristics.

*Gas-Phase Chemical Kinetic Analysis and By-Product Correlation.*

- 2) **Task 2.** Develop or modify, as needed, plasma chemistry codes for use in modeling chemical kinetic reactions and for comparison of experimental results with code predictions.
- 3) **Task 3.** Identify and estimate quantities formed of by-products generated during the experiments of Task 1.
- 4) **Task 4.** Application of codes developed during the performance of Task 2 to simulate representative experimental data generated during the performance of Tasks 1 and 2.

*Liquid-Phase Pulsed Corona Experiments.*

- 5) **Task 5.** Develop and design a pulsed corona discharge reactor for use in aqueous solutions.

## **B. BACKGROUND**

This section reviews previous research on pollutant removal from waste streams using non-thermal plasma techniques such as electron beams, dielectric barrier discharge, and corona discharge. Additional details are reported in the final report for Phase I of this project. Details on the operation and conduction of liquid phase experiments will be reported in the next report due in May 1997 as required by the contract.

### **Electron Beams**

Electron beam treatment to prevent pollution was first initiated in Japan in 1970 by the Japan Atomic Energy Research Institute in collaboration with Ebara Corporation. Several pilot plant studies of electron beam process applications to coal-fired powered plants have been made in Europe and in the U.S. This process is particularly attractive for the treatment of large volumes of gaseous effluents such as those coming out of utility power plants (Frank et al., 1993).

In the electron beam process, irradiation of the flue gas with energetic (300-800 keV) electrons initiates electron-gas reactions to produce radicals that have high enough energy to oxidize  $\text{NO}_x$  and  $\text{SO}_2$  to nitric acid and sulfuric acid, respectively. In the presence of ammonia ( $\text{NH}_3$ ), these acids are converted into ammonium sulfate and ammonium nitrate. These salts are later recovered as a dry powder using a conventional particle collector (Frank et al., 1993, Matzing, 1991).

The reaction mechanism involved in the removal of NO<sub>x</sub> and SO<sub>2</sub> in electron beam treatment was investigated by Tokunaga et al. (1984). Reactions of NO and SO<sub>2</sub> were studied under the irradiation of electron beams using various gas compositions ranging from a simple system (nitrogen-NO) to a more complex system (nitrogen-oxygen-water vapor-NO-SO<sub>2</sub>) which is close to the composition of an actual flue gas. For the NO-nitrogen gas mixture at a gas temperature of 100 °C, a dose of 3 Mrad, and an initial NO concentration of 250 ppm, 10% of the NO was converted into NO<sub>2</sub> and 3% of the NO was converted to N<sub>2</sub>O. The remaining NO was anticipated to be decomposed mainly to nitrogen and oxygen. In the case of a NO<sub>2</sub>-nitrogen mixture at a dose of 6 Mrad, 60% of the NO<sub>2</sub> formed NO and N<sub>2</sub>O, and 40% of the NO<sub>2</sub> was decomposed to nitrogen and oxygen. For different NO and NO<sub>2</sub> concentrations in a gas containing 3% oxygen and 97% nitrogen at 100 °C, the final concentrations of NO and NO<sub>2</sub> were represented by the following empirical equation:

$$\frac{[NO]}{[NO_2]^2} = 0.027 \text{ ppm}^{-1} \quad (1)$$

The total NO concentration was observed to increase with dose rate for initially low concentrations of NO (50-100 ppm), and was not observed to follow the above empirical relation. The presence of water vapor (2.2% to 12.9%) enhanced the NO removal and the formation of HNO<sub>3</sub> at a gas temperature of 120 °C. The addition of additives such as carbon monoxide (0-1.13 %) and ammonia (0-2000 ppm) were observed to have a positive effect on the removal of NO. For a 1.13% addition of carbon monoxide, NO removal was enhanced by 50% at 1 Mrad, and an increase of 14% was found in the NO removal efficiency with the addition of 2000 ppm of NH<sub>3</sub>.

A kinetic model for the radiation-induced oxidation of nitrogen oxides to include temperature dependence and the presence of sulfur dioxide was developed by Busi et al. (1987). An increase in temperature from ambient to 120 °C decreased the removal efficiency of NO. Matzing (1991) considered detailed theoretical and model results for the electron beam dry scrubbing process (EBDS). The major radical source was shown to come from positive ion formation, which led to NO<sub>x</sub> removal by both oxidative and reductive reaction pathways. The relative humidity of the gas played a crucial role in the removal efficiencies. The addition of ammonia led to the formation of

aerosols, and a linear correlation was found between  $\text{N}_2\text{O}$  formation and the stoichiometric ratio of added ammonia.

Among the disadvantages of using the electron beam process are high cost, large physical size of electron beam generators, X-ray hazards, the necessity of ammonia addition, and aerosol formation (Frank et al., 1993).

### **Dielectric Barrier Discharge**

Dielectric barrier discharge (DBD) or silent discharge has been studied for the removal of  $\text{SO}_2$  (Sardja et al., 1990; Dhali et al., 1991) and  $\text{NO}_x$  (Chang et al., 1992). In DBD, a repetitive pulsed or AC voltage is applied in order to sustain a discharge between two separated electrodes having a dielectric material covering each. Ions produced by the discharge traverse the space between the electrodes, and are then stored in the surface of the dielectric materials. Hence, a sparkless reactive plasma with a high electron temperature and a low gas temperature is produced which enhances the chemical reactions desired for  $\text{SO}_2/\text{NO}_x$  removal.

In DBD, the gas is exposed to many such discharge pulses. Excitation of an atmospheric pressure plasma in this fashion is quite efficient because arcs between electrodes are prevented by the short duration of the individual current pulses, and the electron energy of the plasma is well matched with the energy required to produce the electronic and dissociative states of molecular gases (Chang et al., 1992). Chang et al. (1992) found that under dry conditions the NO removal efficiency decreased with an increasing concentration of  $\text{O}_2$  at room temperature. In addition, the efficiency of NO removal increased in the presence of water vapor in the system at room temperature. At elevated temperatures (130-160 °C), increasing  $\text{H}_2\text{O}$  (> 9%) concentration and decreasing  $\text{CO}_2$  (< 3%) concentration resulted in increasing NO removal efficiencies. NO removal efficiency was found to be sensitive to gas temperature, gas composition, and power deposition.

Dielectric discharge can also be produced by utilizing a reactor filled with ferroelectric material between two metal electrodes connected to a high voltage AC power supply. An electric field of high intensity is formed around each dielectric pellet, thereby producing high energy free electrons (Mizuno et al., 1987).

## Corona Discharge

Corona discharge exists in several forms including DC corona, AC corona, or pulsed corona, of positive corona or negative polarity, depending on the type and polarity of the electric field and on the electrode geometry (uniform or non-uniform). Pulsed streamer corona discharges have been considered for the removal of pollutants both in the gas phase (Clements et al., 1989; Dinelli et al., 1990; Masuda et al., 1990) and in the liquid phase (Clements et al., 1985; Sharma et al., 1993; Joshi et al., 1995). The use of pulsed corona for flue gas treatment is being pursued industrially in several places such as at a coal burning thermal power station at ENEL (Dinelli et al., 1990).

DC corona has been used in the removal of  $\text{NO}_x$  in place of an electron beam, and it was found that the removal rate was enhanced but the power consumption was very high. DC corona consumes high electric power since it accelerates negative ions as well as electrons. Since oxidizing species such as  $\cdot\text{OH}$  and  $\cdot\text{O}$  are produced in a very short time only by electrons with a sufficient energy, it is imperative to accelerate only the electrons, and not the ions, in order to reduce the power consumption. An effective method is to use a very sharp high voltage pulse with a nanosecond range duration time, because this allows rapid acceleration of electrons with minimum ion acceleration even under ordinary gas pressure (Masuda et al., 1990). Due to the nanosecond duration of the applied pulse, much higher electric fields can be applied without causing sparking between the electrodes.

Simultaneous removal of  $\text{NO}_x$  and  $\text{SO}_2$  from flue gas by the application of short duration voltage pulses was considered in an electrode geometry similar to that of an electrostatic precipitator (Dinelli et al., 1990). Nitrogen oxide removal efficiency of 33% together with a sulfur dioxide removal efficiency of 75% was obtained when both contaminants were present at levels of 420 ppmv and 360 ppmv, respectively, in 90 °C air containing ammonia for 6  $\text{Wh/Nm}^3$  energy input into the gas. The energy efficiency of this process is such that with 1 kWh input to the gas, a removal of about 25 g of nitrogen oxide and about 70 g of sulfur dioxide was achieved with the addition of 40 g of ammonia. The use of hydrated lime was also considered as a possible substitute for ammonia for the neutralization of the nitric and sulfuric acid compounds to form salts. Optimization of ammonia injection and gas temperature along with better electrical design of the reactors was suggested to improve the energy efficiency.

In a negative pulsed streamer corona process,  $\text{NO}_x$  concentration remained unchanged up to a critical peak field intensity for a  $\text{NO-NH}_3$ -air mixture ( $\text{NH}_3$  : 180 ppm) (Masuda et al., 1990). Beyond this critical field intensity,  $\text{NO}_2$  was also removed, and its removal depended upon the gas residence time and the amount of ammonia addition. Ammonia addition enhanced the removal of  $\text{NO}_2$  but not that of  $\text{NO}$ . The efficiency of  $\text{NO}$  removal by using negative pulsing was found to be a function of the specific power of pulsing  $P/Q$  (corona power/ gas flow rate) divided by the inverse of the square root of the residence time.

$\text{NO}_x$  removal from dry air mixed with ammonia in a pipe/nozzles-to-plate electrode corona discharge system has also been considered (Ohkubo et al., 1994). The gases were introduced into the discharge zone through the pipe electrode coming out of the nozzles. The addition of ammonia led to the formation of ammonium nitrate aerosol particles which were deposited on the electrodes. The characteristics of the corona discharge were significantly affected by the addition of inert gases such as argon. The addition of these gases helped to obtain a stable streamer corona for higher  $\text{NO}_x$  removal efficiency.

Mizuno et al. (1995) noted that the removal of  $\text{NO}_x$  gases can be achieved by using square-wave voltage pulses having frequencies on the order of several hundred Hz for the energization of cylinder-type plasma chemical reactors. The performance was noted to be better at lower gas temperatures, and the use of ethylene as an additive to the flue gas significantly enhanced the  $\text{NO}_x$  removal efficiency. They observed the formation of acetic acid in the analysis of the reaction products, but it was not quantified.

Simultaneous removal of  $\text{NO}_x$ ,  $\text{SO}_2$  and fly ash ( $\text{RO}_x$ ) using the application of a semi-wet type corona discharge reactor has been considered (Okazaki et al., 1995). The semi-wet type discharge reactor consisted of a cylindrical pyrex glass tube and a stainless steel discharge wire electrode at the center, with a water film covering the inner surface of the glass tube. For an initial concentration of 300 ppm of  $\text{NO}$  and 500 ppm of  $\text{SO}_2$ , 90% of  $\text{NO}_x$  and nearly 100% of  $\text{SO}_2$  were removed at the same time, even in a gas containing a high oxygen concentration of about 15%.

Tas (1995) investigated the plasma-induced conversion of  $\text{NO}$  as a function of several parameters including the composition of the gas mixture, the presence of catalyst materials, and the type of catalyst material. The energy efficiency of the conversion of  $\text{NO}$  to  $\text{NO}_2$  can be increased

by a factor of 2 for pure bulk gas of helium or nitrogen with 1000 ppm of NO by using a silica catalyst. The energy input was varied by controlling the pulsing frequency of the discharge in the reactor. The addition of oxygen to the bulk gas depressed the dissociative conversion of NO, and at a high power input and for an initial concentration of 1000 ppm, equation (1) corresponded well with the measured conversion of NO. With the addition of water, NO<sub>2</sub> was expected to be converted to HNO<sub>3</sub>, however HNO<sub>3</sub> was not detected.

Figure 1 compares the energy efficiency of NO removal at high concentrations of NO by Mizuno et al. (1995) and Tas (1995), and Figure 2 shows a summary of energy efficiency of NO removal at low concentrations of NO by Masuda et al. (1990) and Ohkubho et al. (1994). As seen in Figure 1, the addition of 500 ppm of ethylene increased the NO removal for the same power per unit volume divided by the square root of time in dry air. The data of Mizuno et al. (1995) and Tas (1995) for the case of NO removal in the presence of water are very close.

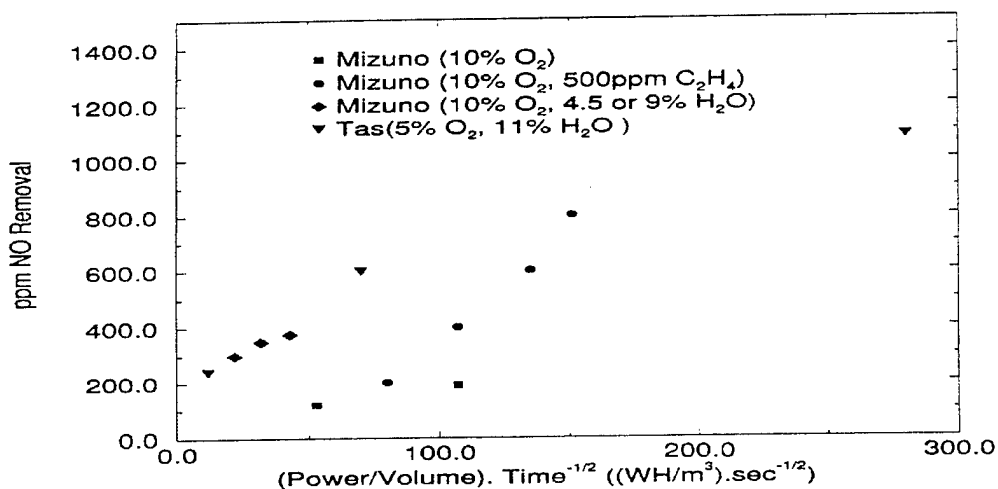


**Figure 1.** Summary of Energy Efficiency of NO Removal at High Concentrations.

Figure 2 shows that the NO removal in the presence of ammonia considered by Masuda and Nakao (1990) was far different from that observed by Ohkubho et al (1994). In all of the above cases where NO removal was considered by pulsed streamer corona discharge, there were certain

dissimilarities such as the nature of the electrode and the polarity of the field. No theoretical justification for this type of plot is available at present, however it serves as a convenient means to compare data under a variety of power conditions.

Modeling of the chemical reactions taking place during the pulsed streamer corona process has been developed in order to understand the evolution of the concentrations of different chemical species (Penetrante et al., 1993). For a power input of  $0.05 \text{ W/cm}^3$  and for an initial concentration of 400 ppm NO at 300 K, 200 ppm of the initial NO was predicted to be converted back to  $\text{N}_2$  and 200 ppm to  $\text{NO}_2$ . Of this 200 ppm of  $\text{NO}_2$ , 180 ppm was converted to  $\text{N}_2\text{O}$  and 20 ppm to  $\text{N}_2\text{O}_5$ . When the temperature was increased to 400 K, only 100 ppm of the initial NO was converted to  $\text{NO}_2$  and another 100 ppm was converted to  $\text{N}_2\text{O}$ . With the addition of 10% water and 15%  $\text{CO}_2$ , from an initial 400 ppm NO about 120 ppm was converted to  $\text{HNO}_3$  and 50 ppm was converted to  $\text{N}_2\text{O}$ . The ozone produced was about 50 ppm and the residual  $\text{NO}_x$  present was around 10 ppm. This model prediction, however, has not yet been confirmed by experimental results.

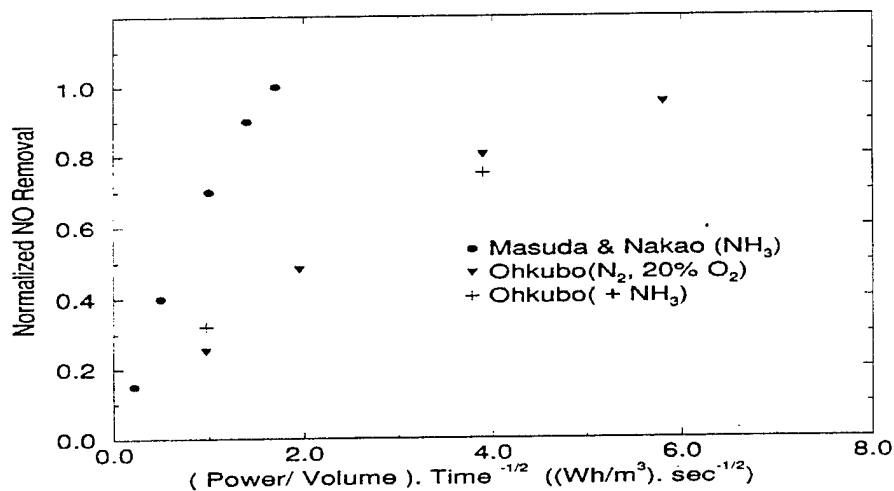


**Figure 2.** Summary of Energy Efficiency for NO Removal at Low Concentration.

Recent experimental studies by Wolf et al. (1996) of dielectric barrier discharges have shown that NO removal depends not only on the power density delivered to the reactor, but also on the



absolute value of the applied voltage. This agrees with the work of Masuda et al. (1990) and Mizuno et al. (1995) who found the same result for pulsed corona reactors. Penetrante et al. (1996) have claimed that the performance of dielectric barrier discharge reactors should be the same as that of pulsed corona reactors, and that the performance of each should only depend upon the power density delivered to the reactor and not upon the field strength or characteristic shape of the voltage pulse. They showed that NO removal versus power density was the same for specially designed corona and dielectric barrier reactors. Wolf et al. (1996) constructed a dielectric barrier reactor that would operate at higher fields and found that the power density was lowered for a given NO removal.

### **Physical Characteristics of the Pulsed Corona Discharge**

Different types of corona discharges can occur in non-uniform electric fields, depending upon the polarity and the nature of the applied electric field. Positive pulsed corona proceeds from corona onset to a burst pulse corona to streamer corona, then to glow corona and, finally, spark discharge as the applied voltage is increased. In the case of negative pulsed corona, the initial form is Trichel pulse corona, followed by pulseless corona and then spark discharge as the voltage is increased. A Trichel pulse refers to the regular current pulse produced when the voltage applied to a negative electrode is gradually increased to produce ionization. These pulses are extremely regular in both magnitude and repetition rate. The frequency of the Trichel pulse repetition starts with 2 kHz near onset, and it may attain a few MHz before the onset of glow corona (Naseer, 1971). Positive corona depends more on photoionization for its propagation, while the negative corona propagates by impact ionization of the gas molecules (Chang et al., 1993).

In pulsed streamer corona, the ionization grows from the high voltage electrode into a background field which is purely geometric. The discharge assumes the form of a number of branched, tree-like streamers, whose starting points are discrete and distributed over the highly stressed region with a specific density (Dinelli et al, 1990). Photoionization is generally assumed to be the mechanism that supplies secondary seed electrons and triggers the avalanches.

The streamer formation in a DC anode (positive) corona can be described as a Townsend avalanche which is a conceptual description of the electron multiplication processes. The process

begins with free electrons in a strong electric field gaining energy to collide with gas molecules and lose energy by a variety of collision process (e.g. elastic scattering, excitation, ionization), thereby producing secondary electrons and positive ions (Creyghton, 1994). The electrons produced through collision further produce electrons through secondary reactions, resulting in an electron avalanche. As a result, the head of the electron avalanche and the positive ions, which are left behind the avalanche, form a sort of dipole. The electron avalanche is said to be "critical" when the dipole field reaches a value comparable to the external applied field. The electric field is enhanced in front of the head of the electron avalanche, while the electric field is reduced in between the avalanche head and the positive ions which are left behind. Still further back in the avalanche, the electric field between the positive ions and the cathode is enhanced.

The electron avalanche has an increased velocity and light emission intensity. These avalanches are referred to as anode directed streamers (ADS). Also, as the electrons propagate towards the anode there is a buildup of positive ions. In the presence of a space charge field and initial free electrons at the cathode side of the avalanche, cathode directed streamers (CDS) can be formed. The CDS propagate as a result of secondary avalanches which neutralize the positive concentration of the previous avalanches, leaving a new positive ion concentration behind at a shorter distance from the cathode (Creyghton, 1994). During the primary avalanche propagation excited gas molecules are also produced which act as a source for electrons. These electrons serve as a source for secondary avalanches required for CDS propagation.

Streamer discharges are hence highly localized "space charge waves" which enhance the applied field in front of the wave (active region) and propagate because of electron avalanche formation in this high field. Along the track of the wave there remains a weakly ionized plasma filament (passive region), along which the conduction current flows to the high voltage electrode, supplying the energy for streamer advancement (Nasser, 1971). In the case of corona at impulse voltages, the ionic space charge drift and accumulation can be neglected due to the short duration of the pulse width. In the case of non-uniform electrode geometry, the streamer growth assumes radial directions, increasing the number of branches.

The major characteristics of streamers include the length, number, speed of propagation, width, number of electrons and ions, time lag, and electric field distribution. Typical values of

streamer width are in the range of 25 to 100  $\mu\text{m}$  and the speed of propagation is in the range of 0.7-0.9 mm/ns (Creyghton, 1994). Recent experimental and theoretical studies have also shown that the propagation characteristics of positive streamers depend very much upon the degree of electronegativity of the carrier gas. In weakly electronegative gases like atmospheric air, the streamers appear much longer and more branched than in strongly electronegative gas such as  $\text{SF}_6$ . Hence, with large concentrations of  $\text{CO}_2$  and  $\text{H}_2\text{O}$ , the discharge characteristics are very near to those of highly electronegative gases (Gallimberti, 1988).

### Modeling Pulsed Streamer Corona Discharge

In order to model the streamer discharge in a pulsed corona, an understanding of the elementary processes such as ionization, attachment, and photoionization is essential.

A 1-D streamer propagation model has been developed in which the streamer is assumed to possess cylindrical symmetry (Gallimberti, 1972, 1988). The densities of the charged particles along the central axis (x-axis) of the streamer can be calculated solving the continuity equations, i.e., for electrons, positive ions, and negative ions. It is possible to solve for the electric field by solving the Poisson equation once the densities of the charged particles are known:

$$\nabla \cdot E = \frac{(n_p - n_e - n_n)}{\epsilon_o} \quad (2)$$

where  $E$  is the electric field,  $n_p$  is the concentration of positive ions,  $n_e$  is the concentration of electrons,  $n_n$  is the concentration of negative ions and  $\epsilon_o$  is the permittivity of the gas medium considered.

2-D models, in which the radial distribution of charged particles is calculated, have been performed to simulate streamer formation in a uniform electric field (Wang et al., 1990). A 1-D streamer model with an approximation of the Poisson equation has been used to calculate the streamer properties (Creyghton, 1994). The current pulse, net charge, and energy loss have also been calculated for an impulse corona (Gallimberti, 1988).

The solution of the Boltzmann equation is necessary to calculate the electron transport coefficients and kinetic rate coefficients for various inelastic electron-gas collision reactions. The

Boltzmann equation is the continuity equation for electrons in six-dimensional phase space and it describes the time evolution of the electron energy distribution function. The most common technique used to solve the Boltzmann equation has been the moment method in which a spherical harmonic expansion (or Legendre series) of the angular dependence of the velocity is assumed with truncation after the first two terms (Huxley et al., 1974). The electron transport properties were significantly affected by the composition of gas considered.

The kinetic rate coefficients for the electron-gas reactions are functions of the electron energy distribution function. The kinetic rate coefficients can be calculated by

$$k_{eij} = \int_0^{\infty} \left[ \frac{\epsilon}{2m_e} \right]^{1/2} \sigma_{ij}(\epsilon) f(\epsilon) d\epsilon \quad (3)$$

where  $k_{eij}$  is the kinetic rate constant for the electron-gas reaction,  $\epsilon$  is the electron energy,  $m_e$  is the mass of an electron,  $\sigma_{ij}$  is the collisional cross section, and  $f(\epsilon)$  is the electron energy distribution function.

The collision cross section is defined as a measure of the probability of a given type of interaction between a gas molecule and an electron. The cross section is a function of the relative velocity of particles and the energy of the electrons. It varies over several orders of magnitude according to the type of interaction being considered.

The densities of chemical reactive dissociation products have been calculated using a numerical model for streamer-induced chemical kinetics as discussed above (Alekseev et al., 1993, McFarlane et al., 1991; Maroude et al., 1996). Modeling of the electrostatic corona discharge reactor has been done by solving the Boltzmann equation for the electron energy distribution function, which in turn was used to determine the kinetic rate constants for the electron gas collisional reactions (Mukkavilli et al., 1988). For a dry air system, 58 reactions were considered, and 96 reactions were considered for the wet air system. Increase of moisture in the feed air had a negligible effect on the input gases ( $N_2$  and  $O_2$ ), but it was found to reduce the ozone concentration by more than two orders of magnitude and that of  $NO_x$  by a factor of two.

Ozone generation in pulsed corona reactors having point-to-plane and wire-cylinder geometries have been considered with discrete injection of electrons and also with time-varying electronic density (Pignolet et al., 1990; Loiseau et al., 1994). The shape of the electronic injection time profile did not affect the concentration profile of ozone production. The temperature gradient between the electrodes in the wire-to-cylinder geometry had a drastic effect on the electron densities near the wire directly through ozone destruction at high temperatures and indirectly by viscosity, which affects the velocity profile (Loiseau et al., 1994).

Past work in the field of pulsed streamer corona has focused on either primarily experimental results or on purely theoretical modeling. The present work will try to combine both experimental and computational aspects in order to develop an understanding of the basic chemistry taking place during the pulsed streamer corona process. Removal of NO from gases of various compositions including pure nitrogen and air, and the addition of water vapor, ethylene and carbon monoxide will be considered. A kinetic model will be utilized in order to develop a quantitative understanding of the reaction pathways occurring in the system.

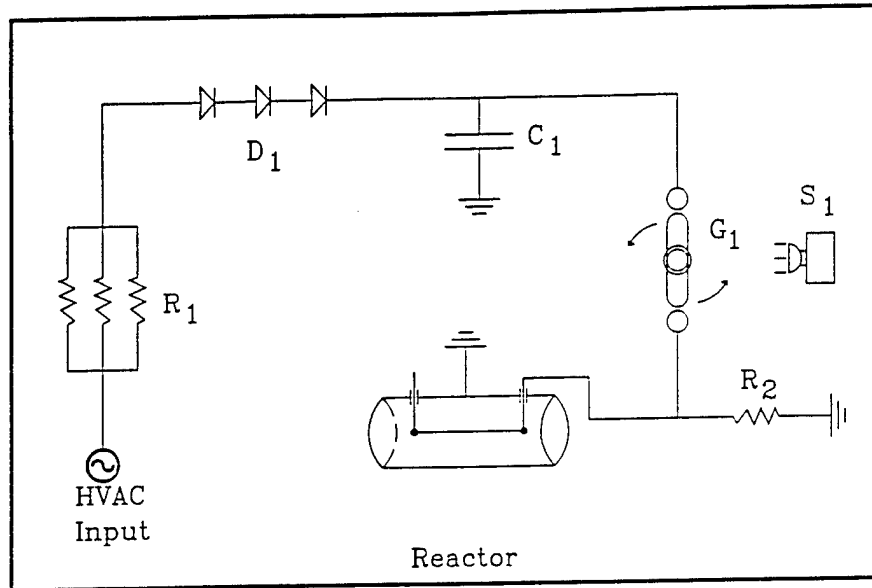
## SECTION II

### EXPERIMENTAL APPARATUS AND PROCEDURES

Non-thermal plasma reactors operated at low temperature, low power consumption, and atmospheric pressure can be classified by their physical geometry and by their method of electrical energization. Among the various types are point-to-plane, point-to-point, packed bed, coaxial, and wire-cylinder electrode geometries. The methods of energization include direct current, alternating current, or pulsed current. In this study, pulsed power was delivered to a wire-cylinder geometry reactor.

#### A. POWER SUPPLY

The pulsed power supply used in this investigation is shown in Figure 3. It consists of two major units: 1) a high voltage transformer/rectifier (T-R) set and 2) a pulse generating apparatus. The power supply used was similar to the configuration used by Clements et al. (1989). The high voltage DC T-R set was modified by eliminating the internal rectifier, thereby producing 0-100 kV AC at 0-28 mA. Output from the T-R set was connected to the pulse generation circuit, where the current passes through a high voltage resistor (333 k $\Omega$ ) and then through a diode array which acts as a half-wave rectifier. The output from the rectifier charged a bank of capacitors (2700 pF) during the charging cycle. A mechanical rotating spark gap having two fixed stainless steel spherical electrodes and a rotating rod electrode was employed to discharge the capacitor bank twice per shaft revolution, synchronized with the AC current (60 Hz). From the output of the spark gap the circuit had two parallel pathways. One of them passed through a load resistor (300 k $\Omega$ ) which enabled the gap to fire. The other was connected to the central wire within the cylindrical reactor, from which the discharge emanated. The generation of pulsed corona discharge by a rotating spark gap was a source of electromagnetic interference, therefore the pulse generating apparatus was encased in an aluminum box to reduce RF noise.



HVAC = 0 - 100 kV, 0 - 28 mA

$R_1 = 333 \text{ k}\Omega$

$R_2 = 300 \Omega$

$D_1 = 60 \text{ kV, 12 A max}$

$C_1 = 2700 \text{ pF}$

$G_1 = \text{Rotating Spark Gap, 1800 RPM, 60 discharges / sec}$

$S_1 = \text{Strobe Lamp}$

Figure 3 : Pulsed Power Supply Diagram

## B. REACTOR SPECIFICATIONS

The pulsed streamer corona reactor used in this study was a stainless steel, 4 inches in diameter and 18 inches long, cylindrical tube. The high voltage electrode (0.109 inches diameter, 12 inches long) was suspended concentric to the grounded outer cylinder resulting in an electrode separation of 2 inches. The active pulsed corona treatment volume of the reactor was 2.45 l. The typical gas flow rate, gas velocity, and residence time in the reactor are from 2.5 to 40 l/min, from 321 to 5134 cm/s, and from 3.6 to 60.0 seconds, respectively. The high voltage ceramic feed-through conductors as well as the center electrode were fabricated of # 304 stainless steel to prevent any corrosion and rust formation inside the reactor.

## C. ANALYTICAL INSTRUMENTATION

Analysis of the outlet gases from the reactor included the measurement of NO, NO<sub>2</sub>, O<sub>3</sub>, N<sub>2</sub>O, and hydrocarbon breakdown products. Nitrogen oxides (NO and NO<sub>2</sub>) were measured using a Thermo-Environmental Instruments, Inc., Model 42H chemiluminescence NO<sub>x</sub> analyzer. Ozone was measured using the KI reaction test. N<sub>2</sub>O and hydrocarbon breakdown products were measured using a Hewlett-Packard GC/MS instrument located in the Department of Chemistry at Florida State University. HPLC analysis was also performed on samples obtained by sparging the reactor exhaust gas through a flask of HPLC carrier solvent (i.e., phosphoric acid buffer in de-ionized water). HPLC analysis was used to determine the breakdown products of the ethylene when NO removal was considered in the presence of ethylene in humid air. The pulse waveform characteristics were measured using a Tektronix TDX 460 four channel digitizing oscilloscope with a P6015A 1000x 3.0 pF, 1000 MΩ voltage probe and a current probe (P6016). A Cole-Parmer TriSense velocity/temperature/humidity measurement system was used to measure the gas velocity, temperature, and humidity in the gas system. The analytical instrumentation, the reactor setup, and the gas feed system are shown in Figure 4a.

## D. FEED GAS SYSTEM

The feed gas system (see Figure 4a) consisted of: 1) a compressed air source and pure nitrogen gas cylinders which act as carrier gases, 2) gas cylinders and high pressure regulators



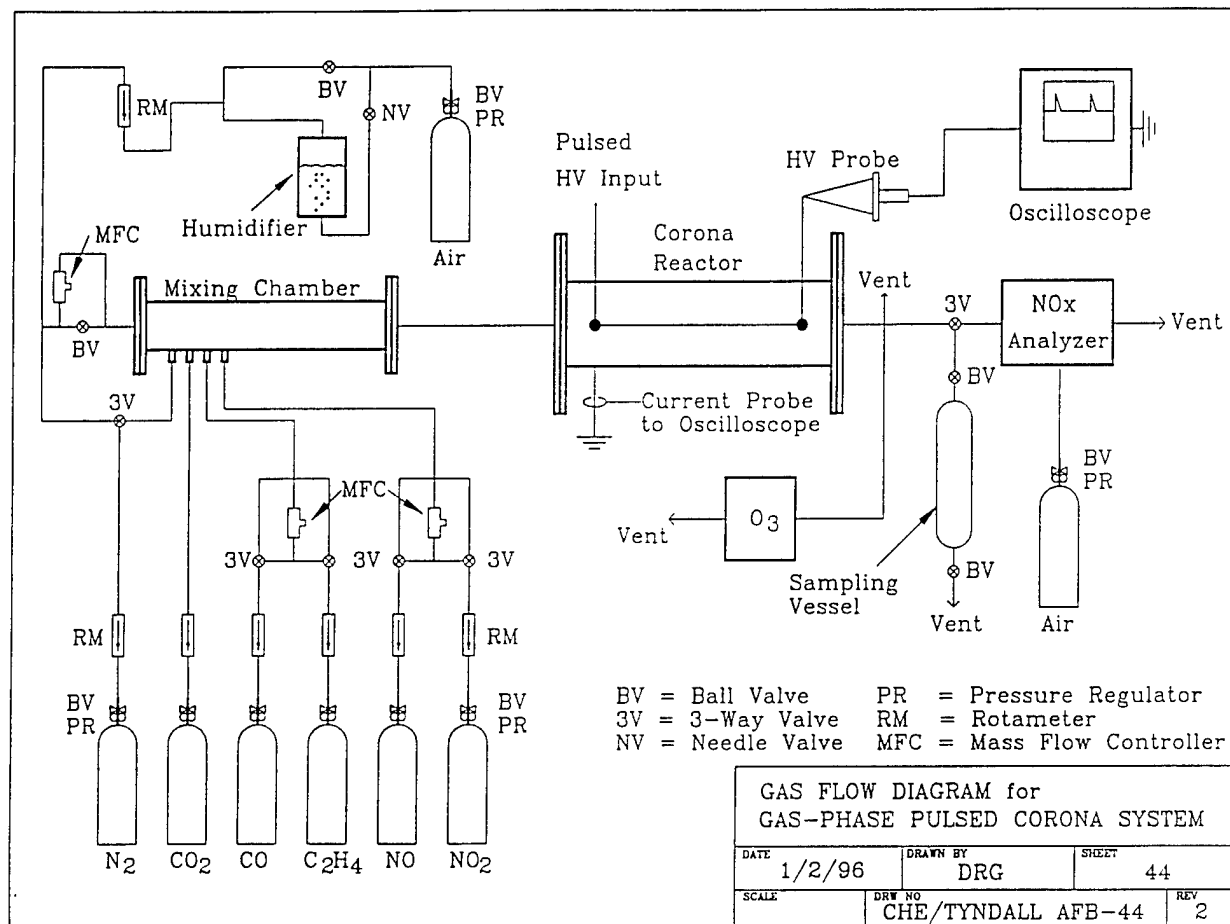


Figure 4 : Experimental Setup

containing 1% NO in dry N<sub>2</sub>, 1% NO<sub>2</sub> in dry N<sub>2</sub>, pure C<sub>2</sub>H<sub>4</sub>, and pure CO, 3) gas cylinders and high pressure regulators containing calibration gases of 100 ppm NO in N<sub>2</sub> and 113 ppm NO<sub>2</sub> in N<sub>2</sub>, 4) a water tank through which the air and the other gas can be bubbled for humidification, 5) flow meters, valves, and mass flow controllers, and 6) a stainless steel gas mixing chamber upstream from the reactor.

The gas cylinders and the regulators were manufactured by Air Products Inc. The water tank used to humidify the air was 26 inches long and 7 inches in diameter. The air was introduced at the bottom of the tank, and was made to bubble through the water column. Flow meters used to monitor the flow rate of the air into the reactor were purchased from Dwyer, Inc. Mass flow controllers used to control the flow of air and the trace gases sent into the reactor were purchased from MKS Instruments Inc. Two controllers of Type 1259C were used to control the flow of NO and ethylene gas. A mass flow controller of Type 1559A was used to control the amount of air or N<sub>2</sub> flowing into the reactor. Trace gases such as NO, ethylene, and CO were mixed with the air in a stainless steel mixing chamber before passing into the reactor. The mixing chamber was 23.5 in. long and had a diameter of 2.5 inches.

## **E. EXPERIMENTAL PROCEDURES**

In order to conduct a typical experiment to consider NO removal at a particular voltage and residence time, the NO<sub>x</sub> monitor as well as the mass flow controllers were turned on at least 2 hours before the start of the experiment to allow them to stabilize. Calibration of the NO<sub>x</sub> monitor was performed by passing the calibration gases of known concentrations of NO and NO<sub>2</sub> into the monitor and calibrating the monitor reading to the corresponding value. Once the mass flow controllers stabilize, the readings were zeroed, if necessary.

The feed air used in the experiments was produced by a central compressed air source from the College of Engineering building. A dedicated regulator/valve filter assembly was adjusted so that the pressure of the air delivered to the gas distribution system was maintained at 20 psig. The air flow rate through the reactor was then adjusted with needle valves and with the mass flow controller corresponding to the required gas residence time in the reactor. The two spherical electrodes and the rod electrode on the rotating spark gap tended to corrode during the course of an

experiment, so they were cleaned using ethanol and sandpaper before running every experiment. The rotating mechanical spark gap was engaged and adjusted so that it was aligned perpendicular to the discharge position when the strobe lamp was in line frequency mode (60 Hz). This ensured full charging of the capacitors by the power supply.

The feed air delivered to the reactor was first passed through a drier (calcium sulfate packed columns) to remove any residual water vapor present in the compressed air. In cases where water vapor was required for an experiment in the system, air was bubbled through a water tank. The flow rate of all feed and trace gases were continually monitored by mass flow controllers and/or by flow meters.

To measure the voltage waveform of the pulsed voltage, the high voltage probe was connected to the central wire electrode to which the high voltage input was connected. The current probe was attached across a wire connecting the outer cylinder of the reactor to the ground. The exact locations at which the voltage and the current were measured are shown in Figure 4. Both the probes were connected to the oscilloscope to measure the different characteristics of the waveforms. Once the flow rate of all the gases had stabilized, the pulsed corona discharge was applied to the reactor.

The pulsed voltage, current, and power waveform characteristics were noted from the oscilloscope, and adequate time was allowed for all the analytical instruments to stabilize. The exhaust gases coming out of the reactor were passed through the  $\text{NO}_x$  monitor to record the concentration of NO and  $\text{NO}_2$ . For trace gas sample analysis, the outlet gases from the reactor were passed through a glass sampling vessel. The gases in the sampling vessel were analyzed by GC/MS for the breakdown products of  $\text{NO}_x$  gases and also for the concentration of ethylene in experiments for which the ethylene was present in the feed gas.

For liquid sample analysis, the exhaust gases were sparged through water in a flask. These water samples were then analyzed by HPLC and ion chromatography. HPLC analysis was performed on a Perkin Elmer HPLC unit using a Supelcogel C-610H organic acid column 30 cm by 7.8 mm. The flow rate was 0.5 ml/min with a mobile phase of 0.1%  $\text{H}_3\text{PO}_4$ . A UV detector set at 210 nm was used and samples were injected through a 300  $\mu\text{l}$  sample loop. HPLC Grade Optima water was used for the mobile phase preparation and for the collection of the samples from the corona reactor.

Exhaust gas from the corona reactor was bubbled through approximately 200 ml of the phosphoric acid mobile phase for specified time intervals of 20 to 30 minutes. Samples of this fluid were analyzed by HPLC. The exhaust gases used for this analysis were obtained from the corona with operating conditions: 1) 50 kV, 2) residence time 44 seconds, 3) 100 ppm NO, 4) 500 ppm C<sub>2</sub>H<sub>4</sub>, 5) carrier gas of compressed air humidified to 85.5% relative humidity at 75 °C.

Ozone concentration was determined by using the KI method specified in Greenberg et al. (1992). This involved the use of two traps in series each containing 200 mL of 2% KI solution at the output of the corona reactor. The entire output flow from the reactor was sparged into each trap in series. The traps were exposed to the output stream for 10 minutes. After exposure both solutions were transferred to separate beakers and titrated against 0.05 N Na<sub>2</sub>S<sub>2</sub>O<sub>3</sub> solution. When the solutions lose their yellow color, 1 to 2 mL of starch indicator solution was added. Titration was continued until the solution was clear. Ozone concentration is calculated using the equations given by Greenberg et al. (1992).

Once the readings of the 1) NO<sub>x</sub> concentration, 2) rise time, 3) peak voltage, 4) pulse width of the voltage waveform, 5) peak current, and 6) pulse width of the current waveform were measured, the power to the reactor was turned off and the reactor and the spark gap were grounded with a grounding rod. The valves of the gas cylinders were closed and the reactor was then purged for several minutes with clean, dry compressed air.

## F. LIQUID PHASE REACTOR SPECIFICATIONS

A new liquid phase reactor was designed and constructed following the general design of reactors used in previous studies (Sharma et al., 1993, Joshi et al., 1995). The reactor consists of a 1 liter jacketed glass vessel shown in Figure 4b. A glass u-tube runs from outside the jacketed reactor to a male ground glass connector on the inside of the reactor. A high voltage wire will be introduced into the reactor through this tube; the wire will connect with a stainless steel discharge needle facing upwards. Opposite the needle, a pancake-shaped grounded electrode is suspended from a ground glass fitting centered in the top of the reactor lid. Another ground glass fitting will allow gas to be introduced into the reactor, while a third fitting will be impermeable.

The improvements in the reactor design from the previous reactors used in our laboratory are

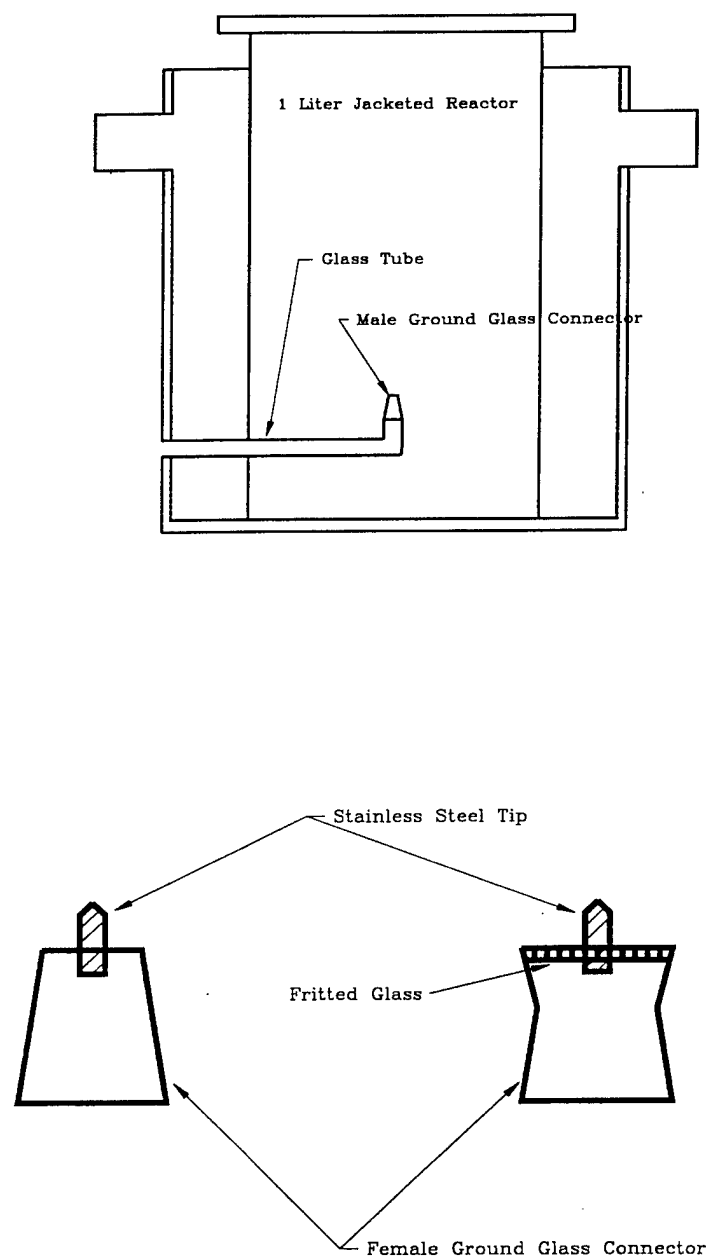


Figure 4b. Liquid Phase Reactor and Electrode Tip Design.

the following. Reactor volume has been increased from 550 ml to one liter, and glass is used as the vessel material. The high voltage input wire will be introduced from the side of the reactor and will not be in close proximity to the ground electrode. This will also allow for a perfectly round ground electrode that will not have any sharp edges. The addition of the water jacket will allow for easier control of the reactor temperature. Finally, the new design of the electrode tip will allow for easy removal of the electrode from the reactor and replacement of the discharge electrode.

### SECTION III

#### REACTION MODELING

In a pulsed corona discharge in a gaseous medium, free electrons gain energy from an imposed electric field and lose energy through collisions with neutral gas molecules. This transfer of energy to the gas molecules leads to the formation of a variety of new species including ions, metastables, atoms, and free radicals. These products are chemically active and react with the other gas molecules to form new stable compounds. The modeling of the reactor is a complicated process and certain assumptions are made to analyze the system.

The kinetic rate constants for the electron-gas reactions depend upon the imposed electric field and also on the gas composition. In this work, a model was constructed with the help of experimental data to consider the concentration of different molecular species during the pulsed corona discharge. A global approach was adopted where only dissociation reactions of major constituents of the gas were considered in the reaction model. The kinetic rate constants for the dissociation reactions were obtained for the experimental data on NO removal and NO<sub>2</sub> formation and removal in various gas streams.

The modeling effort here accounted for the chemistry in pulsed streamer corona discharge by considering two chemical reaction sets. During the time frame of pulsing (pulse-on period), the electron concentration was assumed to be fixed, and the reaction set included the gas molecule dissociation reactions in order to calculate the concentration profile of different species. During the time between the pulsing (pulse-off period), the electron concentration was assumed to be zero, and so the reaction set which did not have the dissociation reactions was used to calculate the concentration profile. These two reaction sets were interchanged repeatedly to simulate the pulse-on, pulse-off aspect of the discharge.

The pulse width of the voltage pulse, which was the time at the half maximum, varied between 500-700 nanoseconds. The total pulse duration from the inception of the rise time to the complete decay of the voltage peak was 1 microsecond. In the present modeling, the pulse width was assumed to be 1 microsecond and the time between the two pulses was assumed to be 16.667 milliseconds, corresponding to a pulse frequency of 60 Hz. Hence the reaction set with electron

dissociation reactions was used to calculate the concentration profile for 1 microsecond followed by the reaction set which did not include the dissociation reactions to calculate the concentration profiles for the next 16.667 milliseconds repeatedly until the final total time equaled the residence time in the reactor.

This method was similar to the model used by Loiseau et al. (1994) for computing ozone production in a cylindrical oxygen-fed ozonizer. For example, Figure 5 shows the concentration profile of ozone computed by the code used in the present study that alternately employed the two reaction sets to simulate the pulse-on and pulse off aspect of the discharge. As in the figure, during the pulse-on period the oxygen radicals are produced and hence ozone formation increased rapidly, and during the pulse-off period the ozone production level was flat.

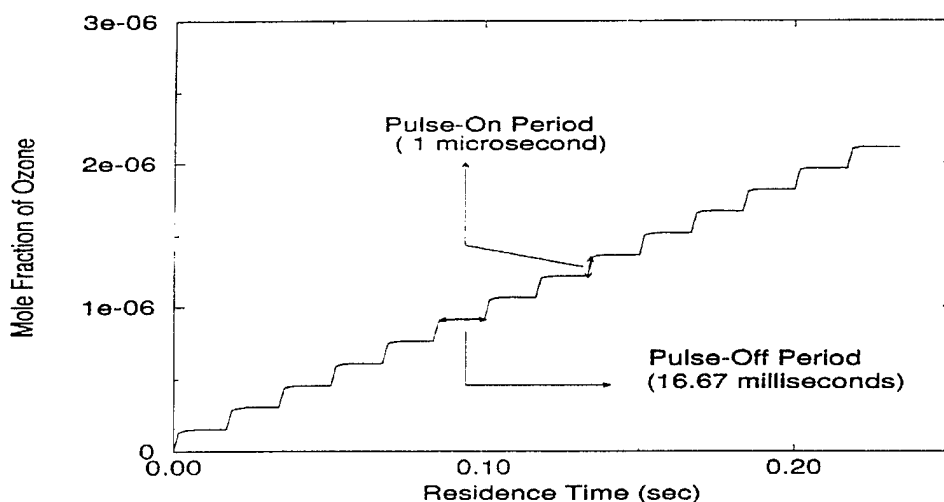


**Figure 5.** Ozone Concentration Profile to Illustrate Modeling Method.

The following were the assumptions made for the model used here:

1. Isothermal system. There is no appreciable heating of the gas during the residence time in the reactor.
2. Plug-flow model. The model does not account for the axial and radial dispersion in the reactor.
3. There is no variation in the concentration of electrons during the pulse-on period either in



space or in time.

4. Reactions involving metastables, ions, and photo-ionization are neglected.
5. The model does not account for the variation in electric field strength from the anode wire to the cathode cylinder.

The molar species continuity equations for all the species is given by:

$$\frac{\partial c_i}{\partial t} + u \cdot \nabla c_i = D_i \nabla^2 c_i + \sum_j v_{ij} R_{ij} \quad (4)$$

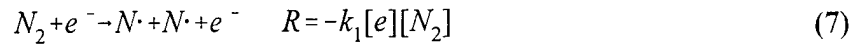
where  $c_i$  is the concentration of species  $i$ ,  $t$  is the time,  $u$  is the molar average velocity vector,  $D_i$  is the diffusion coefficient,  $v_{ij}$  is the stoichiometric coefficient of the  $i$ th species in the  $j$ th reaction and  $R_{ij}$  is the reaction rate. For a plug flow reactor model without axial dispersion or molecular diffusion the equation reduces to:

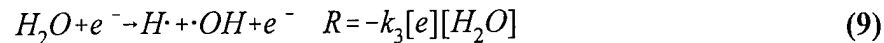
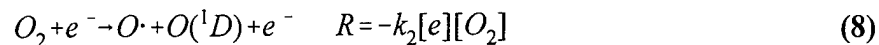
$$u_x \frac{dc_i}{dx} = \sum_j v_{ij} R_{ij} \quad (5)$$

In terms of residence time ( $\tau = x/u_x$ ) in the reactor, the equation becomes:

$$\frac{dc_i}{d\tau} = \sum_j v_{ij} R_{ij} \quad (6)$$

The above system of ordinary differential equations has been solved using the CHEMKIN software (Kee et al., 1994). A set of reactions was considered which included only one electron-molecule collision reaction per each major constituent ( $N_2$ ,  $O_2$ ,  $H_2O$ ). The dissociation reactions considered which were dependent upon the electric field are:





Reaction (7) represents the production of nitrogen free radicals by all possible mechanisms including dissociation, ionization, and excitation. The kinetic rate constant for this global reaction is dependent upon the electric field applied and hence would vary with the external applied field. Similarly, the rate constants for reactions (8) and (9) represent the global kinetic rate constants for the production of oxygen and hydroxyl radicals, respectively. Although ionization is a major process taking place in the corona discharge, it was assumed in the present model that the ions do not play a major role in the chemistry of the neutral gas molecules.

The set of reactions used for modeling NO removal in the case of nitrogen, dry air, and humid air is shown in Table 1. The rate constants for these reactions are obtained primarily from the atmospheric chemistry literature (Willis & Boyd; 1976, Baulch et al.; 1983, Demore et al., 1987; and Atkinson et al., 1989), and were cross-checked with the NIST Database (NIST Standard Reference Data Base 17.0, 1994). The criterion for choosing the reactions was to consider reactions of neutral species having significant kinetic rate constants ( $> 1.0 \times 10^7 \text{ cm}^3 \text{ mole}^{-1} \text{ sec}^{-1}$ ).

Table 1 : List of Chemical Reactions Considered for Modeling

Chemical Reactions	Rate Constants ( $cm^3.mole^{-1}.sec^{-1}$ )	Source
$N_2 \longrightarrow 2N\cdot$	$K_1[E]$	Expt. Data.
$O_2 \longrightarrow O\cdot + O(^1D)$	$K_2[E]$	Expt. Data.
$N\cdot + N\cdot \longrightarrow N_2$	$6.38 \times 10^{10}$	Willis & Boyd, 1976.
$N\cdot + O\cdot \longrightarrow NO$	$1.45 \times 10^{11}$	Willis & Boyd, 1976.
$N\cdot + NO \longrightarrow N_2 + O\cdot$	$2.04 \times 10^{13}$	Willis & Boyd, 1976.
$N\cdot + O_2 \longrightarrow NO + O\cdot$	$5.36 \times 10^7$	Atkinson et al., 1989.
$N\cdot + NO_2 \longrightarrow 2NO$	$1.81 \times 10^{12}$	Atkinson et al., 1989.
$N\cdot + NO_2 \longrightarrow N_2O + O\cdot$	$1.81 \times 10^{12}$	Atkinson et al., 1989.
$O\cdot + O\cdot \longrightarrow O_2$	$1.02 \times 10^{11}$	Willis & Boyd, 1976.
$O\cdot + O_2 \longrightarrow O_3$	$7.83 \times 10^9$	Willis & Boyd, 1976.
$O\cdot + O_3 \longrightarrow 2O_2$	$4.82 \times 10^9$	Willis & Boyd, 1976.
$O(^1D) \longrightarrow O\cdot$	$6.95 \times 10^8$	Demore et al., 1987.
$O(^1D) + NO_2 \longrightarrow NO + O_2$	$2.95 \times 10^{13}$	Schofield, 1979.
$O(^1D) + O_3 \longrightarrow 2O_2$	$7.23 \times 10^{13}$	Atkinson et al., 1989.
$O(^1D) + O_3 \longrightarrow 2O\cdot + O_2$	$7.23 \times 10^{13}$	Atkinson et al., 1989.
$O(^1D) + N_2O \longrightarrow N_2 + O_2$	$2.95 \times 10^{13}$	Demore et al., 1987.
$O(^1D) + N_2O \longrightarrow 2NO$	$4.04 \times 10^{13}$	Demore et al., 1987.
$NO + O_3 \longrightarrow NO_2 + O_2$	$8.43 \times 10^9$	Demore et al., 1987.
$NO + O\cdot \longrightarrow N\cdot + O_2$	$2.77 \times 10^9$	Demore et al., 1987.
<i>continued on next page</i>		

<i>continued from previous page</i>		
Chemical Reactions	Rate Constants ( $cm^3.mole^{-1}.sec^{-1}$ )	Source
$NO + O \cdot \longrightarrow NO_2$	$1.40 \times 10^{12}$	Atkinson et al., 1989.
$NO + NO_3 \longrightarrow 2NO_2$	$1.75 \times 10^{13}$	Demore et al., 1987.
$NO + NO_3 \longrightarrow 2NO + O_2$	$1.84 \times 10^{11}$	Sutherland et al., 1975.
$NO_2 + O_3 \longrightarrow NO_3 + O_2$	$1.93 \times 10^7$	Atkinson et al., 1989.
$NO_2 + O \cdot \longrightarrow NO + O_2$	$5.84 \times 10^{12}$	Atkinson et al., 1989.
$NO_2 + NO_3 \longrightarrow$		
$NO + NO_2 + O_2$	$6.45 \times 10^8$	Baulch et al., 1983.
$N_2O_4 + M \longrightarrow 2NO_2 + M$	$2.06 \times 10^9$	Baulch et al., 1983.
$2NO_3 \longrightarrow 2NO_2 + O_2$	$1.92 \times 10^8$	Baulch et al., 1983.
$NO_3 + O \cdot \longrightarrow NO_2 + O_2$	$1.02 \times 10^{13}$	Demore et al., 1987.
$O_3 + N \cdot \longrightarrow NO + O_2$	$6.02 \times 10^7$	Baulch et al., 1983.
$2NO_2 + M \longrightarrow N_2O_4 + M$	$3.06 \times 10^{14}$	Baulch et al., 1987.
$NO_2 + O \cdot \longrightarrow NO_3$	$1.29 \times 10^{12}$	Atkinson et al., 1989.
$H_2O \longrightarrow H \cdot + OH \cdot$	$K_3[E]$	Expt. Data
$N \cdot + OH \cdot \longrightarrow NO + H \cdot$	$1.45 \times 10^{13}$	Demore et al., 1987.
$O(^1D) + H_2 \longrightarrow H \cdot + OH \cdot$	$6.02 \times 10^{13}$	Demore et al., 1987.
$O(^1D) + H_2O \longrightarrow 2OH \cdot$	$1.33 \times 10^{14}$	Demore et al., 1987.
$O \cdot + H \cdot \longrightarrow OH \cdot$	$1.08 \times 10^{12}$	Willis & Boyd, 1976.
$O \cdot + HO_2 \longrightarrow OH \cdot + O_2$	$3.4 \times 10^{13}$	Atkinson et al., 1989.
$O \cdot + OH \cdot \longrightarrow O_2 + H \cdot$	$1.99 \times 10^{13}$	Atkinson et al., 1989.
$OH \cdot + H_2 \longrightarrow H_2O + H \cdot$	$4.03 \times 10^9$	Atkinson et al., 1989.
$OH \cdot + OH \cdot \longrightarrow H_2O + O \cdot$	$1.08 \times 10^{12}$	Atkinson et al., 1989.
<i>continued on next page</i>		

<i>continued from previous page</i>		
Chemical Reactions	Rate Constants ( $cm^3.mole^{-1}.sec^{-1}$ )	Source
$OH\cdot + OH\cdot \longrightarrow H_2O_2$	$9.93 \times 10^{12}$	Atkinson et al., 1989.
$OH\cdot + HO_2\cdot \longrightarrow H_2O + O_2$	$6.63 \times 10^{13}$	Atkinson et al., 1989.
$OH\cdot + H_2O_2 \longrightarrow H_2O + HO_2\cdot$	$1.02 \times 10^{12}$	Atkinson et al., 1989.
$OH\cdot + H\cdot \longrightarrow H_2O$	$1.45 \times 10^{13}$	Atkinson et al., 1989.
$H\cdot + O_2 \longrightarrow HO_2\cdot$	$8.49 \times 10^{11}$	Atkinson et al., 1989.
$H\cdot + O_3 \longrightarrow OH\cdot + O_2$	$1.67 \times 10^{13}$	Atkinson et al., 1989.
$H\cdot + HO_2\cdot \longrightarrow H_2 + O_2$	$3.37 \times 10^{12}$	Atkinson et al., 1989.
$H\cdot + HO_2\cdot \longrightarrow 2OH\cdot$	$4.34 \times 10^{13}$	Atkinson et al., 1989.
$H\cdot + HO_2\cdot \longrightarrow H_2O + O\cdot$	$1.45 \times 10^{12}$	Atkinson et al., 1989.
$H\cdot + H_2O_2 \longrightarrow H_2O + OH\cdot$	$6.02 \times 10^{10}$	Willis & Boyd, 1976.
$HO_2\cdot + HO_2\cdot \longrightarrow H_2O_2 + O_2$	$1.02 \times 10^{12}$	Demore et al., 1987.
$NO + OH\cdot \longrightarrow HNO_2$	$9.03 \times 10^{12}$	Atkinson et al., 1989.
$NO_2 + OH\cdot \longrightarrow HNO_3$	$1.45 \times 10^{13}$	Demore et al., 1989.
$NO_2 + OH\cdot \longrightarrow HO_2\cdot + NO$	$1.39 \times 10^{13}$	Atkinson et al., 1989.
$HNO_2 + OH\cdot \longrightarrow NO_2 + H_2O$	$2.95 \times 10^{12}$	Atkinson et al., 1989.
$HNO_3 + OH\cdot \longrightarrow H_2O + NO_3$	$9.03 \times 10^{10}$	Atkinson et al., 1989.
$OH\cdot + H\cdot \longrightarrow H_2 + O\cdot$	$1.96 \times 10^7$	Loirat et al., 1987.
$H_2O_2 + H\cdot \longrightarrow HO_2\cdot + H_2$	$3.12 \times 10^9$	Warnatz, et al., 1984.
$H_2O_2 + O\cdot \longrightarrow OH\cdot + HO_2\cdot$	$1.03 \times 10^9$	Atkinson et al., 1989.
$O_3 + HO_2\cdot \longrightarrow OH\cdot + 2O_2$	$1.17 \times 10^9$	Levine et al., 1985.
$O_3 + OH\cdot \longrightarrow HO_2\cdot + O_2$	$3.36 \times 10^{10}$	Atkinson et al., 1989.
$HNO_2 + O\cdot \longrightarrow NO_2 + OH\cdot$	$1.81 \times 10^9$	Kaiser et al., 1978.
<i>continued on next page</i>		

*continued from previous page*

Chemical Reactions	Rate Constants ( $cm^3.mole^{-1}.sec^{-1}$ )	Source
$HNO_3 + HNO_2 \longrightarrow$		
$NO_2 + H_2O$	$9.64 \times 10^6$	Kaiser et al., 1977.
$HNO_3 + O \cdot \longrightarrow NO_3 + OH \cdot$	$1.81 \times 10^9$	Kaiser et al., 1978.
$HNO_3 + H \cdot \longrightarrow HNO_2 + OH \cdot$	$6.02 \times 10^{10}$	Baulch et al., 1983.
$NO_3 + H \cdot \longrightarrow NO_2 + OH \cdot$	$6.63 \times 10^{13}$	Boodaghians et al., 1988.
$NO_3 + OH \cdot \longrightarrow NO_2 + HO_2$	$1.39 \times 10^{13}$	Boodaghians et al., 1988.
$NO_3 + HO_2 \longrightarrow HNO_3 + O_2$	$7.63 \times 10^{11}$	Hoffmann et al., 1988.
$NO_3 + HO_2 \longrightarrow$		
$NO_2 + OH \cdot + O_2$	$3.05 \times 10^{12}$	Hoffmann et al., 1988.
$N \cdot + HO_2 \longrightarrow NO + OH \cdot$	$1.33 \times 10^{13}$	Brune et al., 1983.
$NO + HO_2 \longrightarrow NO_2 + OH \cdot$	$4.66 \times 10^{12}$	NIST Database.
$NO + HO_2 \longrightarrow HNO_3$	$8.43 \times 10^{10}$	NIST Database.

## SECTION IV

### EXPERIMENTAL RESULTS & DISCUSSION

#### A. PHYSICAL DISCHARGE CHARACTERISTICS

The physical aspects of the corona discharge including the corona onset voltage, the peak voltage, the pulse rise time, and the pulse width were measured at the location where the pulsed discharge was delivered to the centrally located high voltage discharge wire electrode.

First, a power supply calibration was made to find the relation between the applied AC voltage delivered to the pulse forming network and the voltage indicated on the control section of the transformer/rectifier (dial voltage). A plot of the applied voltage versus the dial voltage is shown in Figure 6. The applied voltage refers to the peak AC output voltage of the transformer as measured by the high voltage probe and the oscilloscope. This figure shows an apparent linear relationship between the dial voltage and the applied voltage. Linear regression was performed on the data, and the correlation coefficient was found to be 0.9998 and the slope of the line to be 0.964.

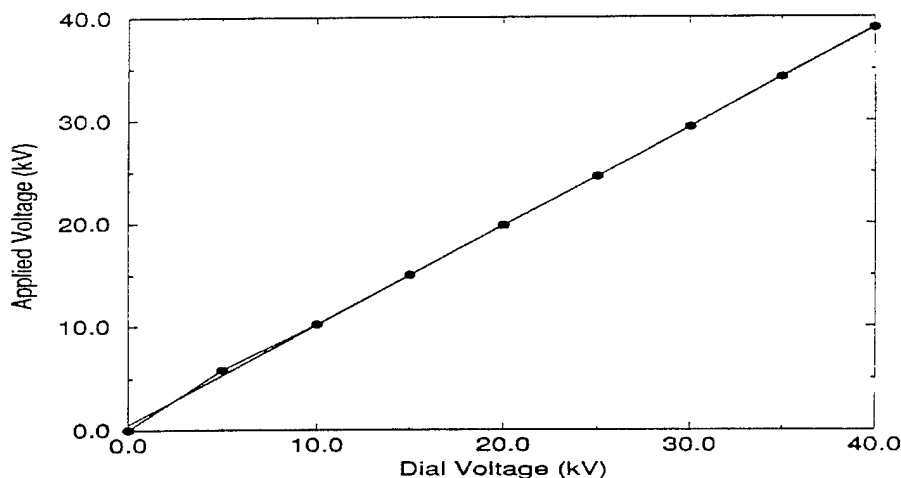


Figure 6. Power Supply Calibration.

Pulsed corona onset (corona initiation voltage) in the reactor was found to occur at a pulsed input voltage of between 13 and 14 kV in an atmosphere of dry air and at about 10 kV in a dry

nitrogen atmosphere. Below the onset of corona, the voltage and the current readings measured at the reactor using the oscilloscope were very small. Above the corona onset the peak voltage and the current increased dramatically. The rise time of the voltage pulse was found to vary between 15 and 30 nanoseconds.

A plot of a typical voltage waveform is shown in Figure 7. As seen in the figure, there is a sharp increase in the voltage, i.e., a very short rise time, followed by an exponential decay of the voltage. The pulse width at half-maximum of the voltage pulse varied from 500 to 700 nanoseconds. The current waveform is shown in Figure 8. The current pulses were shorter in width ( $< 300$  nanoseconds) when compared to the voltage pulses. The power input per pulse was calculated by multiplying the voltage and the current waveforms and measuring the area under the resulting waveform. A plot of the pulsed power waveform is shown in Figure 9. Table 2 summarizes the peak voltage, the rise time, and the pulse width of the pulsed voltage as a function of dial voltage in a dry air atmosphere.

As the table shows, the peak pulsed voltage was significantly higher than the dial voltage, and both the rise time and the pulse width increased with an increase in the applied voltage. As originally conceived, the pulse generating circuit did not include a load resistor in parallel with the reactor electrodes (see Figure 3). However, it was found that the spark gap would not fire even at high input voltages because the effective resistance of the gap between the reactor

Table 2: Voltage Characteristics of the Pulse in Dry Air

Dial Voltage (kV)	Peak Voltage (kV)	Rise Time (ns)	Pulse Width (ns)
30	38.8	13.5	449
35	44.8	16.5	616
40	51.4	18.0	627
50	59.6	29.0	694



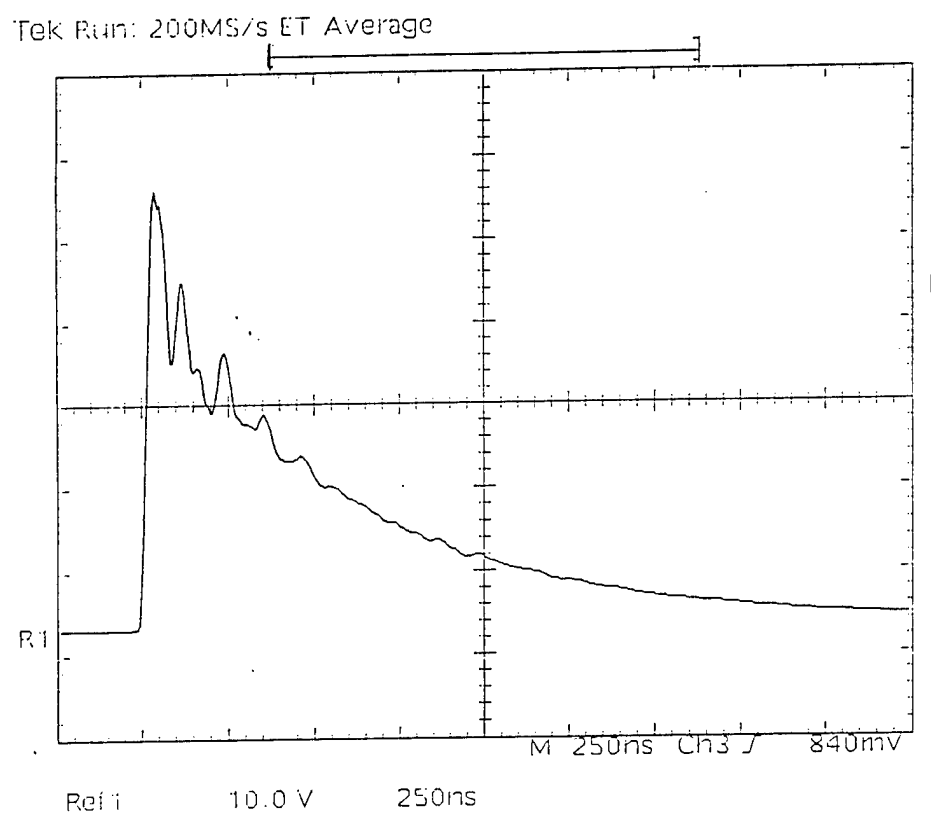


Figure 7 Voltage Waveform in an Atmosphere of Dry Air at 40 kV

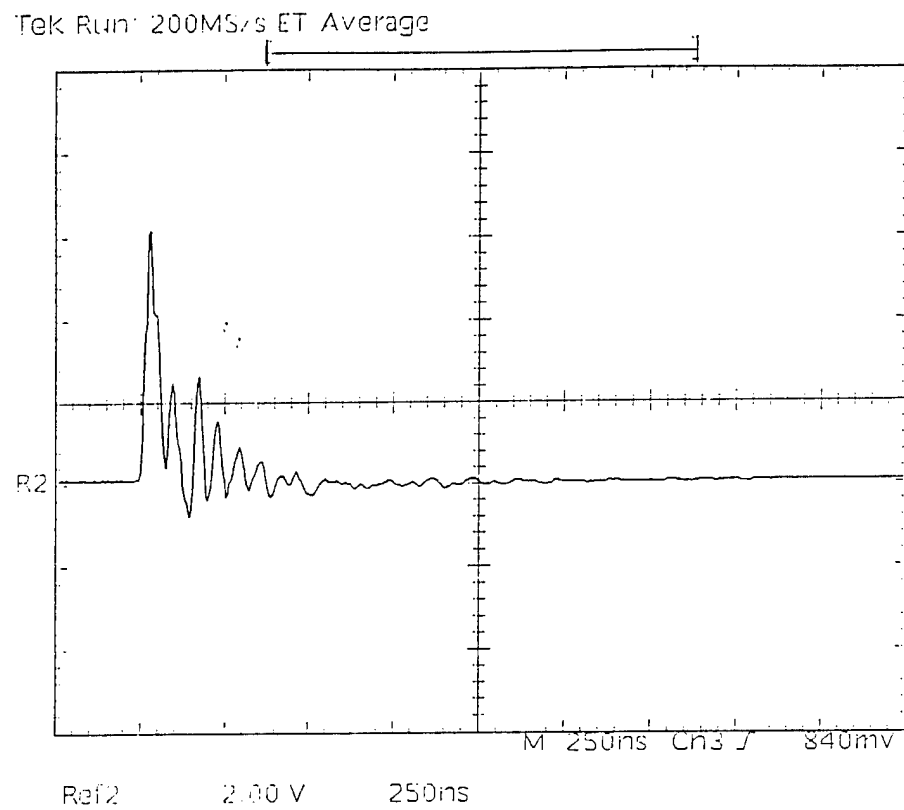


Figure 8 Current Waveform in an Atmosphere of Dry Air at 40 kV

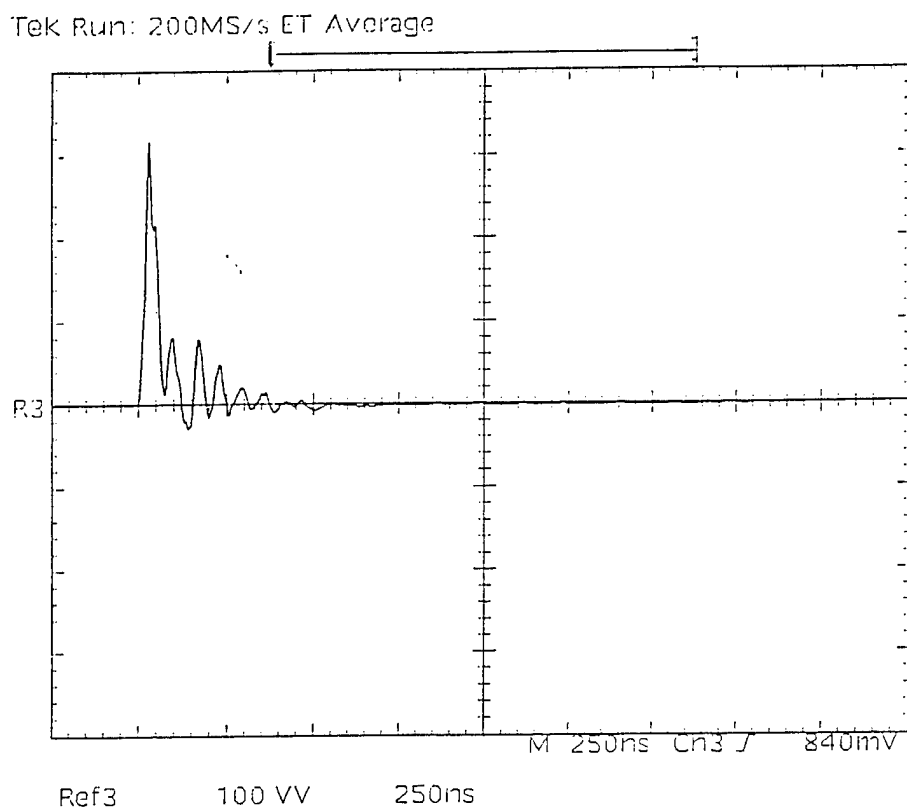


Figure 9 Power Waveform in an Atmosphere of Dry Air at 40 kV

electrodes was too high. In order to decrease the effective resistance of the gap between the outer grounded cylinder and the high voltage wire electrode, a load resistance was connected from the spark gap output to ground in parallel to the two reactor electrodes. The nature of the voltage waveform was affected by the value of the load resistance. As the resistance of the load resistor was decreased from 300  $\Omega$  to 77.1  $\Omega$ , the decay time (time required for the voltage to drop from its maximum value to its minimum value) for the voltage pulses increased. A load resistor of 300  $\Omega$  was used in all the experiments conducted for NO removal.

In this study, the pulse frequency was kept constant at 60 Hz and the voltage was varied in order to increase the energy input into the reactor. Table 3 shows the peak value of the current waveform and the corresponding energy per unit pulse calculated as a function of applied voltage. The power delivered to the reactor was determined by multiplying the energy per pulse by the frequency of pulsing. With the Tektronix current probe P6021, the energy input varied from 8.0 mJ/pulse to 148.0 mJ/pulse in the case of dry air. No differences in the pulse characteristics were observed when humid air was fed to the reactor.

Table 3: Current & Power Characteristics of the Pulse in Dry Air

Dial Voltage (kV)	Peak Current (A)	Energy per Pulse (mJ)	Power (watts)
30	42	8.0	0.48
35	52	20.	1.20
40	64	56.	3.36
50	82	148.	8.88

The energy delivered per pulse was close to that reported by Tas (1995) (6-7 mJ/pulse). The power was found to vary from 0.48 to 8.88 watts. Mizuno et al. (1995) reported an input power of 20 to 40 watts which is higher than the values obtained in the present study. The power density varied from 1.4 to 158 J/l which is in the range of that reported by Wolf et al. (1996) and Penetrante et al. (1996).

Experiments were designed to determine the extent of NO removal from several gases

with different compositions in order to study the reaction mechanisms for NO removal. The experiments were conducted at four different residence times and at four different voltages. All of the experiments were repeated twice to insure the reproducibility of the results. The average concentration determined in two similar runs was used to plot the figures of NO and NO<sub>2</sub> concentrations as functions of residence time and operating voltages. As an initial case, experiments on NO removal in an atmosphere of nitrogen was considered. This was followed by experiments in dry air, humid air, and finally in the presence of gas additives including carbon monoxide and ethylene.

## **B. NO REMOVAL IN NITROGEN**

NO removal experiments in an atmosphere of dry nitrogen were conducted at different residence times (7.2, 14.5, 29.0, and 44.0 seconds) and at different dial voltages (30, 35, 40, and 50 kV). The initial concentration of NO during the experiments was 100 ppmv.

The NO removal data as a function of residence time for different voltages is shown in Figure 10a. It was observed that the NO concentration decreased as the residence time in the reactor was increased at a particular voltage. In addition, as the applied voltage was increased for a particular residence time, the NO concentration decreased. Complete removal of NO was observed at the higher voltages of 40 and 50 kV at a residence time of 44.0 seconds.

The NO<sub>2</sub> concentration profile as a function of residence time for different dial voltages is shown in Figure 10b. A maximum of 8 ppm NO<sub>2</sub> formation was measured with the NO<sub>x</sub> monitor at the voltages of 40 and 50 kV. The concentration profiles of NO<sub>2</sub> at 35, 40, and 50 kV passed through maxima as the residence times in the reactor increased. Also, as the voltage was increased, the time corresponding to the maximum concentration decreased. At 30 kV the NO<sub>2</sub> concentration was steadily increasing with the residence time. These profiles indicate that at higher voltages (35, 40, & 50 kV), NO<sub>2</sub> is an intermediate product, and at longer residence times NO<sub>2</sub> was reduced back to molecular nitrogen and oxygen. At 30 kV, the amount of power input was not sufficient to reduce the NO<sub>2</sub> formed. Approximately 97% removal of NO<sub>x</sub> was obtained at high voltages (40 and 50 kV) and at a residence time of 44.0 seconds.

Penetrante et al. (1996) and Wolf et al. (1996) plot the NO concentration versus the

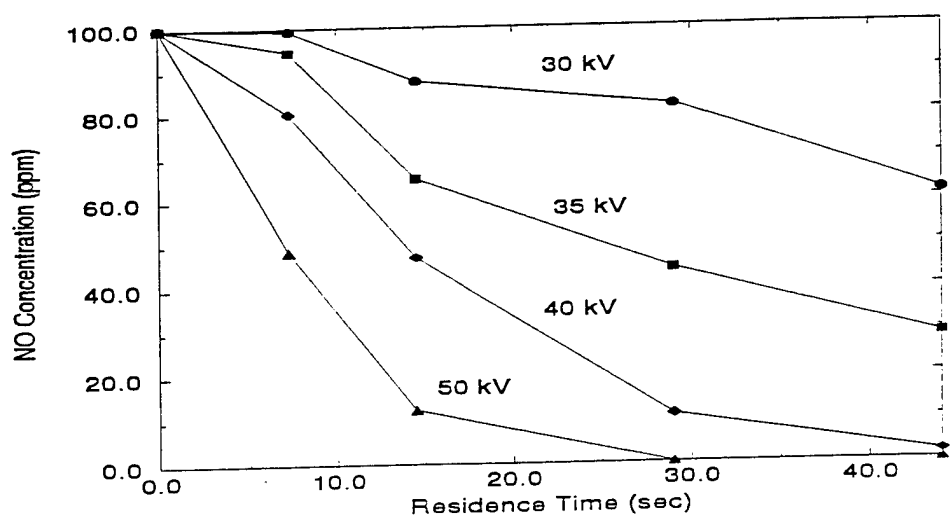


Figure 10a NO Concentration Profile in an Atmosphere of Nitrogen

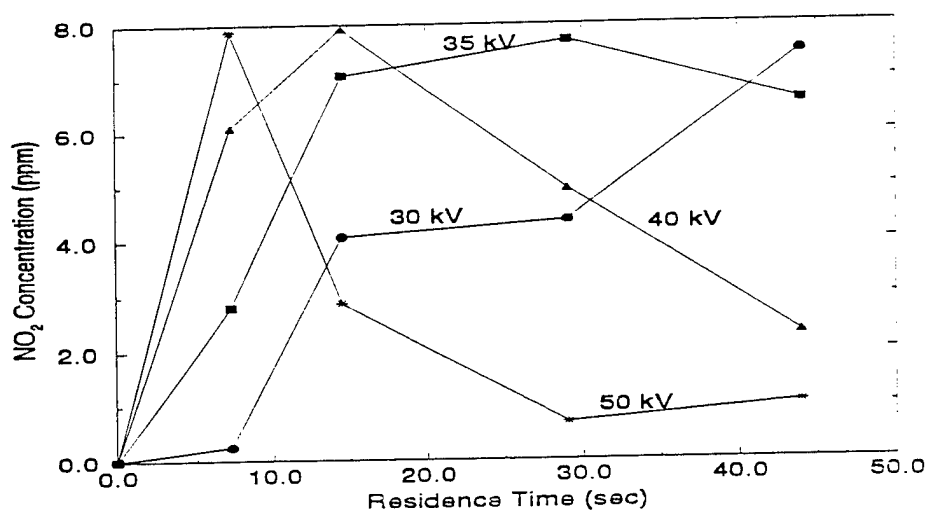


Figure 10b NO<sub>2</sub> Concentration Profile in an Atmosphere of Nitrogen

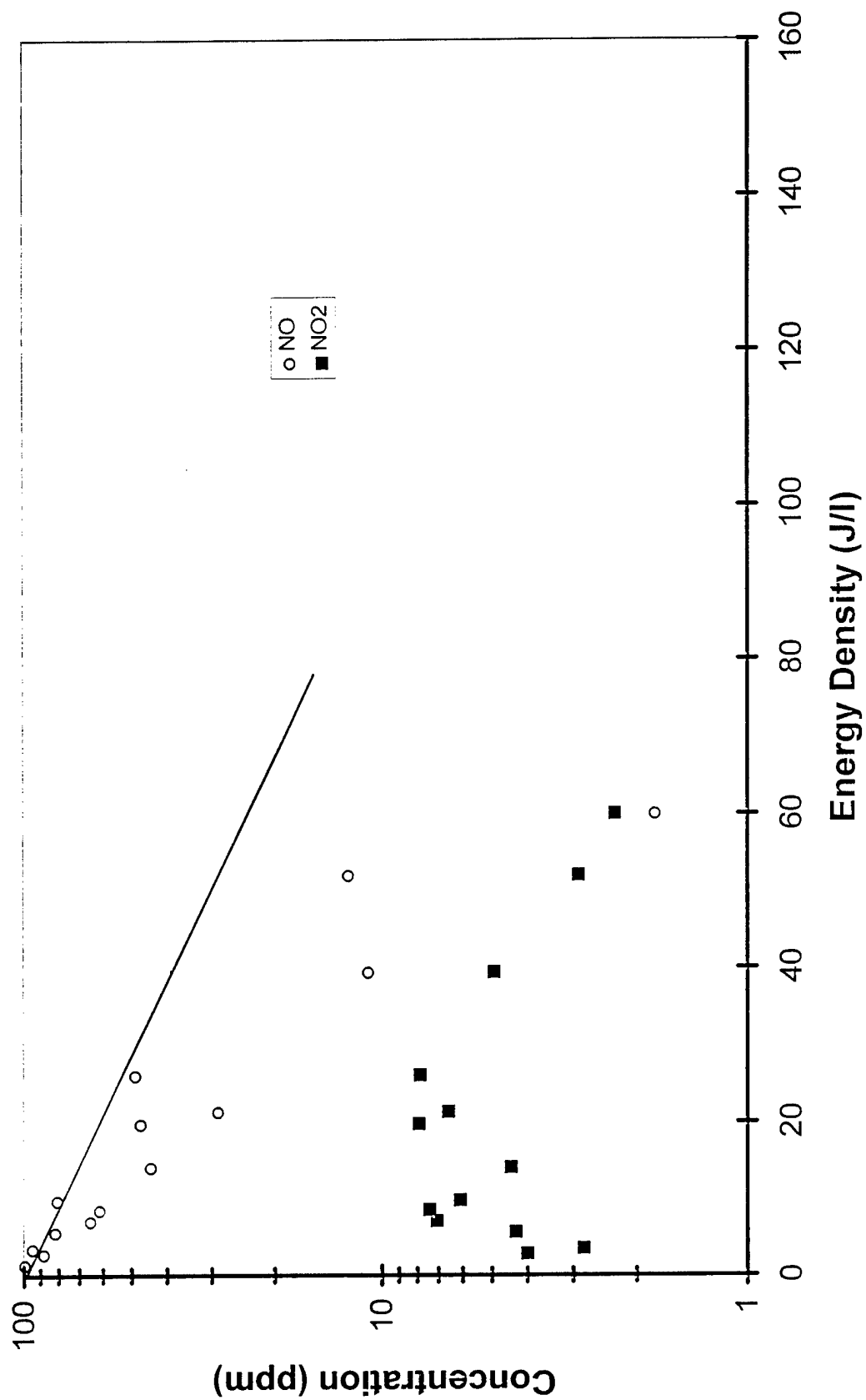
power density. Figure 11 shows our NO and NO<sub>2</sub> data plotted versus power density with a comparison to the theoretical predictions of Penetrante. The data of Penetrante et al. (1996) and Wolf et al. (1996) for lower voltages and applied fields follow the theoretical line of Penetrante et al. (1996), however, the data of Wolf et al. (1996) for higher field intensities and our data show a significantly lower power density for a given NO removal.

The kinetic model described earlier was used to determine the rate constant for the nitrogen dissociation reaction by fitting the model to the NO experimental data. The number of chemical reactions considered to calculate the concentration profiles of different species was 31. Figure 12 shows the mole fractions of NO, NO<sub>2</sub>, and N<sub>2</sub>O calculated by the model as a function of residence time at 50 kV. Experimental values of the NO<sub>2</sub> concentration profile at 50 kV in Figure 11 qualitatively match with the model profile of NO<sub>2</sub> at 50 kV shown in Figure 12 (100 ppm = 0.0001 in terms of mole fraction). The maximum value of NO<sub>2</sub> concentration in the model profile is around 17 ppm whereas the maximum value found by the experiments at 50 kV was around 8 ppm. Figure 12 also shows a small formation of N<sub>2</sub>O. Essentially the model predicts around 90% reduction of initial NO to molecular nitrogen and oxygen in an atmosphere of nitrogen at 50 kV.

The model profile of NO and the experimental data are shown in Figure 13. As seen in Figure 13, the model profiles match very well with the experimental values at 35, 40, and 50 kV at longer residence time. There is a slight deviation of the model from the experimental points at 30 kV. The experimental data of NO removal at 7.2 seconds residence time for all the voltages except 50 kV were less than that predicted by the model.

The rate constant of nitrogen dissociation as a function of applied voltage thus obtained by fitting the model to the experimental data is shown in Figure 14. This figure shows an almost linear relation of the rate constant as a function of applied electrical field. Of course, since the field is non-linear with power as shown in Table 3, the reaction rate constant is a non-linear function of the power delivered to the reactor. Many theoretical studies of pulsed corona and other non-thermal plasma reactors report the pseudo first-order rate constant for electron collision reaction to be of the form  $k' = [E/n]k$ , where  $k'$  is the pseudo first order rate constant,  $[E/n]$  is the reduced field, i.e. value of electrical field divided by the gas density, and  $k$  is the true second-

## NO / NO<sub>2</sub> Concentration in Nitrogen





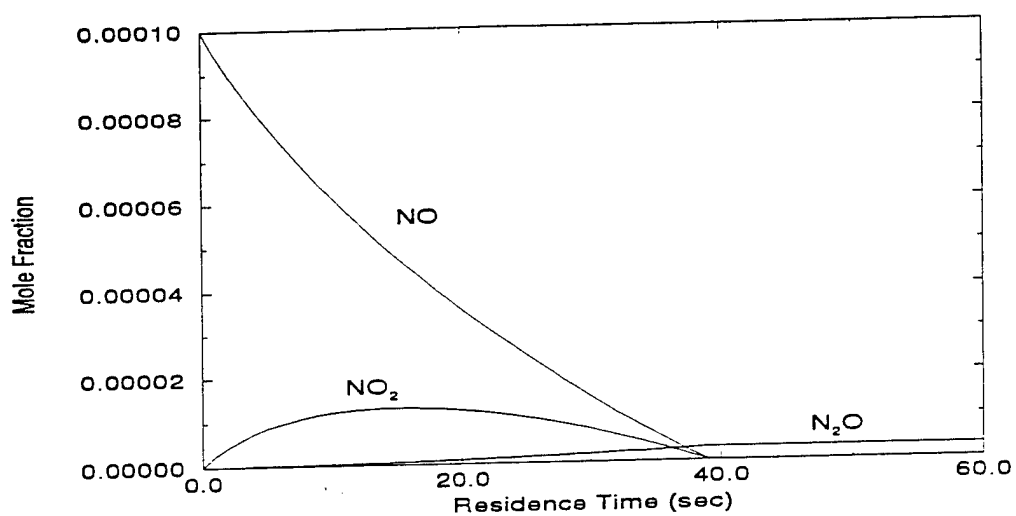


Figure 12 Model Profile of Different Species in an Atmosphere of Nitrogen

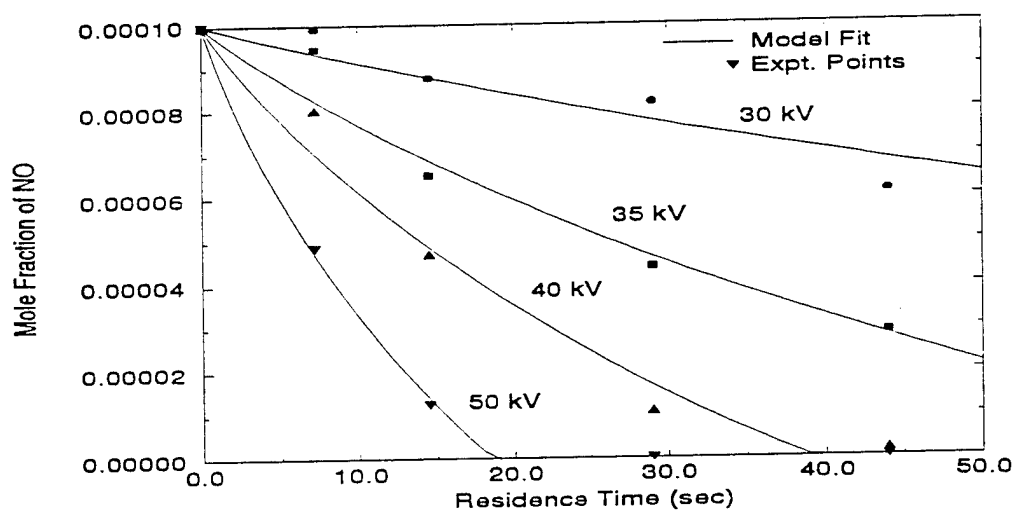
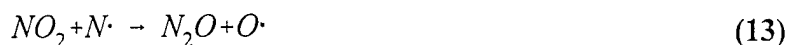


Figure 13 Model Fit for NO Concentration Profile in an Atmosphere of Nitrogen

order rate constant for the electron molecule collision. For constant gas density, this relationship would predict a linear dependence upon the electrical field as seen in our study.

The rate constant determined is a pseudo first-order rate constant, which is essentially the electron concentration multiplied by the actual second-order dissociation rate constant as in Equations 7, 8, and 9. Both experimental and modeling results indicate that the main reaction pathway for NO removal in nitrogen is through reduction to molecular nitrogen. The main reactions responsible for the removal are:



As the applied voltage is increased, the amount of nitrogen radicals produced by Equation 10 increases. The reactions responsible for NO removal are Equations 11 and 12. Equation 11 results in the formation of NO<sub>2</sub> but Equations 13 and 14 are fast enough to reduce the NO<sub>2</sub> formed back to N<sub>2</sub> and to N<sub>2</sub>O.

Tokunaga et al. (1984) used an electron beam to consider NO removal as a function of dose rate in an atmosphere of nitrogen, and concluded that NO was mainly decomposed to nitrogen and oxygen. The products from the irradiation were analyzed and NO<sub>2</sub> and N<sub>2</sub>O were

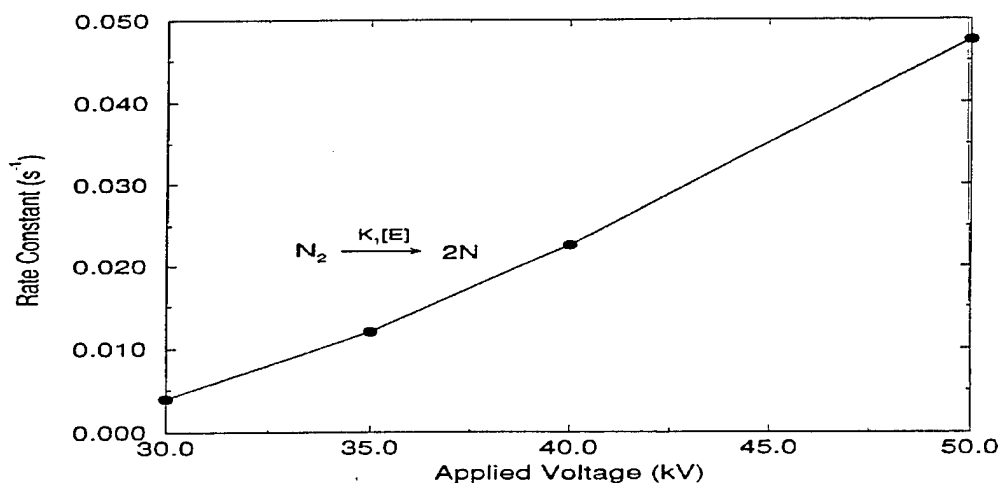


Figure 14. Rate Constants for Nitrogen Dissociation in Pure Nitrogen

present in very small amounts ( $\text{NO}_2=10\%$ ,  $\text{N}_2\text{O}=3\%$ ). Tas (1995) used pulsed streamer corona discharge to consider NO removal in an atmosphere of nitrogen, and concluded that the reduction pathway was the main path for the removal of NO in nitrogen. This conclusion is also supported by other studies (Wolf et al., 1996; Penetrante et al., 1996).

Penetrante et al. (1995) considered in detail the kinetics of corona discharge by solving for the electron energy distribution function to calculate the kinetic rate constants for the electron-gas reactions in order to predict the profile of different species for the case of NO removal in an atmosphere of nitrogen. The chemical kinetics calculation included 287 reactions and 37 species involving charged as well as neutral species. This model also predicts the reduction of NO as the main pathway for NO removal. It is important, however, to note that in the present study the model developed for the case of NO removal in nitrogen has considered only 13 neutral species and 31 chemical reactions as compared to the vast number of reactions considered by Penetrante et al. (1995). It is, therefore, possible to characterize the chemical reactions taking place in the pulsed streamer corona reactor by considering the neutral species reactions.

### C. NO REMOVAL IN DRY AIR

Experiments on NO removal in an atmosphere of dry air at various voltages (30, 35, 40, and 50 kV) and at different gas residence times (3.6, 7.2, 14.5, 29.0, and 60.0) were conducted to study the effect of oxygen addition on the NO and NO<sub>2</sub> concentration profiles.

The feed air used for the study was from a compressed air source from the building. The compressed air source was passed through a series of drier columns (anhydrous calcium sulfate) to remove the water vapor in the air. The initial NO concentration was about 116 ppm.

The concentration of NO<sub>2</sub> varied from 0 ppm to 25 ppm as the residence time in the reactor (without corona) increased. This indicated that a small fraction of the initial NO was oxidized to NO<sub>2</sub> when mixed with air in the reactor even in the absence of corona discharge. The temperature of the gas varied from 12.9 to 19 °C during the experiments.

NO concentration profiles as a function of residence time for different pulsed voltages are shown in Figure 15. NO concentration decreased as the applied voltage was increased for a particular residence time. It also decreased as the residence time was increased for a particular voltage. Comparing Figures 10 and 15, the rate of NO removal was faster in the case of dry air than in nitrogen. At 50 kV in an atmosphere of nitrogen 90% of NO was removed whereas in dry air almost 100% removal was observed at 14.5 seconds residence time. Using an initial concentration of 250 ppmv of NO, Chang et al. (1992) observed that at room temperature, the addition of oxygen reduces the NO removal rate in case of dielectric barrier discharge. This is in contradiction to what was observed in the experiments conducted in this study. Tas (1995) also observed that for an initial concentration of 1200 ppm, the NO removal decreased with an increase in the oxygen composition on the feed gas.

The NO<sub>2</sub> concentration profiles are shown in Figure 16. The NO<sub>2</sub> concentration increased with residence time for all voltages at short residence times. The NO<sub>2</sub> profiles at 40 and 50 kV go through maxima and the concentrations decrease slightly at longer residence times. NO<sub>2</sub> concentration profiles at 30 and 35 kV increase steadily with residence time. Unlike the NO<sub>2</sub> profile in the case of NO removal in nitrogen, the removal of NO<sub>2</sub> in dry air was not observed at longer residence times and at high voltages.

The results indicate that most of the NO was converted into NO<sub>2</sub> at the tested voltages and

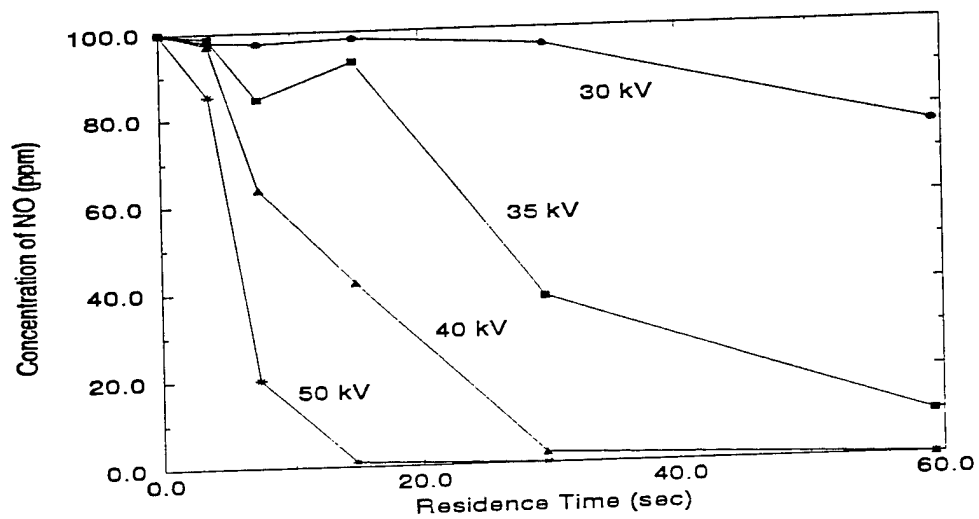


Figure 15 NO Concentration Profile in an Atmosphere of Dry Air

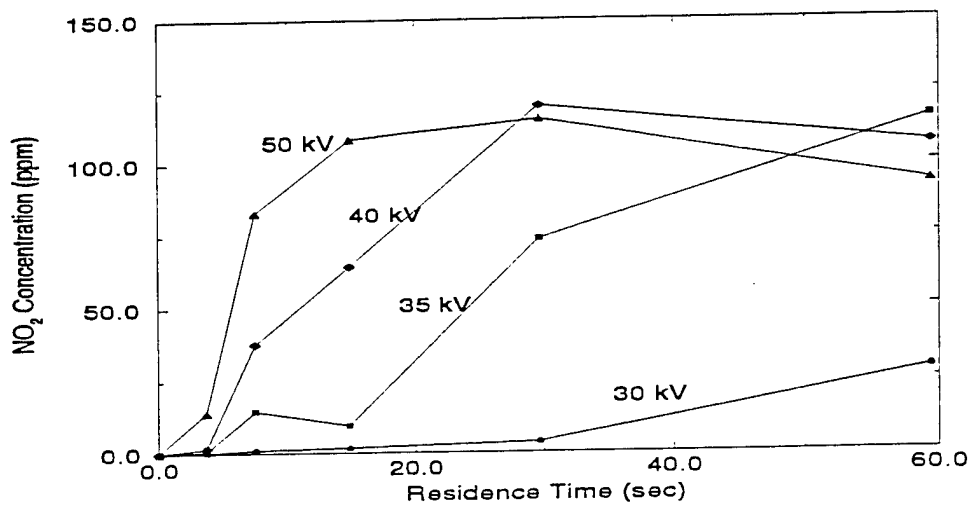


Figure 16 NO<sub>2</sub> Concentration Profile in an Atmosphere of Dry Air

residence times. Total  $\text{NO}_x$  was higher than the initial NO concentration at 14.5 and 29.0 seconds residence time and at 50 kV. This indicated that there was  $\text{NO}_x$  formation from the dry air itself during the discharge. To confirm this, an experiment to consider the formation of NO and  $\text{NO}_2$  in the pulsed corona discharge in dry air was conducted. It was observed that at 60 seconds residence time and at an applied voltage of 50 kV, the formation of  $\text{NO}_2$  was 10 ppm. Tokunaga et al. (1984) also noticed an increase in the total  $\text{NO}_x$  concentration when the initial concentration of NO was around 50-100 ppm. For an initial concentration of 100 ppm of NO, the  $\text{NO}_x$  concentration at a dose rate of 5 Mrad was 120 ppm, and it was found to increase with dose rate for a gas composition of 3% oxygen in an atmosphere of nitrogen.

A measurement of  $\text{N}_2\text{O}$  was made for the 44.0 second residence time experiment at 50 kV, and the concentration was found to be 17 ppm. The measurement was made by a GC/MS analysis of the gas sample coming out of the outlet of the reactor.

For the case of NO removal in dry air, the two unknown rate constants corresponding to the nitrogen and oxygen dissociation were obtained by fitting the model profiles with the experimental data for NO and  $\text{NO}_2$ . The model profiles of NO,  $\text{NO}_2$ ,  $\text{N}_2\text{O}$ , and  $\text{O}_3$  are shown in Figure 17 for the treatment cases at 50 kV. NO removal corresponded with  $\text{NO}_2$  formation at shorter residence times, and at the longer residence times the  $\text{NO}_2$  concentration leveled out at 80% of the initial NO. The  $\text{O}_3$  concentration increased only after a significant lag time where the NO concentration decreased. This is due to the fact that in the presence of NO, the amount of ozone formation due to oxygen radicals reacting with oxygen molecules is very small when compared to oxygen radicals reacting with NO to produce  $\text{NO}_2$ . Once the NO molecules were removed, ozone formation was unhindered and the slope of the ozone concentration as a function of residence time started increasing. The  $\text{N}_2\text{O}$  concentration as predicted by the model for a residence time of 44.0 seconds at 50 kV is around 15 ppm which matches well with the experimentally observed value. This is a significant observation since  $\text{N}_2\text{O}$  data was not used in fitting the model, i.e., the  $\text{N}_2\text{O}$  measurement provides an independent check of the model. In case of  $\text{NO}_2$ , however, there was around 20% deviation between the model profile and the experimental values at 50 kV.

The model profile for NO and the experimental points used to fit the model are shown in Figure 18. As seen in the figure, there is a deviation between the experimental points and the model

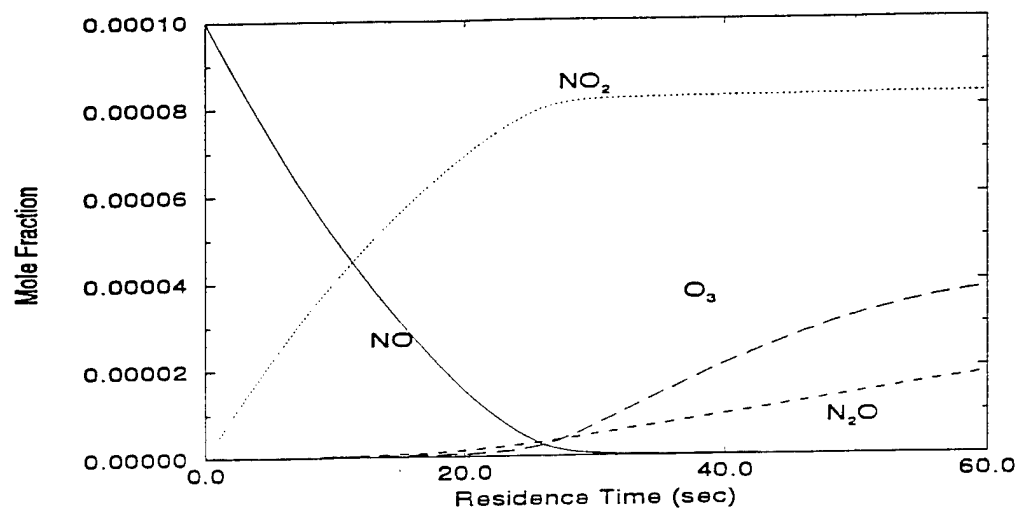


Figure 17 Model Profile of Different Species in an Atmosphere of Dry Air

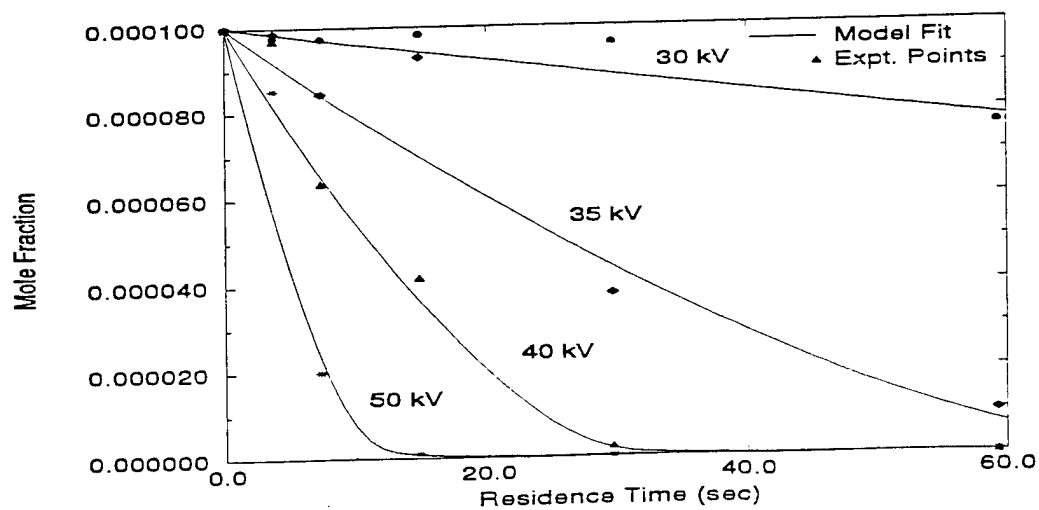


Figure 18 Model Fit for NO Concentration Profile in an Atmosphere of Dry Air

at short residence time (3.6 seconds). One reason for this behavior could be that at short residence time, the flow pattern in the reactor was highly turbulent and hence the reactor would operate more like a well-mixed reactor than as a plug-flow reactor. The model profile for NO fits well with the experimental points at longer residence times.

The main reaction mechanisms for the removal of NO in an atmosphere of dry air was through the oxidation of NO to NO<sub>2</sub> and the main reactions in addition to Reactions 11 to 14 are:



Reaction 15 produces the necessary oxygen radicals required for the oxidation of NO. Reaction 11 converts the NO to NO<sub>2</sub> and Reaction 13 converts the NO<sub>2</sub> formed into N<sub>2</sub>O. The ozone formation was significant once the NO molecules are removed and Reaction 16 is the corresponding reaction pathway.

The rate constants obtained for nitrogen and oxygen dissociation as a function of applied voltage are shown in Figure 19. The slope for the oxygen dissociation is higher than that for nitrogen dissociation in air. The nitrogen dissociation rate constant in dry air was not the same as in the case of a pure nitrogen feed gas. The rate constant was 0.0475 s<sup>-1</sup> in an atmosphere of nitrogen at 50 kV but in dry air the rate constant was reduced to 0.03 s<sup>-1</sup> at the corresponding voltage. The presence of electronegative gas such as oxygen is known to have an effect on the nitrogen dissociation (Chang et al., 1992).

The differences in the rate constants for nitrogen and oxygen dissociation in dry air are functions of the applied voltage. At low voltage (30 kV) the rate constants are almost equal (approximately .01 s<sup>-1</sup>) and at the high voltage (50 kV) the rate constants are 0.025 s<sup>-1</sup> for nitrogen dissociation and 0.25 s<sup>-1</sup> for oxygen dissociation. This factor of ten difference is significantly smaller than theoretical studies (Penetrante et al., 1995) where it is predicted that the G-values for oxygen



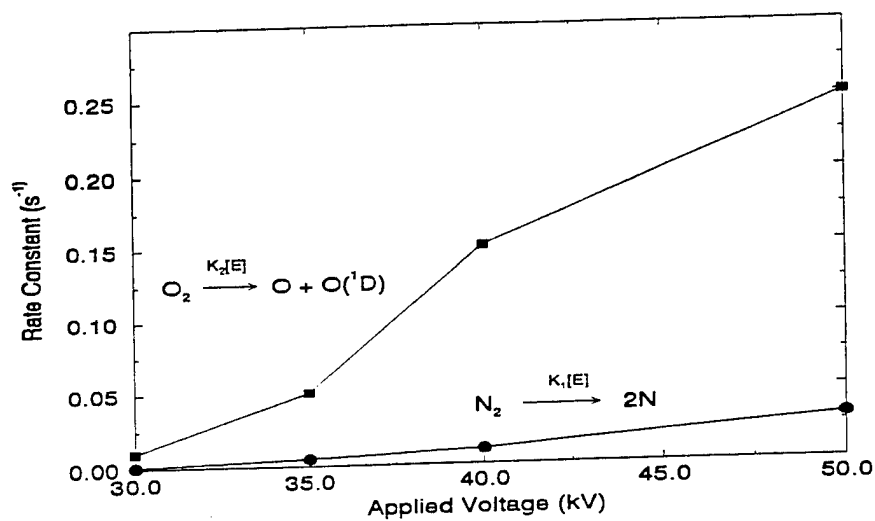


Figure 19 Rate Constants of Nitrogen and Oxygen Dissociation as a Function of Applied Voltage in an Atmosphere of Dry Air

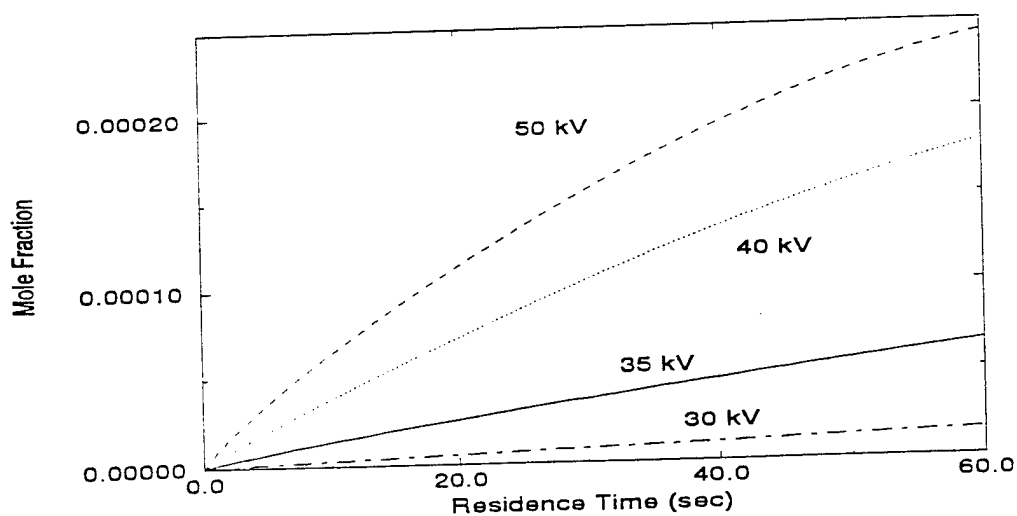


Figure 20  $O_3$  Concentration Profile Predicted by the Model

and nitrogen dissociation would differ by about 600 times. It should also be noted that these theoretical studies also do not predict a field dependence as seen in our work.

Tokunaga et al. (1984) conducted experiments for NO removal in a dry mixture of nitrogen and oxygen ( $N_2$  97%,  $O_2$  3%) using an electron beam, and they concluded that for high initial concentrations of NO and at high dose rate, the ratio of the final concentrations of NO and  $NO_2$  after the treatment were given by the empirical relation of Equation 1. Tas (1995) also considered the removal of NO from dry air and concluded that the empirical relation holds true. However, experiments and modeling conducted in the present work do not follow the empirical relation suggested by Tokunaga et al (1984). That relation holds true only for cases in which the initial concentration of NO was very high (500-1000 ppm). Penetrante (1993) considered modeling the concentration profiles of NO and  $NO_2$  in an atmosphere of dry air at room temperature, and he concluded that for an initial concentration of 400 ppm of  $NO_2$ , 50% of the initial NO was converted into  $NO_2$ , which was later again converted to  $N_2O$  and  $N_2$ . In that study, the model prediction for an initial concentration of 100 ppm is 80% conversion of the initial NO to  $NO_2$  and 20 ppm  $N_2O$  formation.

#### **D. OZONE FORMATION IN DRY AIR**

The formation of ozone in dry air with pulsed streamer corona treatment was considered at 50 kV and with a residence time of 44.0 seconds. Measurements by the KI solution method gave ozone concentration under these conditions of approximately 670 ppm. The amount of ozone predicted by the model is shown in Figure 20. The model predicts 200 ppmv of ozone to be produced at a gas residence time of 44.0 seconds and at 50 kV, whereas the value observed in the experiment was 670 ppm. Further refinement of the model to account for this variation is under development and more extensive measurements of ozone concentration under a wider range of conditions is being performed. It should be noted that the KI solution gives a fairly accurate measurement of ozone level and that the thesis of Mr. Kalyana reported measurements of up to 1200 parts per million as measured by a commercial ozone monitor. This level of ozone is too low to be accurately measured by the ozone monitor according to the manufacturer's specifications.

## E. NO REMOVAL IN HUMID AIR

Water vapor is present in concentrations of up to 5% by mole in the exhaust gases produced by the combustion of fossil fuels or from jet cell engines (Spicer et al., 1992). The hydroxyl radicals produced from the pulsed corona-induced dissociation of water molecules react with  $\text{NO}_2$  to form  $\text{HNO}_3$ .

Experiments were conducted in order to test the removal of NO in humid air. The feed air was humidified by passing it through a humidifier bringing the water content to 83% relative humidity at 18 °C. This corresponds to 1.5% of gas composition by volume. As in previous experiments the voltage was varied at different residence times (7.2, 14.5, 29.0, and 44.0 seconds), and the NO and  $\text{NO}_2$  outlet concentrations from the reactor were monitored.

Figure 21 shows the concentration profile of NO as a function of residence time for different dial voltages. When compared with Figure 15 corresponding to NO removal in dry air, the amount of NO removal for the operating voltages of 35, 40, and 50 kV in humid air was less than that of dry air. At an operating voltage of 50 kV, 80% removal of NO was observed at a residence time of 7.2 seconds in dry air. In the presence of water at the same operating conditions, 75% removal of NO was observed. Hence the addition of water did not enhance the NO removal. However, with dielectric discharge, Chang et al. (1992) reported an increase in the removal efficiency of NO with the addition of water for an initial concentration of 250 ppmv of NO.

Figure 22 shows the concentration profiles of  $\text{NO}_2$  as functions of residence time and operating dial voltage. The  $\text{NO}_2$  concentration undergoes a maximum at about 14.5 seconds residence time for 35 and 40 kV. The maximum for 50 kV was at 7.2 seconds while the 30 kV profile had a steady increase in the concentration. The concentration of  $\text{NO}_2$  was less than 5 ppm for all the voltages at a residence time of 44.0 seconds. The maximum concentration of  $\text{NO}_2$  attained was 22 ppm for the case of 50 kV. Around 95% removal of total  $\text{NO}_x$  was observed for 40 and 50 kV voltages at a gas residence time of 44.0 seconds. Thus, with the addition of water, the  $\text{NO}_2$  concentration decreased significantly. The  $\text{NO}_2$  concentration was 2.5 ppm at 50 kV at a residence time of 29.0 seconds in the case of humid air compared to 86.4 ppm in the case of dry air at corresponding conditions.

In order to measure the possible formation of  $\text{HNO}_3$  from  $\text{NO}_2$ , the exhaust gases from the

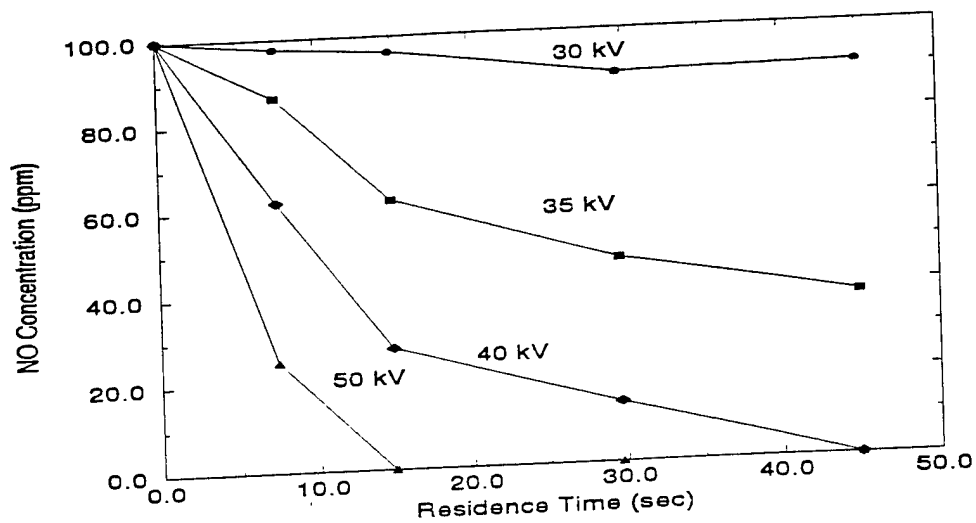


Figure 21 : NO Concentration Profile in an Atmosphere of Humid Air

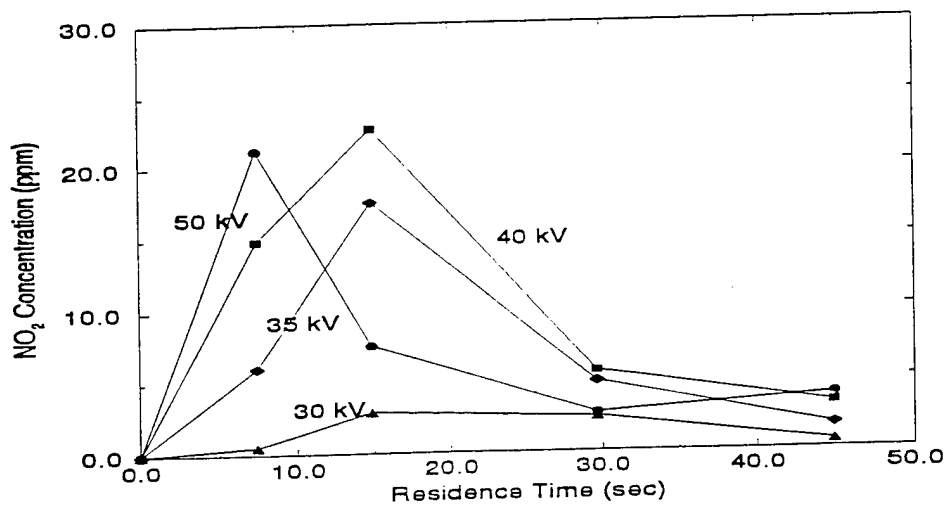


Figure 22 : NO<sub>2</sub> Concentration Profile in an Atmosphere of Humid Air

reactor were sparged through de-ionized water. The operating voltage was 50 kV and the gas residence time was 44.0 seconds. The liquid sample was then analyzed for nitrate by ion chromatography. The concentration of  $\text{NO}_3^-$  in the sample was 900 ppb by weight which corresponds to 1.64 ppmv of  $\text{HNO}_3$  in the gas sample. The amount measured as nitrates is significantly lower when compared with the removal of  $\text{NO}_2$ .

The important reactions which are responsible for the reduced concentration of NO, are:



The model profiles of NO,  $\text{NO}_2$ ,  $\text{HNO}_2$ , and  $\text{HNO}_3$  are shown in Figure 23 corresponding to pulsed voltages of 50 kV. The number of chemical reactions considered to model the reactions taking place in the presence of water in the system was 74. The  $\text{NO}_2$  profile undergoes a maximum concentration of 50 ppm at 16 seconds residence time. The model predicts up to 35% conversion of initial NO to  $\text{HNO}_3$ .  $\text{HNO}_2$  is an important intermediate product and is an important route for NO removal. The nitric acid produced tends to form aerosols. Future work should consider the study of aerosol formation.

Figure 24 shows the NO model profile versus the experimental data used to fit the model for calculating the rate constant for water dissociation. As the graph shows, the model matches the experimental points at short residence times, but deviates from it at longer residence times. In calculating the rate constant for the water molecule dissociation, an assumption has been made that the rate constants for oxygen and nitrogen dissociation were not affected by the addition of water. That may possibly explain some of the deviation of the model from the experimental points.

The maximum concentration of  $\text{NO}_2$  as observed in the experiments was around 20 ppm for the case of 50 kV pulsed voltage while the model predicts a maximum of 50 ppm. The  $\text{NO}_2$

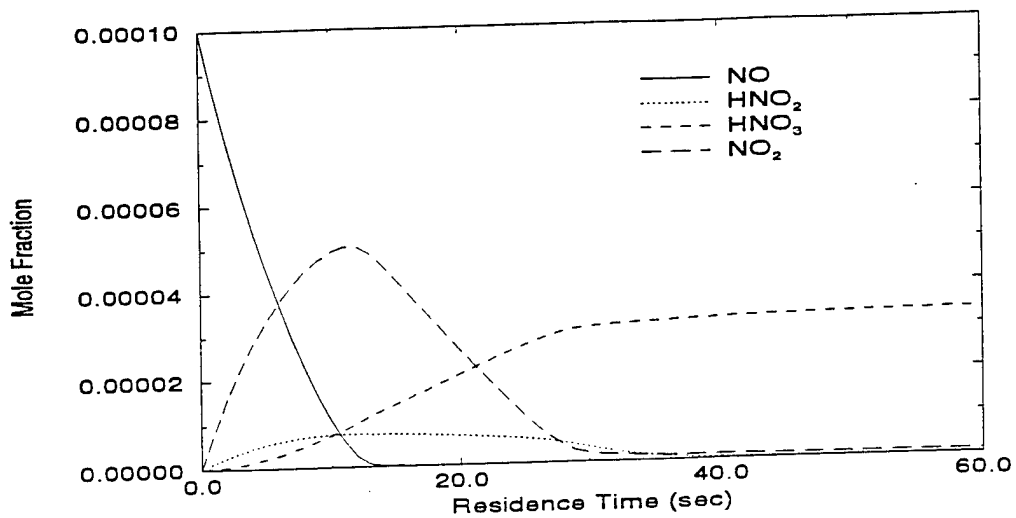


Figure 23 Model Profile of Different Species in an Atmosphere of Humid Air

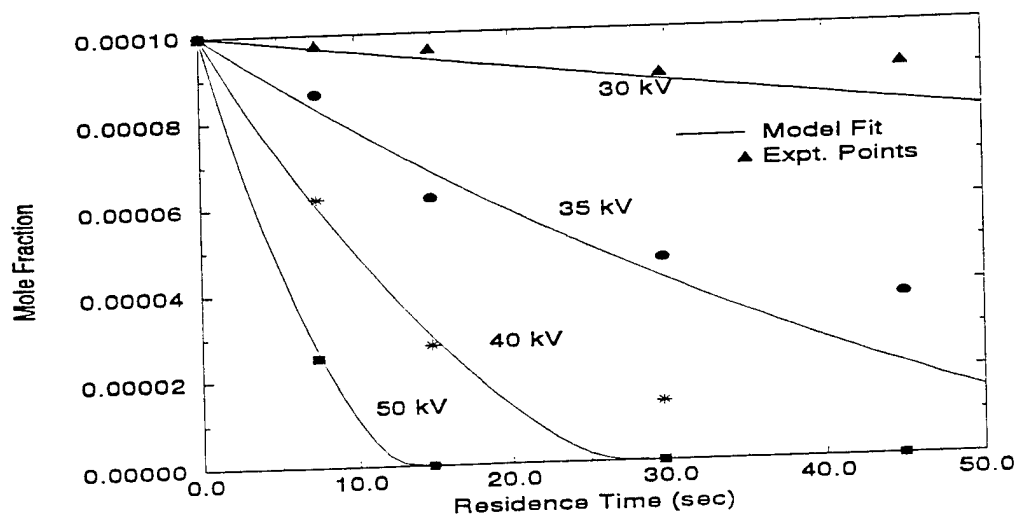


Figure 24 Model Fit for NO Removal in an Atmosphere of Humid Air

concentration profile predicted by the model for various voltages is shown in Figure 25. From Figure 25, the NO<sub>2</sub> concentration for the cases of 40 and 50 kV goes through a maximum, while in the cases of 30 and 35 kV there is a steady increase in the concentration of NO<sub>2</sub>. But the experimental data shown in Figure 22 indicate that at all of the voltages except 30 kV, the NO<sub>2</sub> concentration goes through a maximum.

The kinetic rate constant for the water dissociation obtained by fitting the model with the experimental data is shown in Figure 26 as a function of operating dial voltage. The rate constant increases monotonically with the applied voltage. Tokunaga et al. (1984), Chang et al. (1992), and Tas (1995) observed that the addition of water enhances the NO removal as well. But in this study the addition of water did not enhance the NO removal. One of the reasons is that at high concentrations of initial NO and NO<sub>2</sub> (~ 1000 ppm) in dry air, the final concentrations of NO and NO<sub>2</sub> come to equilibrium as suggested by the empirical relation given by Equation 1. With the addition of water, NO<sub>2</sub> removal takes place due to the formation of HNO<sub>3</sub> from NO<sub>2</sub>. Since there is a decrease in the NO<sub>2</sub> level, the corresponding equilibrium concentration of NO also decreases according to the Equation 1. Hence the enhanced removal of NO noticed in the presence of water is not due to the direct reaction of NO with the hydroxyl radicals. However, the experiments conducted in this study indicate that the empirical Equation 1 does not hold when the initial concentration of NO is low (~100 ppm).

## F. THE EFFECT OF CO ON NO REMOVAL IN HUMID AIR

Carbon monoxide is one of the important constituents of combustion gases. The addition of 500 ppm of CO to humid air was studied to consider NO removal under these conditions. Tokunaga et al. (1984) showed that the addition of CO enhanced NO removal due to the production of HO<sub>2</sub> radicals by the following reaction mechanism:



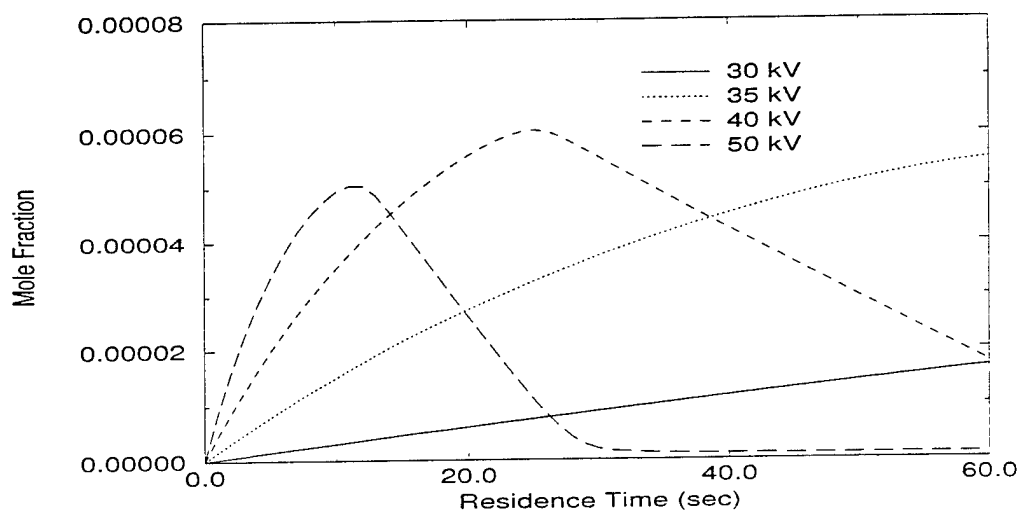


Figure 25 : NO<sub>2</sub> Model Profile in an Atmosphere of Humid Air

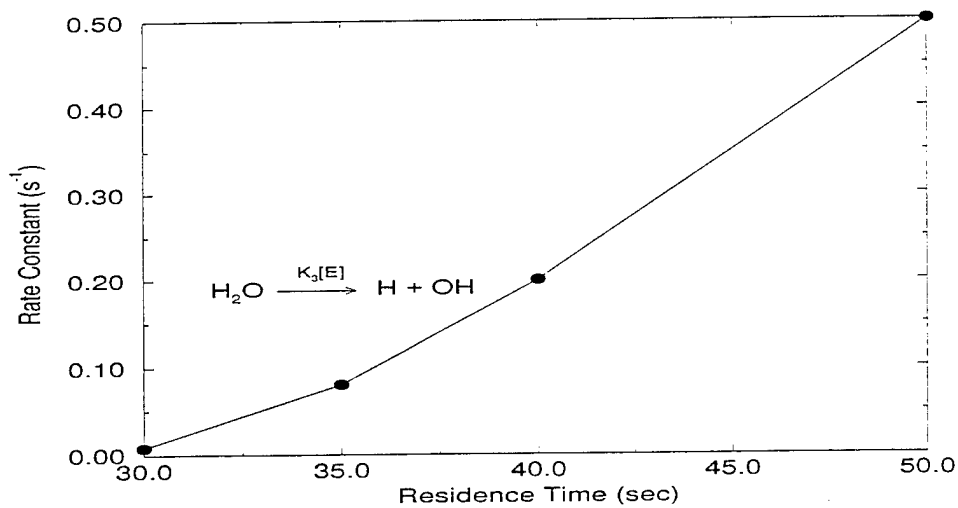


Figure 26 : Rate Constants of Water Dissociation as a Function of Applied Voltage in an Atmosphere of Humid Air





Experiments to determine NO removal with the addition of CO were performed at different voltages (30, 35, 40, and 50 kV) and at different gas residence times (7.2, 14.5, 29.0, and 44.0 seconds). The inlet concentration of CO was maintained at 500 ppm. The concentration of NO and NO<sub>2</sub> as a function of residence time for different operating voltages are shown in Figures 27 and 28, respectively. Comparing the concentration profiles of NO removal without CO (Figure 21) and with CO (Figure 27), CO did not have any effect on the NO removal. The NO concentrations at 7.2 seconds residence time were 62.6 ppm and 29.5 ppm at 40 and 50 kV, respectively, in the presence of CO. In the absence of CO in the system (see Figure 21) the NO concentration at these voltages for the same residence time were 62.0 and 25.6 ppm.

Figures 22 and 28 can be compared for NO<sub>2</sub> concentration profiles to conclude that the presence of CO at 500 ppm does not affect the NO<sub>2</sub> profile. The NO<sub>2</sub> concentrations at 7.2 seconds residence time were 16.6 and 24.9 ppm for 40 and 50 kV, respectively, with the presence of CO in the system. The corresponding NO<sub>2</sub> concentrations in the absence of CO in the system at 7.2 seconds residence time was 14.8 and 21.8 ppm for the cases of 40 and 50 kV. The amount of CO added might be too small to provide a significant increase in the NO removal. The minimum concentration with which Tokunaga et al. (1984) observed any change in the NO removal was 0.29% (2900 ppm) of CO.

The kinetic model profiles of NO, NO<sub>2</sub>, and HNO<sub>3</sub> for NO removal in humid air in the presence CO for the case of 50 kV are shown in Figure 29. To analyze the concentration profile in this case, Equation 20 was considered. The model profile obtained in this case is very similar to the

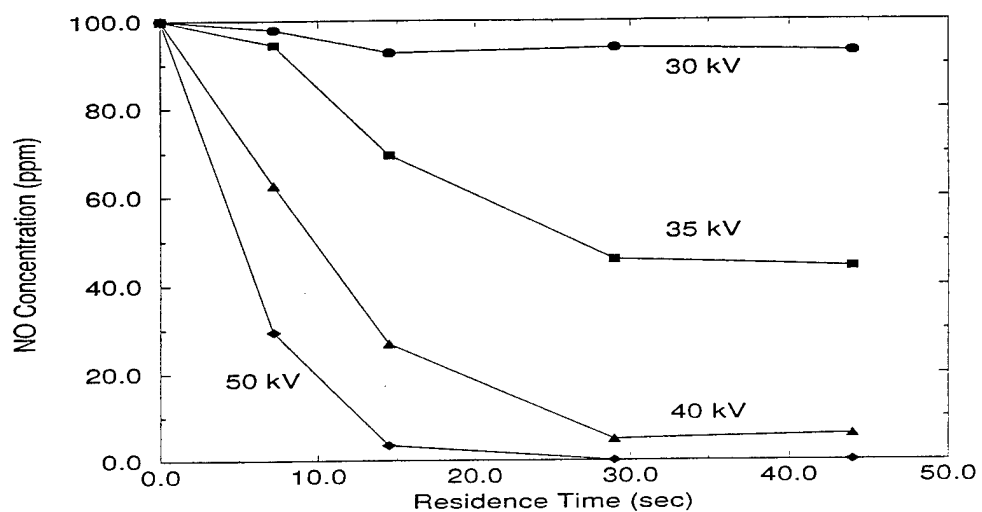


Figure 27 : NO Concentration Profile in an Atmosphere of Humid Air and CO

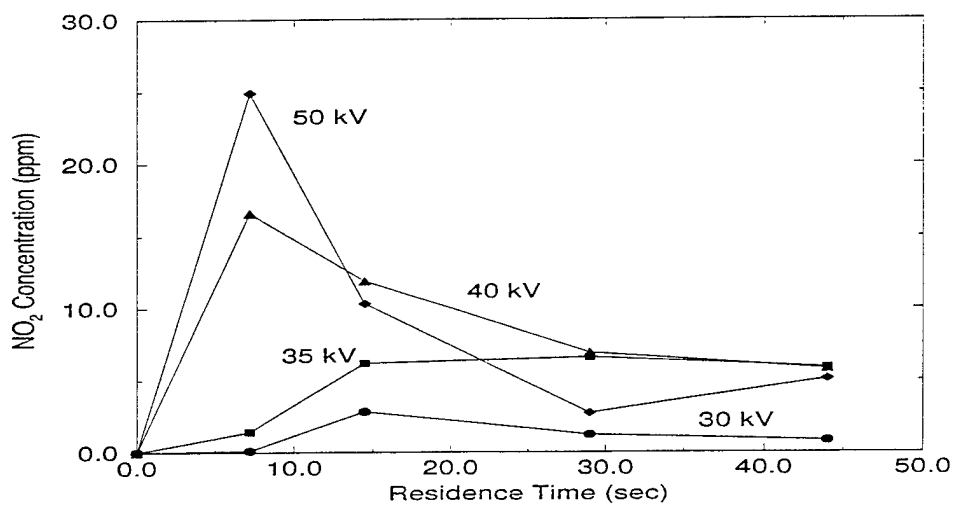


Figure 28 : NO<sub>2</sub> Concentration Profile in an Atmosphere of Humid Air and CO

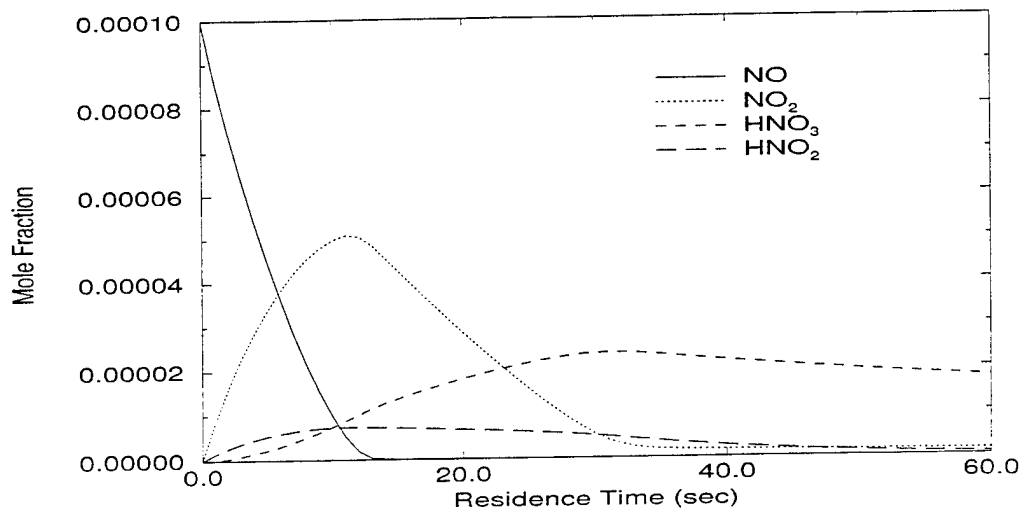


Figure 29 Model Profile of Different Species in the Presence of 500 ppm of CO in Humid Air

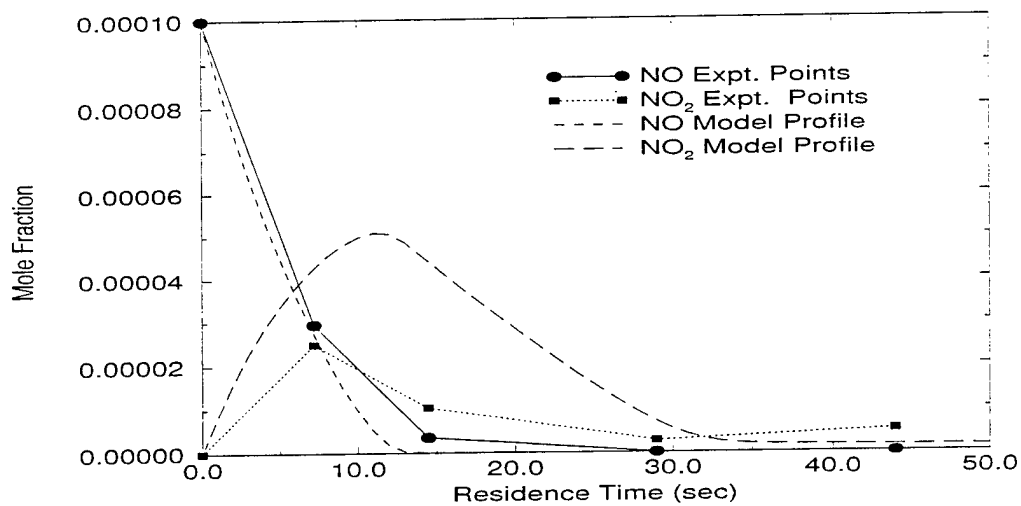


Figure 30 Comparison of the Model Prediction of NO and NO<sub>2</sub> Profile with Experimental Data in Case of NO Removal in the Presence of 500 ppm of CO in Humid Air

model profiles obtained in the case of NO removal in humid air (see Figure 23). The addition of a single reaction of carbon monoxide does not significantly affect the species concentration profiles at this initial CO concentration.

Figure 30 compares the NO and NO<sub>2</sub> profiles in the presence of CO predicted by the model to the experimental points. As seen in the figure, the profile of NO matches well with the experimental points. The NO<sub>2</sub> profile of the model qualitatively matches the experimental points but the values are significantly different. The maximum concentration predicted by the model is around 50 ppm whereas the maximum observed concentration of NO<sub>2</sub> was around 22 ppm. The addition of high concentrations of CO (> 0.5%) to consider the removal of NO may be considered for future work.

### **G. NO REMOVAL FROM AIR IN THE PRESENCE OF ETHYLENE**

The atmospheric chemistry of NO<sub>x</sub> and hydrocarbons has been well characterized by Atkinson et al. (1984), Seinfeld (1986), and Grosjean et al. (1996). The reactions of ethylene in the atmosphere with hydroxyl radicals, ozone, and dissociated oxygen may also be applicable in the pulsed streamer corona reactor.

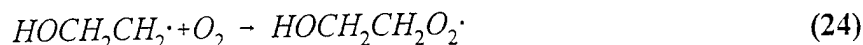
Mizuno et al. (1993) considered the effect of hydrocarbons on the removal efficiency of NO<sub>x</sub> from the exhaust of a diesel engine. They observed that at a gas temperature of 30°C the NO<sub>x</sub> removal efficiency was 22% for an input power of 37.5 W. With the addition of 500 ppm of ethylene, a rapid increase in the NO<sub>x</sub> removal rate (60% for an input power of 35 W) was observed. Among the additives considered, ethylene had the greatest effect on the removal efficiency of NO<sub>x</sub> compared with other additives such as methane and propane.

Vogtlin and Penetrante (1993) conducted experiments on the removal of NO<sub>x</sub> in the presence of hydrocarbon additives such as ethylene and octane at high gas temperatures of 100 to 200°C. Octane was the hydrocarbon used as an additive at a concentration ranging from 0.8 to 8 times the initial NO<sub>x</sub> concentration. At a ratio of 8:1, 93.75% of the initial NO was removed and 45.5% of the initial NO<sub>x</sub> was removed at an energy cost of 29 eV per NO<sub>x</sub> molecule removed. When the molar ratio was lowered to 4:1 for a gas composition of 5% O<sub>2</sub>, 10% H<sub>2</sub>O, 15% CO<sub>2</sub>, and 70% N<sub>2</sub> (flue gas composition), almost 100% NO was removed and 45% of NO<sub>x</sub> was removed at an energy consumption of 80 eV per removed NO<sub>x</sub> molecule. No byproducts identification was made during

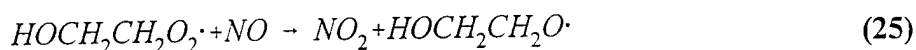
the study. The hydrocarbon additives were found to be recycling the hydroxyl radicals during the oxidation and reduction of NO. Hence, the efficiency of a particular hydrocarbon was therefore limited by the reaction rate of this hydrocarbon with hydroxyl radicals.

Wolf et al. (1996) also considered the effects of hydrocarbons on NO<sub>x</sub> removal in a dielectric barrier discharge reactor. They found that the addition of 500 ppm, 1000 ppm, and 2000 ppm ethylene greatly increased the removal of 500 ppm NO from humid gas containing 10% water, 77 % nitrogen, and 13 % oxygen. They observed only a small amount of ethylene decomposition under these conditions. They found similar effects for the addition of toluene.

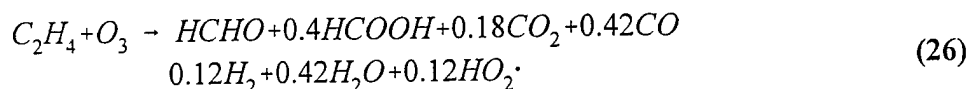
In the natural atmosphere, ethylene reacts primarily with hydroxyl radicals since the concentration of ozone and dissociated oxygen are very small. Hydroxyl radicals directly attack ethylene to produce peroxy radicals which further react with oxygen molecules through the following reactions:



NO is converted to NO<sub>2</sub> through the following reaction:



The HOCH<sub>2</sub>CH<sub>2</sub>O radical is known to react with oxygen to give glycolaldehyde (HOCH<sub>2</sub>CHO) and formaldehyde (CH<sub>2</sub>O). The formaldehyde produced in the above reactions can further react with hydroxyl radicals to produce hydroperoxy radicals. Direct reactions of ethylene with ozone also leads to the production of formaldehyde, formic acid, carbon dioxide, and carbon monoxide in the atmosphere (Seinfeld, 1986) through the reaction



Grosjean et al. (1996) studied the reactions of ozone with ethylene and found that under atmospheric conditions ethylene reacts with ozone to produce primarily (>99 %) formaldehyde with very trace amounts of glyoxal and cyclohexanone.

Ethylene also reacts with dissociated oxygen and hydrogen through the following reactions:



The radicals such as  $HCO \cdot$ ,  $CH_3 \cdot$ , and  $HOCH_2CH_2 \cdot$  react with  $NO$  and  $NO_2$  to form other products.

## DRY AIR

A series of  $NO_x$  removal experiments at different voltages (30, 35, 40, and 50 kV) and residence times (7.2, 14.5, 29.0, and 44.0 seconds) with 500 ppm of ethylene present in dry air was considered.

In dry air, the main reaction mechanism for ethylene breakdown was through reactions with oxygen radicals to produce other radicals such as  $HCO \cdot$ ,  $CH \cdot$ ,  $CH_2 \cdot$  and  $CH_2O \cdot$ . Figure 31 shows the

variation of NO concentration as a function of residence time for various operating voltages. As can be seen in the figure, the NO concentration quickly decreased at higher voltages. When Figures 15 and 31 are compared, it can be seen that the presence of ethylene greatly enhances NO removal. NO removal in the case of dry air and in the absence of ethylene at 7.2 seconds residence time and at an operating voltage of 50 kV was 80%. The addition of ethylene increases the removal efficiency to almost 100% at the same operating conditions. The  $\text{CH}_3\cdot$  and  $\text{HCO}\cdot$  radicals produced from ethylene breakdown react with NO, to form a variety of compounds such as  $\text{CH}_3\text{NO}\cdot$  and  $\text{HNO}\cdot$  thereby enhancing the NO removal. Also,  $\text{HCO}\cdot$  radicals increase the production of hydroperoxy radicals, which are known to enhance the NO removal:



Figure 32 shows the  $\text{NO}_2$  concentration profile as a function of residence time for various operating voltages.  $\text{NO}_2$  concentration increased monotonically with residence time for the lower voltages (30 & 35 kV), and at higher voltages (40 & 50 kV) the concentration passes through a maximum. At the highest voltage of 50 kV and at longest residence time of 44.0 seconds, 45% removal of  $\text{NO}_2$  is observed in the presence of 500 ppm of ethylene as compared to 5% removal of  $\text{NO}_2$  in dry air without ethylene. When Figures 16 and 32 are compared the  $\text{NO}_2$  concentration in the presence of ethylene (Figure 32) is significantly smaller at higher voltages (40 & 50 kV) and at longer residence times as compared to the profile in Figure 16 (no ethylene). The  $\text{HCO}\cdot$  radicals react with  $\text{NO}_2$  to form  $\text{HNO}_2$ . The  $\text{HCO}\cdot$  radicals also produce  $\cdot\text{OH}$  radicals by reaction with oxygen radicals. The corresponding reactions are:



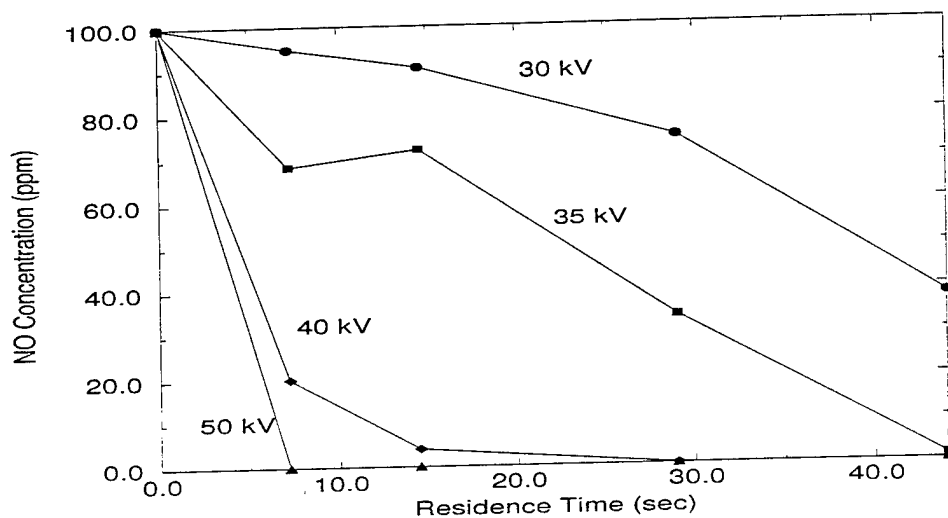


Figure 31 NO Concentration Profile in an Atmosphere of Dry Air and 500 ppm of Ethylene

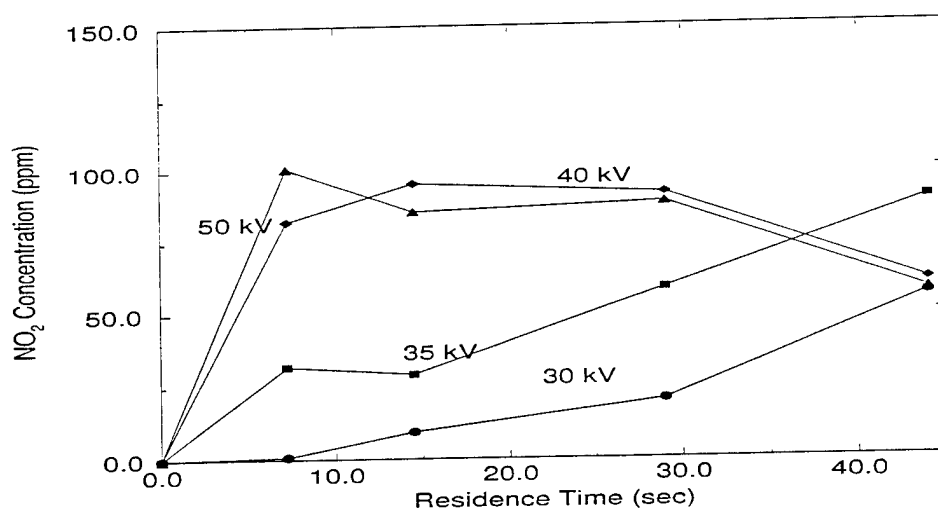


Figure 32 NO<sub>2</sub> Concentration Profile in an Atmosphere of Dry Air and 500 ppm of Ethylene



The hydroxyl radicals produced by Reaction 34 help in the breakdown of ethylene and also



in the removal of  $NO_2$ . Thus,  $HCO\cdot$  is a very important reactive radical which acts as a pathway for hydroxyl and hydroperoxy radicals and also acts as a source for the removal of  $NO_2$ . Some of the  $NO_2$  is also reduced by the methyl radicals to  $NO$ . But, the main reaction mechanism for the removal of  $NO_2$  is through conversion to  $HNO_2$ .

A list of additional reactions that are considered for modeling  $NO$  removal in the presence of ethylene is shown in Table 5. The model concentration profiles for various chemical species for the case of 50 kV are shown in Figures 33 and 34. Figure 33 shows the concentration profiles of  $NO$ ,  $NO_2$ ,  $HNO_2$ , and  $O_3$  as functions of residence time along with the experimental data of  $NO$  and  $NO_2$  for the case of 50 kV. The rate constants for the oxygen and nitrogen dissociation are assumed to be the same as those calculated from the  $NO$  experimental data for the dry air case. As shown in Figure 33 there is a significant formation of  $HNO_2$ , and the experimentally observed  $NO$  removal was faster than that predicted by the model. At a residence time of 7.2 seconds for an operating voltage of 50 kV, 70% removal of  $NO$  is predicted by the model as compared to 100% removal of  $NO$  found in the experiment. In addition, the model shows 10 ppm of  $NO_2$  for a voltage of 50 kV at a residence time of 29.0 seconds. The amount of  $NO_2$  corresponding to the experiment at the same operating conditions is 91.6 ppm. There is a significant difference between the model and the experiments in this case.

Figure 34 shows the main products expected from ethylene breakdown in the pulsed streamer corona reactor that were predicted by the model. The concentrations of  $CO$  and  $CH_2O$  increase steadily with residence time.

## HUMID AIR

A series of experiments at different voltages (30, 35, 40, and 50 kV) and residence times (7.2, 14.5, 29.0, and 44.0 seconds) was conducted to consider the effect of ethylene on  $NO$  removal in humid air. The presence of water leads to the corona-induced production of hydroxyl radicals which

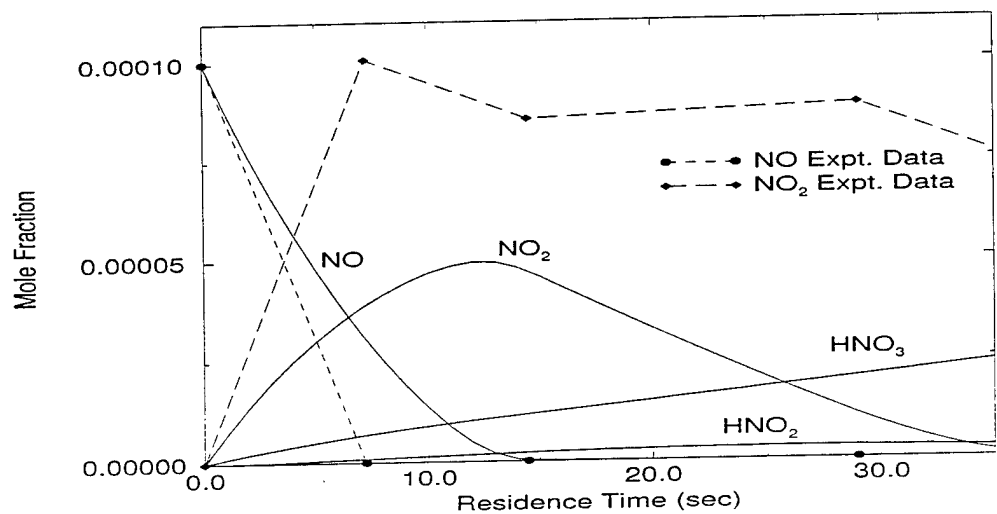


Figure 33 Concentration Profile of Different Species Predicted by the Model for NO Removal in the Presence of 500 ppm Ethylene in Dry Air With the Experimental Data

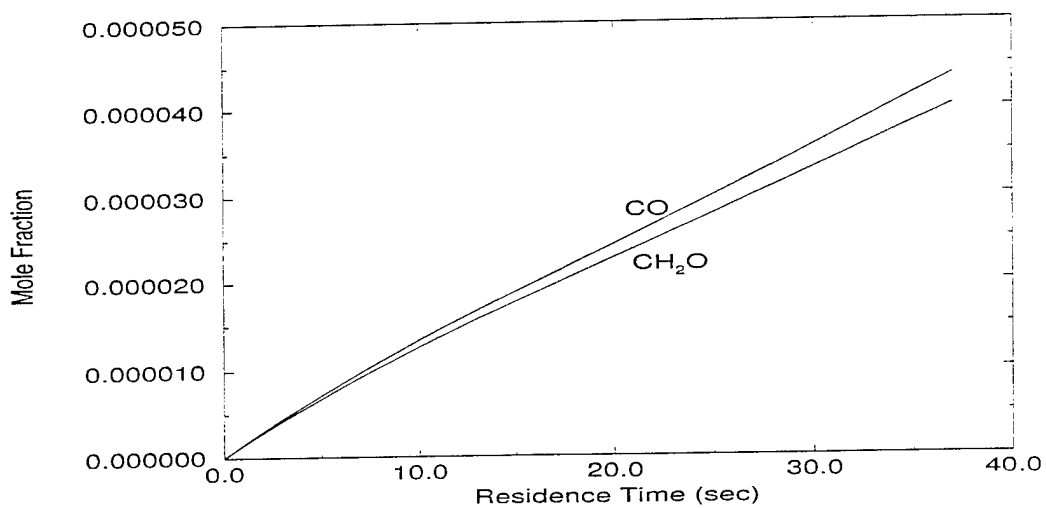


Figure 34 . Concentration Profile of Breakdown Products Predicted by the Model for NO Removal in Dry Air with 500 ppm Ethylene

should lead to more ethylene removal than that observed in dry air. Figure 35 shows the profiles for ethylene breakdown in the cases of dry and humid air as predicted by the model.

The concentration profiles of NO as a function of residence time in humid air with ethylene for various operating voltages are shown in Figure 36. The rate of NO removal is lower compared to the profile obtained for dry air with ethylene (Figure 31). The concentration of NO at 7.2 seconds residence time was 17 ppm in humid air as opposed to almost 0 ppm in the dry air (both with ethylene).

The concentration profiles of NO<sub>2</sub> in humid air with ethylene are shown in Figure 37. The NO<sub>2</sub> concentration profiles go through maxima similar to the NO<sub>2</sub> profiles in humid air without the presence of ethylene (Figure 25). The maximum concentration of NO<sub>2</sub> at 50 kV was about 24.4 ppm at a gas residence time of 7.2 seconds, which compares well with the NO<sub>2</sub> maximum concentration of 21.2 ppm in humid air without ethylene. Hence, ethylene does not significantly affect NO<sub>2</sub> removal in the presence of water. The model profiles indicate that the main breakdown product formed from NO<sub>2</sub> in the case of humid air and 500 ppm ethylene is HNO<sub>2</sub> as opposed to HNO<sub>3</sub> in humid air with no ethylene. More extensive experimental analysis of nitrite and nitrate products is needed to confirm this prediction.

The concentration profiles of NO, NO<sub>2</sub>, HNO<sub>2</sub>, and HNO<sub>3</sub> in humid air with 500 ppm of ethylene predicted by the model are shown in Figure 38 along with the experimental data of NO and NO<sub>2</sub>. The model profile of NO matches very well with the experimental data. The profile of NO<sub>2</sub> predicted by the model also qualitatively matches with the experimental data. The model concentration profiles of the main byproducts formed from ethylene breakdown such as glycolaldehyde (HOCH<sub>2</sub>CHO), formaldehyde (CH<sub>2</sub>O), and CO are shown in Figure 39. To calculate the profile, the rate constants for nitrogen, oxygen, and water dissociation have been assumed to be the same as that obtained for NO removal from humid air.

To confirm the validity of the model, a series of experiments to determine the byproducts formed by the dissociation of ethylene in dry air was conducted at 50 kV and at 44.0 seconds residence time. The gas sample analysis by GC/MS indicated the complete breakdown of ethylene. For 500 ppm ethylene one would expect 1000 ppm CO<sub>2</sub> if complete conversion were achieved; however, 130 ppm of CO<sub>2</sub> was observed thereby indicating only partial degradation. HPLC analysis

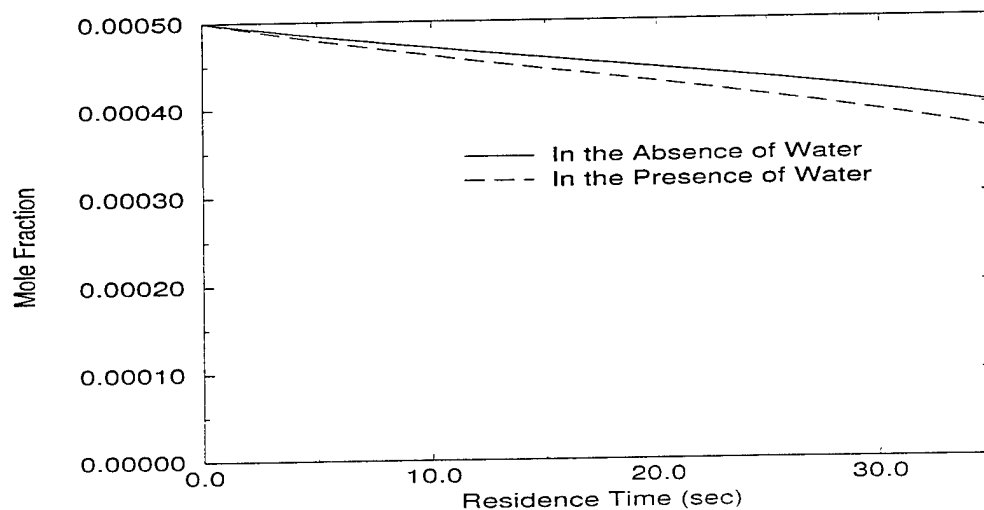


Figure 35 : Ethylene Model Profile With and Without the Presence of Water in Case of NO Removal from Air

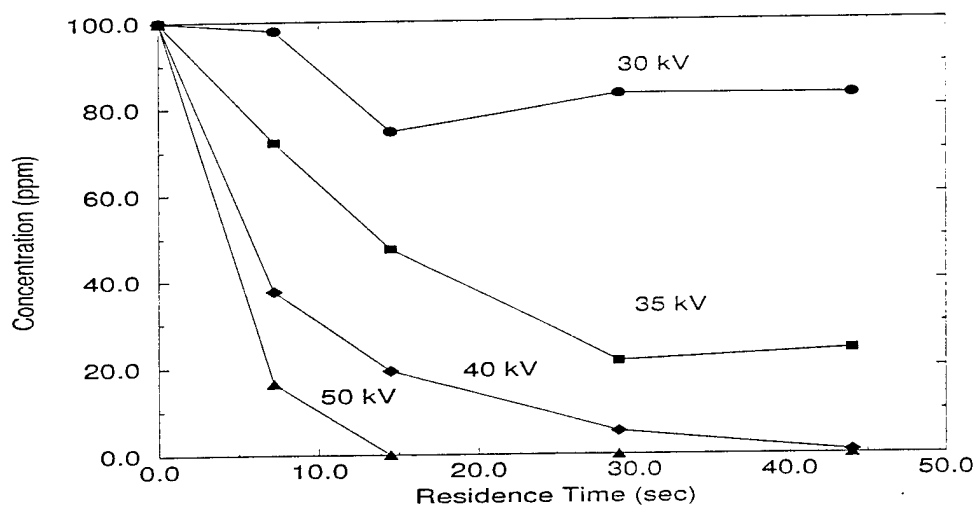


Figure 36 : NO Concentration Profile in an Atmosphere of Humid Air and 500 ppm of Ethylene

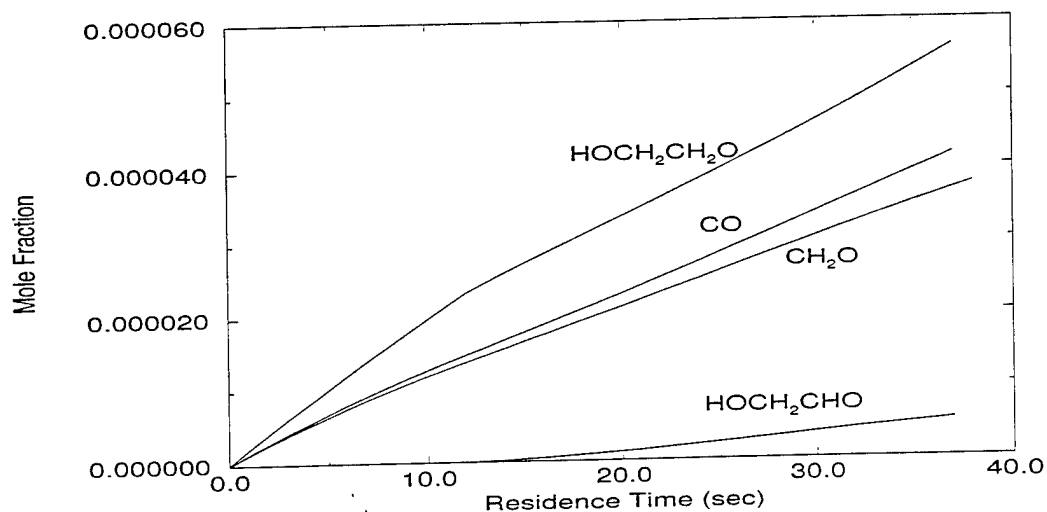


Figure 37 : Concentration Profile of Breakdown Products Predicted by the Model in Case of NO Removal in Humid Air with 500 ppm of Ethylene

Table 4 : Byproducts Predicted by the Model Due to Ethylene Breakdown

Name	Chemical Formula
Formaldehyde	CH <sub>2</sub> O
Formic Acid	HCOOH
Glycolaldehyde	HOCH <sub>2</sub> CHO
Acetaldehyde	CH <sub>3</sub> CHO
Ethylene Glycol	OHCH <sub>2</sub> CH <sub>2</sub> OH
Carbon Monoxide	CO
Carbon dioxide	CO <sub>2</sub>
Methyl Nitrate	CH <sub>3</sub> NO
Hydrogen Cyanide	HCN

of the liquid samples from dry air showed no peaks, however, analysis of humid air reactor samples showed four peaks (Figure 40). One of these peaks was positively identified to be formic acid. Mizuno et al. (1995) considered the removal of  $\text{NO}_x$  gases from dry air and found acetic acid to be an important byproduct. Acetic acid was not identified as one of the byproducts in the present analysis, nor is it predicted by any of the reaction mechanisms from the atmospheric chemistry literature. Table 5 shows the list of chemical compounds that could be formed from the ethylene removal.

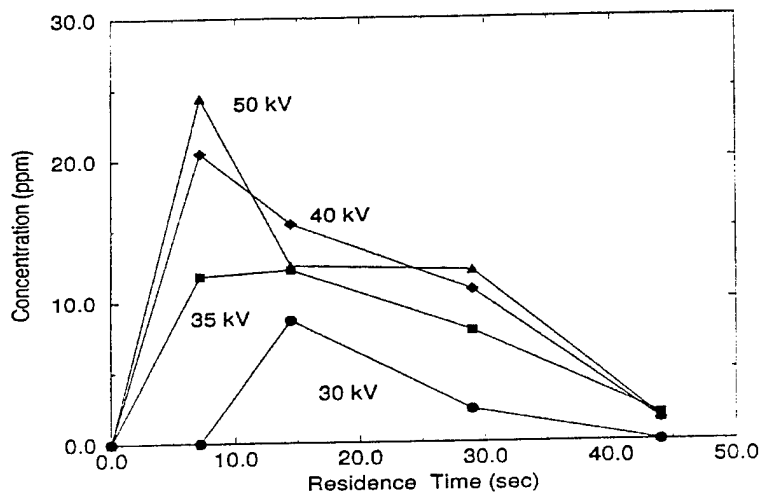


Figure 38  $\text{NO}_2$  Concentration Profiles in an Atmosphere of Humid Air and 500 ppm Ethylene.

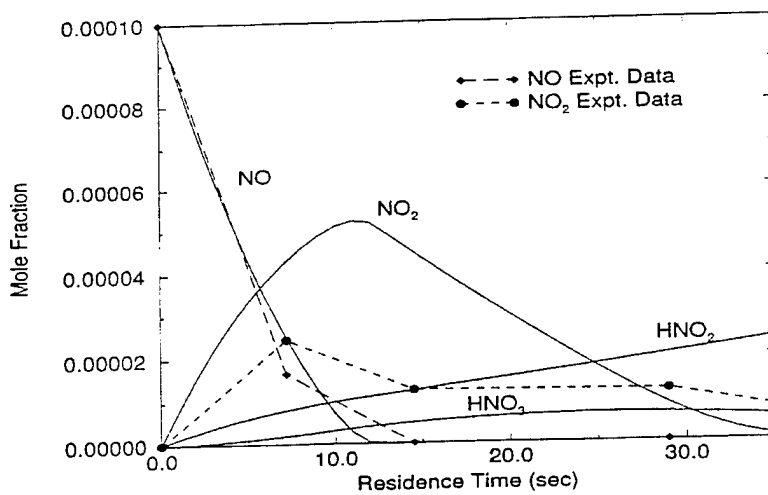


Figure 39 Concentration Profiles of Various Species Predicted by the Model in the Case of NO Removal in the Presence of 500 ppm Ethylene in Humid Air.

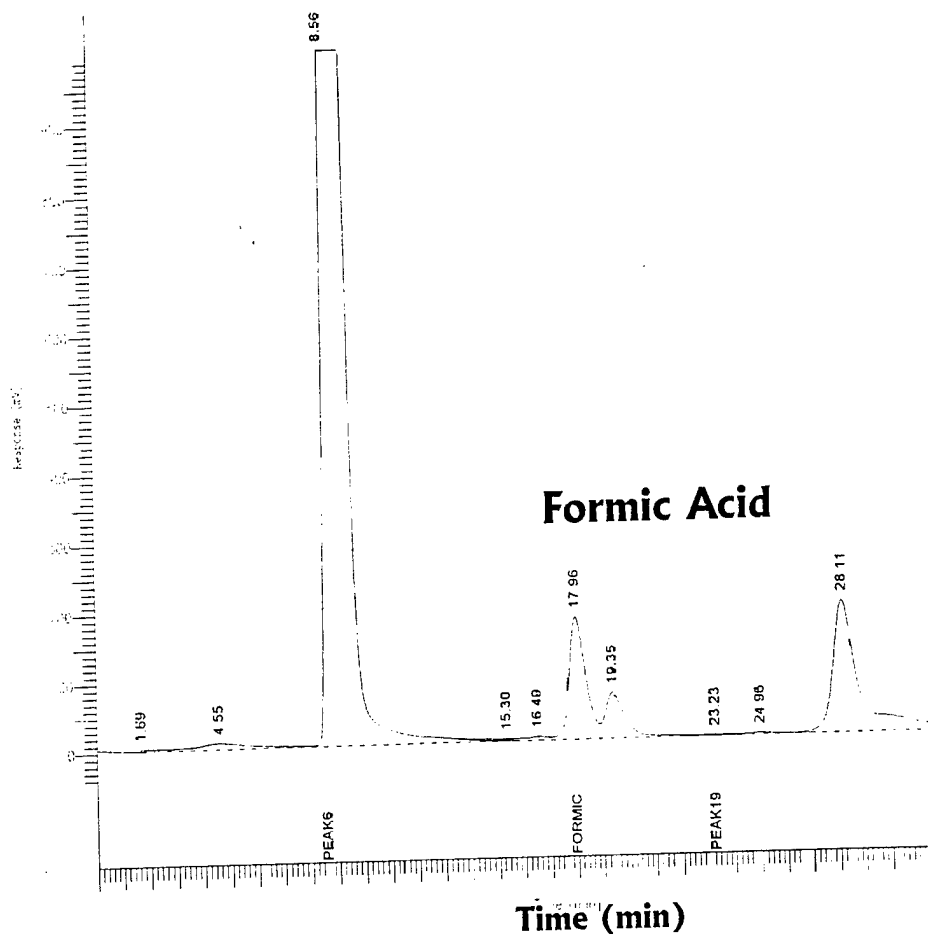


Figure 40. Chromatogram from HPLC Analysis of Gas Samples from Corona Experiment at 50 kV with NO, ethylene, and humid air



Table 5: Additional List of Chemical Reactions Considered for Modeling NO Removal in the Presence of Ethylene

Chemical Reactions	Rate Constants ( $cm^3.mole^{-1}.sec^{-1}$ )	Source
$C_2H_4 + O \cdot \longrightarrow CH_3 + HCO \cdot$	$4.39 \times 10^{11}$	NIST
$C_2H_4 + O \cdot \longrightarrow CH_2 + CH_2O$	$3.98 \times 10^{11}$	NIST
$C_2H_4 + O \cdot \longrightarrow H \cdot + CH_2CHO$	$3.76 \times 10^{11}$	NIST
$C_2H_4 + O \cdot \longrightarrow C_2H_3 + OH \cdot$	$1.46 \times 10^9$	NIST
$C_2H_4 + N \cdot \longrightarrow HCN + CH_3$	$9.93 \times 10^{10}$	NIST
$C_2H_4 + H \cdot \longrightarrow C_2H_5$	$6.88 \times 10^{11}$	NIST
$C_2H_4 + OH \cdot \longrightarrow C_2H_4OH \cdot$	$5.42 \times 10^{12}$	NIST
$HCO \cdot + CH_3 \longrightarrow CO + CH_4$	$1.21 \times 10^{14}$	NIST
$HCO \cdot + O \cdot \longrightarrow CO + OH \cdot$	$3.10 \times 10^{13}$	NIST
$HCO \cdot + O \cdot \longrightarrow H \cdot + CO_2$	$3.01 \times 10^{13}$	NIST
$HCO \cdot + OH \cdot \longrightarrow H_2O + CO$	$1.02 \times 10^{14}$	NIST
$HCO \cdot + O_2 \longrightarrow HO_2 + O \cdot$	$3.31 \times 10^{12}$	NIST
$HCO \cdot + NO_2 \longrightarrow CO + HNO_2$	$3.27 \times 10^{29}$	NIST
$HCO \cdot + NO \longrightarrow CO + HNO$	$7.23 \times 10^{12}$	NIST
$HCO \cdot + CH_3 \longrightarrow CH_3CHO$	$1.81 \times 10^{13}$	NIST
$C_2H_4OH \cdot + O_2 \longrightarrow HOCH_2CH_2O_2$	$1.81 \times 10^{12}$	NIST
$2HOCH_2CH_2O_2 \longrightarrow$		
$2HOCH_2CH_2O \cdot + O_2$	$5.0 \times 10^{11}$	NIST

*continued on next page*

continued from previous page		
Chemical Reactions	Rate Constants ( $\text{cm}^3.\text{mole}^{-1}.\text{sec}^{-1}$ )	Source
$2\text{HOCH}_2\text{CH}_2\text{O}_2 \longrightarrow$		
$\text{HOCH}_2\text{CH}_2\text{OH} + \text{HOCH}_2\text{CHO} + \text{O}_2$	$4.04 \times 10^{11}$	NIST
$\text{HOCH}_2\text{CH}_2\text{O}_2 + \text{NO}$		
$\longrightarrow \text{HOCH}_2\text{CH}_2\text{O} \cdot + \text{NO}_2$	$5.42 \times 10^{12}$	NIST
$\text{CH}_3 + \text{HO}_2 \longrightarrow \text{CH}_3\text{O} \cdot + \text{OH} \cdot$	$1.81 \times 10^{13}$	NIST
$\text{CH}_3 + \text{O} \cdot \longrightarrow \text{CH}_3\text{O}$	$1.58 \times 10^{10}$	NIST
$\text{CH}_3 + \text{O} \cdot \longrightarrow \text{H} \cdot + \text{CH}_2\text{O}$	$8.43 \times 10^{12}$	NIST
$\text{CH}_3 + \text{HO}_2 \longrightarrow \text{CH}_4 + \text{O}_2$	$3.61 \times 10^{12}$	NIST
$\text{CH}_3 + \text{NO} \longrightarrow \text{CH}_3\text{NO}$	$1.01 \times 10^{13}$	NIST
$\text{CH}_3 + \text{NO}_2 \longrightarrow \text{CH}_3\text{ONO}$	$7.00 \times 10^{10}$	NIST
$\text{CH}_3 + \text{NO}_2 \longrightarrow \text{CH}_3\text{O} \cdot + \text{NO}$	$1.39 \times 10^{13}$	NIST
$\text{CH}_2\text{O} + \text{O} \cdot \longrightarrow \text{OH} \cdot + \text{HCO} \cdot$	$1.01 \times 10^{11}$	NIST
$\text{CH}_2\text{O} + \text{OH} \cdot \longrightarrow \text{H}_2\text{O} + \text{HCO} \cdot$	$6.03 \times 10^{12}$	NIST
$\text{CH}_2\text{O} + \text{OH} \cdot \longrightarrow \text{HCOOH} + \text{H} \cdot$	$1.21 \times 10^{11}$	NIST
$\text{CH}_2 + \text{OH} \cdot \longrightarrow \text{CH}_2\text{O} + \text{H} \cdot$	$1.81 \times 10^{13}$	NIST
$\text{CH}_2 + \text{HCO} \cdot \longrightarrow \text{CH}_3 + \text{CO}$	$1.81 \times 10^{13}$	NIST
$\text{CH}_2\text{CHO} + \text{O}_2 \longrightarrow \text{CH}_2\text{O} + \text{CO} + \text{OH} \cdot$	$1.81 \times 10^{10}$	NIST
$\text{C}_2\text{H}_5 + \text{O} \cdot \longrightarrow \text{CH}_3\text{CHO} + \text{H} \cdot$	$8.02 \times 10^{13}$	NIST
$\text{C}_2\text{H}_5 + \text{HCO} \cdot \longrightarrow \text{C}_2\text{H}_5\text{CHO}$	$1.81 \times 10^{13}$	NIST
$\text{C}_2\text{H}_5 + \text{HCO} \cdot \longrightarrow \text{C}_2\text{H}_6 + \text{CO}$	$1.21 \times 10^{14}$	NIST
$\text{C}_2\text{H}_3 + \text{OH} \cdot \longrightarrow \text{CH}_3\text{CHO}$	$3.01 \times 10^{13}$	NIST
$\text{CH}_3\text{O} \cdot + \text{HCO} \cdot \longrightarrow \text{CH}_3\text{OH} + \text{CO}$	$9.04 \times 10^{13}$	NIST
continued on next page		

---

---

*continued from previous page*

---

Chemical Reactions	Rate Constants	Source
	( $\text{cm}^3.\text{mole}^{-1}.\text{sec}^{-1}$ )	
$H\cdot + CH_3OH \longrightarrow CH_2OH + H_2$	$8.39 \times 10^{12}$	NIST
$O\cdot + CH_3OH \longrightarrow OH\cdot + CH_2OH$	$4.87 \times 10^9$	NIST
$OH\cdot + CH_3OH \longrightarrow CH_2OH + H_2O$	$6.4 \times 10^{11}$	NIST
$CH_3O\cdot + CH_3OH \longrightarrow CH_3OH + CH_2OH$	$3.1 \times 10^8$	NIST
$NO_3 + CH_3OH \longrightarrow HNO_3 + CH_2OH$	$5.73 \times 10^6$	NIST
$CH_2OH + CH_2OH \longrightarrow HOCH_2CH_2OH$	$4.82 \times 10^{12}$	NIST

---

---

## SECTION V

### CONCLUSIONS

In the present study, it was shown that a pulsed streamer corona discharge can be used to remove  $\text{NO}_x$  from feed gases such as nitrogen and air containing small amounts of other gases such as water, carbon monoxide, and ethylene. A rotating spark gap pulsed power supply providing fast rise time, narrow width, repetitive high voltage pulses to a wire-cylinder geometry gas phase reactor vessel was constructed and employed in this study. Experiments varying the gas composition, the pulsed voltage value, and the gas residence time were performed to determine the NO and  $\text{NO}_2$  removal. The main reaction pathways for NO removal were identified for each of the gas compositions. A model was developed to calculate the concentration profiles of different chemical species under treatment by a pulsed streamer corona discharge. The reaction rate constants for the nitrogen, oxygen, and water molecule dissociations were obtained by fitting the experimental data of NO removal with the model.

Power input into the pulsed corona discharge reactor was calculated using the voltage and current measurements made during experiments with a fast oscilloscope and high voltage and current probes attached to the pulsed power input. The measured peak voltage was significantly higher than the applied voltage, and the pulse rise time varied from 15-30 nanoseconds as the applied voltage was increased from 30 to 50 kV. The pulse width at half maximum varied from 500 to 700 nanoseconds. The energy input varied from 8.0 mJ/pulse at 30 kV to 148 mJ/pulse at 50 kV in an atmosphere of dry air. The power input varied from 0.48 W to 8.88 W at the corresponding conditions.

Figure 41 shows the summary of NO concentration profiles in different atmospheres at a voltage of 50 kV, and Figure 42 shows the summary of the corresponding  $\text{NO}_2$  concentration profiles. As seen in Figure 41, NO removal in the presence of ethylene in dry air was the fastest. The addition of water did not enhance the NO removal. The concentration profiles of NO removal in humid air, in the presence of 500 ppm of CO in humid air, and in the presence of 500 ppm of ethylene in humid air almost match each other. The  $\text{NO}_2$  concentration profiles shown in Figure 42 indicate that in the presence of water,  $\text{NO}_2$  formation is significantly reduced compared to  $\text{NO}_2$

removal in dry air. The addition of ethylene to dry air enhanced the  $\text{NO}_x$  removal as shown in Figure 42. As was observed in the case of NO removal, the  $\text{NO}_2$  concentration profiles in the case of humid air, 500 ppm of CO in humid air, 500 ppm of ethylene in humid air matched each other well.

For the experimental case of pure nitrogen containing NO under pulsed corona treatment, NO was chemically reduced to  $\text{N}_2$ . About 99% removal of  $\text{NO}_x$  was observed at 50 kV pulsed voltage for a gas residence time of 44.0 seconds. The model profiles of NO and  $\text{NO}_2$  matched well with the experimental data, and the model indicated that there was a small amount of  $\text{N}_2\text{O}$  formation during the process.

In the experimental case of dry air containing NO, oxidation mechanisms dominate the reduction pathway and hence NO was converted to  $\text{NO}_2$ . Subsequent removal of  $\text{NO}_2$  was not observed under the current operating conditions (maximum of 50 kV pulsed voltage and 60.0 seconds residence time). The addition of oxygen in dry air as the feed gas increased the rate of NO removal. Chang et al. (1992) reported that in a dielectric barrier discharge system, the addition of oxygen decreased the rate of NO removal. The model developed in the present study predicted 80% conversion of the initial NO to  $\text{NO}_2$ , while the experimental value showed 95% conversion of NO to  $\text{NO}_2$  at 50 kV and at long residence time.

The rate constant for nitrogen dissociation was determined by fitting the model with the NO experimental data. The experiments, as well as the modeling results, match well with the results indicated in the non-thermal plasma treatment literature. The rate constants for nitrogen and oxygen dissociation were determined from the NO removal and the  $\text{NO}_2$  formation data. The reaction rate constant for nitrogen dissociation was found to be different from the value obtained in pure nitrogen. The rate constant was  $0.0475 \text{ s}^{-1}$  in an atmosphere of nitrogen at 50 kV, but in dry air the rate constant was  $0.03 \text{ s}^{-1}$ . Hence, as expected, the rate constant depends upon the composition of the gas.

The  $\text{N}_2\text{O}$  measurement matched well with the model value obtained in the experiment. This result is significant since this is an independent check of the model. To have an additional independent check on the model, experiments were conducted to measure ozone formation in dry air under pulsed streamer corona discharge. The model prediction matched qualitatively with the

experimental value for ozone, however, further work is necessary to fully validate the experimental ozone measurements.

In the case of NO removal from feed air in the presence of water, the addition of water did not enhance NO removal. The  $\text{NO}_2$  concentration was significantly lower due to the water-induced formation of further products from  $\text{NO}_2$  reactions. A very small amount of  $\text{HNO}_3$  was measured as nitrate during the experiments using ion chromatography. The model predicts about 35% conversion of the initial NO to  $\text{HNO}_3$  at 50 kV and at long residence time (60.0 seconds). The experimental measurements did not find such high concentrations of nitric acid. The  $\text{NO}_2$  concentration profile qualitatively matched with the experimental data, but quantitatively the difference was significant.

The presence of 500 ppm of carbon monoxide in humid air did not affect the experimental concentration profiles of NO and  $\text{NO}_2$ . Tokunaga et al. (1984) showed that the removal of NO was enhanced in the presence of 1.13% carbon monoxide by volume. In the present study the amount of carbon monoxide added to the gas may have been too small to have an effect on the concentration of NO. The model profile with and without 500 ppm of carbon monoxide also showed no effect of CO on NO removal.

In the presence of 500 ppm of ethylene, NO removal was significantly enhanced. In dry air with ethylene about 45% removal of  $\text{NO}_2$  was observed. The main reaction pathways for the enhanced removal of NO and  $\text{NO}_2$  are due to the production of highly reactive radicals by the reaction of oxygen atoms with ethylene. The formation of radicals such as  $\text{HCO}\cdot$ , and  $\text{CH}_3\cdot$  react with NO and  $\text{NO}_2$  to enhance their removal. The model indicated that the main reaction pathway for the removal of  $\text{NO}_2$  in dry air is through reaction with  $\text{HCO}\cdot$  radical to form  $\text{HNO}_2$ .

In humid air containing ethylene, additional ethylene breakdown is caused by its reaction with hydroxyl radicals, aiding in the removal of  $\text{NO}_2$ . Complete removal of ethylene under these conditions was found by using GC/MS analysis of the gas samples. Four chromatographic peaks were observed when the sample was analyzed by HPLC. Formic acid was identified as one of these peaks. The amount of formic acid represents less than 1% of the carbon initially fed into the reactor. The production of carbon dioxide was observed for dry air conditions; however, quantitatively only 13% of the input carbon could be accounted for by  $\text{CO}_2$ .

In conclusion, the use of a pulsed streamer corona discharge has been shown to be successful

in the removal of  $\text{NO}_x$  in different gas compositions. The main reaction mechanisms for  $\text{NO}$  removal in various gas compositions under corona discharge were identified in this work. The addition of ethylene was found to enhance both  $\text{NO}$  and  $\text{NO}_2$  removal even in the case of dry air, while water addition assisted  $\text{NO}_2$  but not  $\text{NO}$  removal. The addition of 500 ppm of  $\text{CO}$  in humid air did not enhance  $\text{NO}$  and  $\text{NO}_2$  removal.

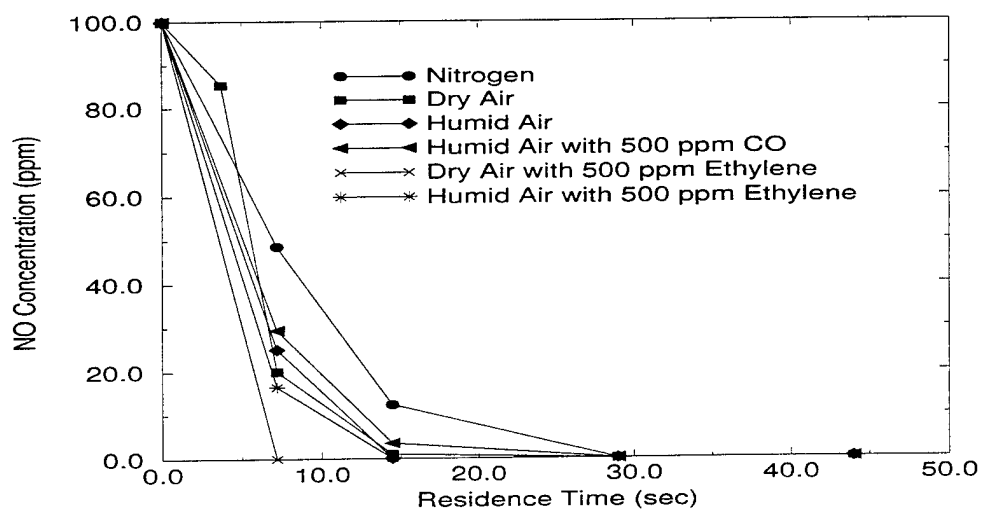


Figure 41 : Summary of NO Removal in Different Atmospheres

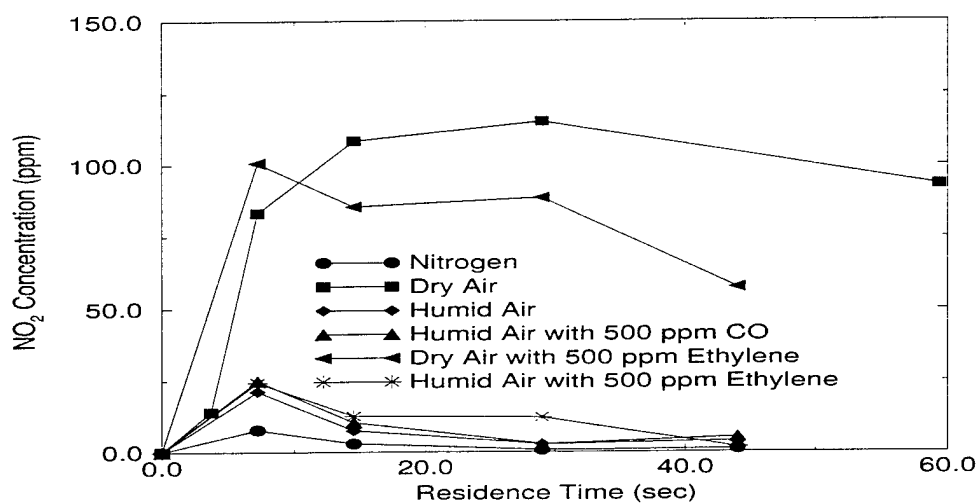


Figure 42: Summary of NO<sub>2</sub> removal in Different Atmospheres



## SECTION VI

### RECOMMENDATIONS

Recommendations from this study include:

- 1) Aerosol Measurements. Experiments conducted to study the removal of  $\text{NO}_x$  in humid air indicated both NO and  $\text{NO}_2$  removal. The atmospheric chemistry literature indicates that both  $\text{HNO}_2$  and  $\text{HNO}_3$  would be produced and could form aerosols. The analysis of aerosols is an important area for future work in order to develop a more complete material balance on the products of reaction. Methods to characterize the size distribution of the aerosols and to measure the concentration of aerosols would be needed for these studies.
- 2) Operating Conditions. Variation of the gas temperature, and additional gas compositions should be considered. The exhaust gases emitted from power plants and jet cell engines are at high temperature and contain large concentrations of carbon dioxide, water vapor, and aerosol particles. The addition of aerosols and operation of the reactor at higher temperatures may be of interest. Further variation of the gas composition through consideration of higher concentrations of NO, CO,  $\text{CO}_2$ , water vapor, and other could be considered.
- 3) Improvements in Experimental Setup. The power input into the system is currently adjusted by increasing the applied voltage. Under the current operating conditions, the maximum voltage achievable is 50 kV. An alternative method to increase the power input into the system would be to vary the frequency of pulsing. Modification of the power supply to allow for frequency variation would be useful in order to further evaluate the difference between the effects of applied field strength and power density on NO removal.
- 4) Reactor electrode materials. It has been observed in the literature that in order to achieve reducing conditions in the reactor, it is desirable to run the reactor with an internal source of

carbon. It may therefore be of interest to operate the reactor with a packed bed of activated carbon or other carbon particles. In addition, the use of carbon electrodes may also be of interest in order to facilitate degradation reactions.

5) Improvements in Modeling. It is currently assumed in the modeling work that the electric field is constant during the pulse-on period. Variation of the electric field pulse shape during the pulse-on period and variation along the electrode length could be introduced to account for non-uniform aspects of the electric discharge.

## REFERENCES

- Alekseev, G. Y., Leuchenko, A. L., and Bityurin, V. A., "Flue Gas Cleaning of the Electrostatic Corona, Part 11 Chemical Kinetics and Heat and Mass Transfer in NO<sub>2</sub>/SO<sub>2</sub> Removal", *Research Report IVTAN-ANRA 93/2*, MOSCOW, 1993.
- Atkinson, R. and Lloyd, A. C., "Evaluation of Kinetic and Mechanistic Data for Modeling of Photochemical Smog", *J. Phys. Chem. Ref. Data*, **13**, 2, 1984, 315-444.
- Atkinson, R., Baulch, D. L., Cox, R. A., Hampson, R. F., Kerr, J. A., and Troe, J., "Evaluated Kinetic and Photochemical Data for Atmospheric Chemistry", *J. Phys. Chem. Ref. Data*, **18**, 1989, 881-1097.
- Baulch, D. L., Drysdale, D., and Horne, D. G., "Evaluated Kinetic Data for High Temperature Reactions", 1983, Butterworths, London, Vol. 2.
- Boodaghians, R., B., Canosa-Mas, C., E., Carpenter, P. J., and Wayne, R., P., "The Reactions of NO<sub>3</sub> with OH and H", *J. Chem. Phys. Farad. Trans.*, 2, **84**, 1988, 931-948.
- Brune, Wm., H., Schwab, J., J., and Anderson, J., G., "Laser Magnetic Resonance, Resonance Fluorescence and Resonance Absorption Studies of the Reaction Kinetics of O + OH → H + O<sub>2</sub>, O + HO<sub>2</sub> → OH + O<sub>2</sub>, N + OH → H + NO and N + HO<sub>2</sub> → Products at 300° K Between 1 and 5 torr", *J. Phys. Chem.*, **87**, 1983, 4503-4514.
- Busi, F., Dangelantonio, M., Mulazzani, Q., G., and Rafael, V., "A Kinetic Model for Radiation Treatment of Combustion Gases", *The Science of the Total Environment*, **64**, 1987, 231-238.
- Chang, M. B., Kushner, M. J., and Rood, M. J., "Gas Phase Removal of NO from Gas Streams via Dielectric Barrier Discharges", *Envir. Sc. Techno.*, **26**, 1992, 777-781.
- Chang, J. S., "Energetic Electron Induced Plasma Processes for Reduction of Acid and Greenhouse Gases in Combustion of Flue Gases", *Non-Thermal Plasma Techniques for Pollution Control*, Part A, Eds: Penetrante, B., M. and Sculthesis, S., E.. Springer-Verlag, 1993, 1-32.
- Clements, J., S., Sato., M., Davis, R., H., "Preliminary Investigation of Prebreakdown Phenomena and Chemical Reactions Using a Pulsed High Voltage Discharge in Water", *IEEE Trans. Ind. Appl.*, **IA-23**, 1985, 1372.
- Clements, J. S., Mason, A., Finney, W. C., and Davis, R. H., "Combined Removal of SO<sub>2</sub>/NO<sub>x</sub> and Fly Ash from Simulated Flue Gas Using Pulsed Streamer Corona", *IEEE Trans. on Ind. Appl.*, **25**, No. 1, January/February 1989, 62-69.

Creyghton, Y. L. M., "Pulsed Positive Corona Discharges, Fundamental Study and Application to Flue Gas Treatment", *CIP-DATA Kononkijk biblitheek*, Den Haag, Netherlands, 1994.

Demore, W. B., Molina, M. J., Sander, S. P., Hampson, R. F., Kurylon, M. J., Golden, D. M., Howard, C. J., and Ravishankara, A. R., "Chemical Kinetics and Photochemical Data for Use in Stratospheric Modeling", National Aeronautics and Space Administration, JPL Publication 87-41, 1987.

Dhali, S., K., and Sardja, I., "Dielectric-Barrier Discharge for Processing of  $\text{SO}_2/\text{NO}_x$ ", *J. Appl. Phys.*, **69**(9), 1 May 1991, 6319-6324.

Dinelli, G., Civitano, L., and Rea, M., "Industrial Experiments on Pulse Corona Simultaneous Removal of  $\text{NO}_x$  and  $\text{SO}_2$  from Flue Gas", *IEEE Trans. on Ind. Appl.*, **26**, 1990, 535-541.

Frank, W., N., and Hirano, S., "The History of Electron Beam Processing for Environmental Pollution Control and Work Performed in the United States", *Non-Thermal Plasma Technz'ques for Pollution Control*, Eds: Penetrante, B., M., and Schultheis, S., E., Part B, Springer-Verlag, 1993, 1-26.

Fujii, T., Gobbo, R., Rea, M., "Pulse Corona Characteristics", *IEEE Tran. on Ind. Appl.*, **29**, No. 1, January/February 1993.

Gallimberti, I., "A Computer Model for Streamer Propagation", *J. Phys. D: Appl. Phys.*, **5**, 1972, 2179-2189.

Gallimberti, I., "Impulse Corona Simulation for Flue Gas Treatment", *Pur. Appl. Chem.*, **60**, 1988, 663-674.

Greenberg, A., Clescerl, L., Eaton, A., *Standard Methods for the Examination of Water and Wastewater 18th Edition*, American Public Health Association, 1992, p. 2.42 and p. 4.38.

Grosjean, E., Bittencourt de Andrade, J., Grosjean, D., "Carbonyl Products of the Gas-Phase Reaction of Ozone with Simple Alkenes", *Environ. Sci. Technol.*, **30**, 1996, 975-983.

Hoffmann, A., and Zellner, R., Paper Presented at the 10th Int. Symposium on Gas Kinetics, Swansey, 1988.

Huxley, L., G., H., and Crompton, R., W., "The Diffusion and Drift of Electrons in Gases", Wiley, New York, 1974, 669.

Joshi, A., A., Locke, B., R., Arce, P., and Finney, W., C., "Formation of Hydroxyl Radicals, Hydrogen Peroxide and Aqueous Electrons by Pulsed Streamer Corona Discharge in Aqueous Solution", *Journal of Hazardous Materials*, **41**, April 1995, 3-30.

- Kaiser, E., W., and Wu, C., H., "A Kinetic Study of the Gas Formation and Decomposition Reactions of Nitrous Acid", *J. Phys. Chem.*, **81**, 1977, 187-190.
- Kaiser, E., W., and Wu, C., H., "Upper Limits to the Gas Phase Reactions of HONO with  $\text{NH}_3$  and  $\text{O}(3p)$  atoms", *J. Phys. Chem.*, **81**, 1978, 187-190.
- Kee, R. J, Rupley, F. M., and Miller, J. A., "Chemkin-11: A Fortran Chemical Kinetics Package for the Analysis of Gas Phase Chemical Kinetics", Sandia Report, SAND89-8009B, 1994.
- Kogelschatz, U., Eliasson, B., "Ozone Generation and Applications", in Handbook of Electrostatic Processes, J-S. ,Chang, A.J. Kelly, J.M. Crowley, eds., Marcel Dekker, Inc., New York, 1995, pp581-605.
- Kokkinos, A., Cichanowicz, J., E., Hall, R., E., and Sedman, C., B., "Stationary Combustion  $\text{NO}_x$  Control: A Summary of the 1991 Symposium", *J. Air Waste. Manage. Assoc.*, **41**, 1991, 1252-1259.
- Leslie S., L., "Nitrogen Oxides Control Technology", Noyes Data Corporation, 1992, 4-14.
- Levine, J., S., "The Photochemistry of Atmospheres", Academic Press, 1985.
- Lincoln, D., "Ozone Generation in Gas Phase Pulsed Corona Reactor", *Report Prepared For Department of Chemical Engineering*, FAMU-FSU College of Engineering, 1995.
- Locke, B.R, Swaminathan, K., Finney, W.C., "Laboratory Studies of Nitrogen Oxide Removal by Pulsed Streamer Corona." *Final Report Prepared for USAF*, 1995.
- Loirat, H., Caralp, F., Destriau, F., and Lesclaux, R., "Oxidation of CO by  $\text{N}_2\text{O}$  between 1076 and 1288 K: Determination of the Rate Constant of the Exchange Reaction", *J. Phys. Chem.*, **91**, 1987, 6538-6542.
- Loiseau, J., F., Laoassie, F., Monge, C., Peyrous, R., Held, B., and Coste, C., "Numerical Simulation of Ozone Axial and Radial Distribution in a Cylindrical Oxygen-Fed Ozonizer", *J. Phys. D: Appl. Phys.*, 1994, 63.
- Lucas, S., "Voltage Waveform Characterization of the Pulsed Corona Reactor", *Report Prepared For Department of Chemical Engineering, FAMU-FSU College of Engineering*, 1995.
- McFarlane, J., and Wren, J. C., "Modeling Electric Discharge Chemistry", *AECL-10374 Atomic Energy of Canada Limited*, Whiteshell Laboratories, 1991.
- Masuda, S., and Nakao, H., "Control of  $\text{NO}_x$  by Positive and Negative Pulsed Corona Discharges", *IEEE Trans. Ind. Appl.*, **26**, 1990, 374-383.

- Matzing, H., "Chemical Kinetics of Flue Gas Cleaning by Irradiation with Electrons", *Adv. Chem. phys.*, **80**, 1991, 315-402.
- Mizuno, A., Ito, H., "Basic Performance of an Electrically Augmented Filter Consisting of Packed Ferroelectric Pellet Layer", *J. Electrostatics*, **25**, 1987, 97107.
- Mizuno, A., and Kamase, Y., "A High-Voltage Pulse Source for Electron Beam Generation Using field Emission" *IEEE Trans. on Ind. Appl.*, **25**, No. 1 January/February 1989.
- Mizuno, A., Chakrabarti, A., Okazaki, K., "Application of Corona Technology in the Reduction of Greenhouse Gases and Other Pollutants", *Non- Thermal Plasma Techniques for Pollution Control*, Part B, Eds: Penetrante, B., M and Schultheis, S., E., Springer-Verlag, 1993, 165-185.
- Mizuno, A., Simizu, K., Chakrabarti, A., Dascalescu, L., and Furuta, S., "NO<sub>x</sub> Removal Process Using Pulsed Discharge Plasma", *IEEE Tran. Ind. Appl.*, **31**, No. 5, September-October 1995, 957-963.
- Mukkavilli, S., Lee, C. K., Varghese, K., and Tavalariades, L. L., "Modeling of the Electrostatic Corona Discharge Reactor", *IEEE Trans. Plasma. Sci.*, **16**, 1988, 656-660.
- Naseer, E., "Fundamentals of Gaseous Ionization and Plasma Electronics", Wiley-Interscience. 1971.
- NIST Chemical Database 17, version 6.01. 1994, Eds: Mallard, W., G., Westley, F., Herron, J., T., Hampson, R., F.; National Institute of Standards and Technology (NIST), Gaithersburg, USA.
- Ohkubho, K., Kanazawa, S., Nomoto, Y., Chang, J. S., and Adachi, T., "NO<sub>x</sub> Removal by a Pipe with Nozzle-Plate Electrode Corona Discharge System", *IEEE Trans. Ind. Appl.*, **30**, No. 4. July/August 1994, 856-860.
- Okazaki, K., Mizuno, A., Shimizu, K., Niwa, T., "Application of Semi-Wet Type Corona Discharge Reactor to the Simultaneous Removal of NO<sub>x</sub>, SO<sub>2</sub> and Fly Ash in Pulverized Coal Combustion", *IEEE Tran. Ind. Appl.*, **31**, Nov/Dec. 1995, 1463-1468.
- Ozkan, U., S., Agarwal, S., K., and Marcelin, G., "Reduction of Nitrogen Oxides Emissions". ACS Symposium Series, 1995, 1-52.
- Penetrante, B. M., "Plasma Chemistry and Power Consumption in Non-thermal Plasma", *Non-Thermal Plasma Techniques for Pollution Control*, Part A, Eds: Penetrante, B., M., and Schultheis, S., E, Springer-Verlag 1993, 65-89.
- Penetrante, B. M., Hsiao, M. C., Meritt, B. T., Vogtlin, G. E., Wallman, P. H., "Comparison of Electrical Discharge Techniques for Nonthermal Plasma Processing of NO in N<sub>2</sub>", *IEEE Tran.*

on *Plasma Sci.*, **23**, No. 4, August 1995.

Penetrante, B.M., Hsiao, M.C., Bardsley, J.N., Merritt, B.T., Vogtlin, G.E., Wallman, P.H., Kuthi, A., Burkhart, C.P., Bayless, J.R.M., "Non-Thermal Plasma Techniques for Abatement of Volatile Organic Compounds and Nitrogen Oxides", Workshop on Plasma Based Environmental Technologies, Berlin, Germany, December 6-7, 1995, 18-46.

Penetrante, B.M., M.C. Hsiao, B.T. Merritt, G.E. Voglin, P.H. Wallman, M. Neiger, O. Wolf, T. Hammer, S. Broer, "Pulsed Corona and Dielectric-Barrier Discharge Processing of NO in N<sub>2</sub>", *Appl. Phys. Lett.* **68**, No 26, June 1996, 3719-3721.

Peyrous, R., Pignolet, P., and Held, B., "Kinetic Simulation of Gaseous Species by an Electrical Discharge in Dry or Humid Oxygen", *J. Phys. D: Appl. Phys.*, **22**, 1989, 1658-1667.

Pignolet, P., Hadj-Ziane, S., Held, B., Peyrous, R., Benas, J., M., and Coste, C., "Ozone Generation by Point to Plane Corona Discharge" *J. Phys. D: Appl. Phys.*, **23**, 1990, 1069-1072.

Rutscher, A., Wagner, H.-E., "Chemical Quasi-Equilibria: A New Concept in the Description of Reaction Plasmas", *Plasma Sources Sci. Technol.* **2**, 1993, 279-288.

Sardja, I., and Dhali, S., K., "Plasma Oxidation Of SO<sub>2</sub>" *Appl. Phys. Lett.*, **56**(1), 1 January 1990, 21-23.

Schofield, K., "Critically Evaluated Rate Constants for Gaseous Reactions of Several Electronically Excited Species", *J. Phys. Chem. Ref. Data*, **8**, 1979, 723-763.

Seinfeld, J. H., "Atmospheric Chemistry and Physics of Air Pollution", John Wiley and Sons, New York, 1986.

Sharma, A., K., Locke, B., R., Arce, P., "A Preliminary Study of Pulsed Streamer Corona Discharge for the Degradation of Phenol in Aqueous Solutions", *Hazardous Waste & Hazardous Materials*, **10** (2), 1993, 209-219.

Spicer, C. W., Holdren, M. W., Smith, L. D., and Hughes, D. p, Smith, M. D., "Chemical Composition of Exhaust From Aircraft Turbine Engines", *Journal of Engineering for Gas Turbines and Power*, **114**, January 1992, 111-117.

Suhr, H., Weddigen, G., "Reduction of Nitric Oxide in Flue Gases by Point to Plane Corona Discharge with Catalytical coatings on the Plane Electrode" *Combust. Sci. and Tech.*, **72**, 101-115.

Sutherland, C. D., and Zinn, J., "Chemistry Computations for Irradiated Hot Air", Los Alamos Scientific Laboratory Informal Report LA-6055-MS, 1975, Los Alamos, NM.

Tas, M.A, "Plasma-Induced Catalysis, A Feasibility study and fundamentals", thesis Technische Universiteit Eindhoven, Netherlands, CIP-DATA Koninklijke Bibliotheek, Den Haag, 1995.

Tokunaga, O., and Suzuki, N., "Radiation Chemical Reactions in NO<sub>x</sub> and SO<sub>2</sub> Removal from Flue Gas", *Radz'at. Phys. Chem.*, **24**, 1984, 145-165.

U.S. EPA, "Air Quality Criteria for Oxides of Nitrogen", Research Triangle Park, 1993.

Vogtln, G., E., and Penetrante, B., M., "Pulsed Corona Discharge for Removal of NO<sub>x</sub> from Flue Gas", Non- Thermal *Plasma Techniques for Pollution Control*, Part B, Eds: Penetrante, B., M, and Schultheis, S., E., Springer-Verlag, 1993, 187-198.

Wang, M., C., and Kunhardt, E., E., "Streamer Dynamics", *Phys. Rev. A*, **42**, t990, 465-515.

Warnatz, J., "Rate Coefficients in C/H/O System", *Combustion Chemistry*, Ed: Gardinger, Jr., Springer, 1984, 197-360.

Willis, C., and Boyd, A. W., "Excitation in the Radiation Chemistry of Inorganic Bases", *Int. J. Rad. Phys. Chem.*, **8**, 1976, 71-111.

Wolf, O., Listl, S., Neiger, M. "Experimental Investigations of Nox-Conversion in a Dielectric Barrier Discharge", Proceedings of the Hakone V, International Symposium on High Pressure Low Temperature Plasma Chemistry, Milovy, Czech Republic, September 2-4, 1996, pp324-328.



## APPENDIX A

### NO REMOVAL DATA FROM NITROGEN, DRY, AND HUMID AIR

The concentrations shown in the tables have been normalized for an initial concentration of NO to be 100 ppm and NO<sub>2</sub> concentration to be 0 ppm.

Table A.1: NO and NO<sub>2</sub> Data at 30 kV in an Atmosphere of Nitrogen

Res. Time (sec)	NO Conc. (ppm)		NO <sub>2</sub> Conc. (ppm)		Mean NO	Mean NO <sub>2</sub>
	Run1	Run2	Run1	Run 2		
7.2	99.8	98.8	0	0	99.9	0
14.5	87.6	87.7	3.3	4.8	87.6	4.0
29.0	82.7	80.7	4.1	4.5	81.7	4.3
44.0	57.9	64.5	7.0	7.9	61.2	7.4

Table A.2: NO and NO<sub>2</sub> Data at 35 kV in an Atmosphere of Nitrogen

Res. Time (sec)	NO Conc. (ppm)		NO <sub>2</sub> Conc. (ppm)		Mean NO	Mean NO <sub>2</sub>
	Run1	Run2	Run1	Run 2		
7.26	98.46	90.74	2.6	3.0	94.62	2.80
14.52	64.8	65.43	6.94	7.2	65.11	7.06
29.04	43.85	44.96	8.38	7.02	44.05	4.93
44	28.75	28.55	6.76	7.36	28.65	6.56

Table A.3: NO and NO<sub>2</sub> Data at 40 kV in an Atmosphere of Nitrogen

Res. Time (sec)	NO Conc. (ppm)		NO <sub>2</sub> Conc. (ppm)		Mean NO	Mean NO <sub>2</sub>
	Run1	Run2	Run1	Run 2		
7.2	82.75	78.05	5.17	7.03	80.42	6.10
14.5	47.29	46.95	7.78	8.06	47.12	7.92
29	12.86	8.96	4.46	5.41	10.91	4.93
44	1.58	1.98	2.0	2.06	1.78	2.30

Table A.4: NO and NO<sub>2</sub> Data at 50 kV in an Atmosphere of Nitrogen

Res. Time (sec)	NO Conc. (ppm)		NO <sub>2</sub> Conc. (ppm)		Mean NO	Mean NO <sub>2</sub>
	Run1	Run2	Run1	Run 2		
7.2	48.07	49.17	7.78	8.0	48.62	7.87
14.5	12.36	12.4	2.8	3.0	12.38	2.9
29	0	0	0.76	0.6	0	0.68
44	0	0	0.83	1.24	0	1.03

Table A.5: NO and NO<sub>2</sub> Data at 30 kV in an Atmosphere of Dry Air

Res. Time (sec)	NO Conc. (ppm)		NO <sub>2</sub> Conc. (ppm)		Mean NO	Mean NO <sub>2</sub>
	Run1	Run2	Run1	Run 2		
3.6	97.5	98.1	0	0	97.8	0
7.2	97.2	97.6	0.65	1.62	97.4	1.13
14.5	97.4	99.2	3.3	0	98.3	1.6
29.0	79.8	94.6	28.0	3.7	87.2	15.8
59.0	77.0	73.0	27.3	22.8	75	25.0

Table A.6: NO and NO<sub>2</sub> Data at 35 kV in an Atmosphere of Dry Air

Res. Time (sec)	NO Conc. (ppm)		NO <sub>2</sub> Conc. (ppm)		Mean NO	Mean NO <sub>2</sub>
	Run1	Run2	Run1	Run 2		
3.6	99.0	98.5	0	0	98.7	0
7.2	82.04	87.16	17.5	11.5	84.58	14.5
14.5	90.5	95.4	12.4	6.4	92.9	9.4
29	47.4	28.6	63.4	84.8	38	74.1
59	9.5	10.8	105.1	107.2	10.1	106.1

Table A.7: NO and NO<sub>2</sub> Data at 40 kV in an Atmosphere of Dry Air

Res. Time (sec)	NO Conc. (ppm)		NO <sub>2</sub> Conc. (ppm)		Mean NO	Mean NO <sub>2</sub>
	Run1	Run2	Run1	Run 2		
3.6	98.9	95.4	0	3.0	97.1	1.5
7.2	58.56	68.9	42.1	33.0	63.8	37.6
14.5	44.4	39.2	64.1	64.7	41.8	64.4
29	0	3.8	121.9	117.9	1.9	119.9
59.0	1.1	0	99.4	101.9	0.5	100.6

Table A.8: NO and NO<sub>2</sub> Data at 50 kV in an Atmosphere of Dry Air

Res. Time (sec)	NO Conc. (ppm)		NO <sub>2</sub> Conc. (ppm)		Mean NO	Mean NO <sub>2</sub>
	Run1	Run2	Run1	Run 2		
3.6	75.0	95.7	24.7	3.3	85.3	14.0
7.2	18.8	21.3	82.5	79.8	20.0	81.2
14.5	0	1.9	108.2	108.6	0.9	108.4
29	0	0	111.9	119.0	0	115.4
44	0	0	85.4	87.4	0	86.4

Table A.9: NO and NO<sub>2</sub> Data at 30 kV in an Atmosphere of Humid Air

Res. Time (sec)	NO Conc. (ppm)		NO <sub>2</sub> Conc. (ppm)		Mean NO	Mean NO <sub>2</sub>
	Run1	Run2	Run1	Run 2		
7.2	97.64	97.94	1.0	0	97.79	0.5
14.5	98.66	94.0	2.04	3.62	96.33	2.83
29.0	80.64	88.67	2.42	2.4	84.66	2.4
44	89.59	91.82	1.02	0	90.7	0.5

Table A.10: NO and NO<sub>2</sub> Data at 35 kV in an Atmosphere of Humid Air

Res. Time (sec)	NO Conc. (ppm)		NO <sub>2</sub> Conc. (ppm)		Mean NO	Mean NO <sub>2</sub>
	Run1	Run2	Run1	Run 2		
7.2	86.79	86.14	6.52	5.46	86.46	5.95
14.5	66.49	57.23	16.76	18.24	61.86	17.5
29.0	41.72	51.76	4.02	5.72	46.74	4.87
44.0	43.36	31.12	1.81	1.48	37.2	1.65

Table A.11: NO and NO<sub>2</sub> Data at 40 kV in an Atmosphere of Humid Air

Res. Time (sec)	NO Conc. (ppm)		NO <sub>2</sub> Conc. (ppm)		Mean NO	Mean NO <sub>2</sub>
	Run1	Run2	Run1	Run 2		
7.2	59.94	64.13	15.66	13.97	62.02	14.82
14.5	29.05	26.38	23.26	22.1	27.7	22.68
29	7.9	19.4	5.29	4.75	13.65	5.62
44.0	0	0	2.88	3.54	0	3.21

Table A.12: NO and NO<sub>2</sub> Data at 50 kV in an Atmosphere of Humid Air

Res. Time (sec)	NO Conc. (ppm)		NO <sub>2</sub> Conc. (ppm)		Mean NO	Mean NO <sub>2</sub>
	Run1	Run2	Run1	Run 2		
7.2	28.1	22.06	20.8	21.58	25.08	21.19
14.5	0	0	4.75	10.26	0	7.5
29.0	0	0	2.76	2.62	0	2.69
44.0	0	0	3.81	3.83	0	3.82

## APPENDIX B

### NO REMOVAL DATA WITH THE ADDITION OF CO AND C<sub>2</sub>H<sub>4</sub>

The concentrations shown in the table have been normalized for an initial concentration of NO to be 100 ppm and NO<sub>2</sub> concentration to be 0 ppm.

Table B.1: NO and NO<sub>2</sub> Data at 30 kV in an Atmosphere of Humid Air and CO

Res. Time (sec)	NO Conc. (ppm)		NO <sub>2</sub> Conc. (ppm)		Mean NO	Mean NO <sub>2</sub>
	Run1	Run2	Run1	Run 2		
7.2	98.6	97.5	0.2	0	98.0	0.1
14.5	96.3	88.8	1.5	4.0	92.6	2.8
29.0	94.2	93.3	1.2	1.1	93.8	1.2
44.0	93.2	92.6	1.6	0	92.9	0.8



Table B.2: NO and NO<sub>2</sub> Data at 35 kV in an Atmosphere of Humid Air and CO

Res. Time (sec)	NO Conc. (ppm)		NO <sub>2</sub> Conc. (ppm)		Mean NO	Mean NO <sub>2</sub>
	Run1	Run2	Run1	Run 2		
7.2	94.6	94.3	1.6	1.2	94.5	1.4
14.5	78.0	60.8	3.4	9.0	69.4	6.2
29.0	50.2	41.3	6.4	6.7	45.8	6.6
44.0	45.6	42.6	5.7	6.1	44.1	5.9

Table B.3: NO and NO<sub>2</sub> Data at 40 kV in an Atmosphere of Humid Air and CO

Res. Time (sec)	NO Conc. (ppm)		NO <sub>2</sub> Conc. (ppm)		Mean NO	Mean NO <sub>2</sub>
	Run1	Run2	Run1	Run 2		
7.2	66.3	58.9	13.6	19.5	62.6	16.6
14.5	27.5	26.0	11.5	12.3	26.8	11.9
29.0	5.6	4.2	7.1	6.75	4.9	6.9
44.0	9.6	2.5	5.6	5.9	6.05	5.8

Table B.4: NO and NO<sub>2</sub> Data at 50 kV in an Atmosphere of Humid Air and CO

Res. Time (sec)	NO Conc. (ppm)		NO <sub>2</sub> Conc. (ppm)		Mean NO	Mean NO <sub>2</sub>
	Run1	Run2	Run1	Run 2		
7.2	30.5	28.4	25.6	24.3	29.5	24.9
14.5	4.6	2.3	10.8	9.7	3.5	10.3
29.0	0	0	2.5	2.9	0	2.7
44.0	0	0	5.2	5.0	0	5.1

Table B.5: NO and NO<sub>2</sub> Data at 30 kV in an Atmosphere of Dry Air and 500 ppm Ethylene

Res. Time (sec)	NO Conc. (ppm)		NO <sub>2</sub> Conc. (ppm)		Mean NO	Mean NO <sub>2</sub>
	Run1	Run2	Run1	Run 2		
7.2	91.8	97.9	1.6	0	94.9	0.8
14.5	92.4	88.9	7.6	10.8	90.65	9.2
29.0	79.0	70.4	20.0	20.1	74.7	20.1
44.0	27.9	48.0	68.5	43.4	38.0	56.0

Table B.6: NO and NO<sub>2</sub> Data at 35 kV in an Atmosphere of Dry Air and 500 ppm of Ethylene

Res. Time (sec)	NO Conc. (ppm)		NO <sub>2</sub> Conc. (ppm)		Mean NO	Mean NO <sub>2</sub>
	Run1	Run2	Run1	Run 2		
7.2	65.1	71.9	36.8	27.9	68.5	31.9
14.5	66.4	77.9	34.3	23.9	72.2	29.1
29.0	42.6	24.9	54.0	63.1	33.8	58.5
44.0	1	1.1	91.7	87.0	1.1	89.4

Table B.7: NO and NO<sub>2</sub> Data at 40 kV in an Atmosphere of Dry Air and 500 ppm Ethylene

Res. Time (sec)	NO Conc. (ppm)		NO <sub>2</sub> Conc. (ppm)		Mean NO	Mean NO <sub>2</sub>
	Run1	Run2	Run1	Run 2		
7.2	25.5	14.7	77.2	87.0	20.1	82.1
14.5	4.3	3.7	95.6	94.8	4.0	95.2
29.0	0	0	90.0	93.2	0	91.6
44.0	0	0	63.9	57.3	0	60.6

Table B.8: NO and NO<sub>2</sub> Data at 50 kV in an Atmosphere of Dry Air and 500 ppm Ethylene

Res. Time (sec)	NO Conc. (ppm)		NO <sub>2</sub> Conc. (ppm)		Mean NO	Mean NO <sub>2</sub>
	Run1	Run2	Run1	Run 2		
7.2	0	0	102.3	99.0	0	100.7
14.5	0	0	86.1	84.6	0	85.4
29.0	0	0	88.6	88.4	0	88.5
44.0	0	0	55.0	59.5	0	57.3

Table B.9: NO and NO<sub>2</sub> Data at 30 kV in an Atmosphere of Humid Air and 500 ppm Ethylene

Res. Time (sec)	NO Conc. (ppm)		NO <sub>2</sub> Conc. (ppm)		Mean NO	Mean NO <sub>2</sub>
	Run1	Run2	Run1	Run 2		
7.2	98.3	97.6	0	0	98.0	0
14.5	76.1	73.2	8.3	8.9	74.65	8.6
29.0	92.2	73.9	1.0	3.5	83.1	2.3
44.0	80.0	85.8	0	0	82.9	0

Table B.10: NO and NO<sub>2</sub> Data at 35 kV in an Atmosphere of Humid Air and 500 ppm Ethylene

Res. Time (sec)	NO Conc. (ppm)		NO <sub>2</sub> Conc. (ppm)		Mean NO	Mean NO <sub>2</sub>
	Run1	Run2	Run1	Run 2		
7.2	70.3	74.1	13.2	10.4	72.2	11.8
14.5	68.2	26.7	8.5	15.9	47.4	12.2
29.0	20.6	22.2	7.9	7.7	21.4	7.8
44.0	34.6	13.4	1.5	2.4	24	1.9

Table B.11: NO and NO<sub>2</sub> Data at 40 kV in an Atmosphere of Humid Air and 500 ppm Ethylene

Res. Time (sec)	NO Conc. (ppm)		NO <sub>2</sub> Conc. (ppm)		Mean NO	Mean NO <sub>2</sub>
	Run1	Run2	Run1	Run 2		
7.2	37.8	36.7	19.9	21.2	37.7	20.5
14.5	22.6	15.8	14.7	16.2	19.2	15.4
29.0	3.6	7.0	10.5	11.0	5.3	10.7
44.0	0	1.4	1.1	2.0	0.7	1.5

Table B.12: NO and NO<sub>2</sub> Data at 50 kV in an Atmosphere of Humid Air and 500 ppm Ethylene

Res. Time (sec)	NO Conc. (ppm)		NO <sub>2</sub> Conc. (ppm)		Mean NO	Mean NO <sub>2</sub>
	Run1	Run2	Run1	Run 2		
7.2	15.6	17.4	24.2	24.6	16.5	24.4
14.5	0	0	11.3	13.8	0	12.5
29.0	0	0	9.8	14.5	0	12.1
44.0	0	0	2.0	1.2	0	1.6

## APPENDIX C

### OZONE FORMATION DATA

Table C.1: O<sub>3</sub> Data at 30 kV in an Atmosphere of Dry Air

Res. Time (sec)	O <sub>3</sub> Conc. (ppm)		Mean O <sub>3</sub>
	Run1	Run2	
7.2	0	3	1.5
14.5	9	0	4.5
29	12	15	13.5
44.0	6	9	7.5

Table C.2: O<sub>3</sub> Data at 35 kV in an Atmosphere of Dry Air

Res. Time (sec)	O <sub>3</sub> Conc. (ppm)		Mean O <sub>3</sub>
	Run1	Run2	
7.2	33	21	27
14.5	15	12	13.5
29.0	27	21	24
44.0	24	78	41

Table C.3: O<sub>3</sub> Data at 40 kV in an Atmosphere of Dry Air

Res. Time (sec)	O <sub>3</sub> Conc. (ppm)		Mean O <sub>3</sub>
	Run1	Run2	
7.2	766	96	81
14.5	45	81	63
29.0	294	183	238.5
44.0	453	459	456



Table C.4: O<sub>3</sub> Data at 50 kV in an Atmosphere of Dry Air

Res. Time (sec)	O <sub>3</sub> Conc. (ppm)		Mean O <sub>3</sub>
	Run1	Run2	
7.2	276	258	267
14.5	375	363	369
29	1089	948	1018.5
44.0	1503	1236	1369.5

## APPENDIX D

### COMPUTER CODES

#### D.1 Procedure of Computations

The pulsed nature of the discharge is simulated in the program by considering two reaction sets to calculate the concentration profiles. During the duration of pulsing, the reaction set which has electron-gas dissociation reactions are used. The time duration of the pulse is assumed to be one microsecond. Since the frequency of pulsing is 60 Hz, the time duration between the pulsing is 16.667 milliseconds. To calculate the concentration profile for the time in between two pulses, the reaction set which does not have the electron-gas reactions are considered.

Initially the program calculates the concentration profile of different species using the initial concentrations given in **comp.inp** file and the set of reactions which has the electron-gas reactions given in **chem.inp** for a period of 1 microsecond. After this time, since the pulsing is no longer there, the reaction set is changed to the set which does not have any electron-gas reactions to calculate the concentration profile for the next 16.667 milliseconds. The reaction set is again interchanged after 16.667 milliseconds to calculate the concentration profile for the next 1 microsecond. This procedure is repeated 120 times corresponding to double the frequency of pulsing would give the concentration of different species after a gas residence time of 1 second. The concentration profile after each second is copied into the file called conc.out. The procedure is repeated till the gas residence time in the reactor

is reached. The program is repeated in this case for 7200 times to calculate the concentrations for a gas residence time of 60 seconds.

The plots shown in the model use the **conc.out** to show the concentrations of different species as a function of residence time.

The program **cycle.sh** is used to repeat the iteration 7200 times. The program **comp.sh** is the shell program which uses the fortran programs (**comp.f**, **vode.f**, **cklib.f**, **math.f**) and the input files to calculate the concentration.

The program **comp.f** is the actual fortran program which calls the ODE solver **vode.f** and other subroutines in **cklib.f** and **math.f** to solve the ODE. The ODE solver and the other subroutines are a part of the software called CHEMKIN (Kee, et al., 1994).

## D.2 cycle.sh

```
# This shell programs runs the ccomp.sh program repeatedly till the  
# final time corresponds to the final time in the reactor.  
# In this case, the program runs for 60 seconds.  
# After that the initial concentrations are added to the conc.out  
# to get the concentration profile.
```

```
#!/bin/csh -f  
set icount = 1  
set iend = 7201  
while ($icount != $iend)  
  sh comp.sh comp  
  @ icount++  
end
```

### D.3 comp.sh

```
# This shell program uses the comp.f program to calculate the concentration
# profile. It uses a ODE solver called vode.f and list of subroutines
# listed under cklib.f files from the software called CHEMKIN.
# This is shell program calculates the concentration profile till the
# final time, interchanges the reaction set making the computed final
# concentration of the initial concentration for the next set.
# The outputfile are comp.out, conc.out.
# conc.out has the concentration profile of the species after every second.

#!/bin/sh

# to execute:  sh comp.sh logname &
sh 1> ${1}.log 2>&1 << ENDSH

set -x

#cd /scr/$LOGNAME          #go to user's scratch directory
#mkdir "${1}$$"            #make subdirectory /myrun##
#cd "${1}$$"               #go to /myrun##

cat << EOF > makefile
include chemmake.h
OBJS = comp.o cklib.o vode.o math.o
INPS = therm.dat chem.inp comp.inp
OUTS = chem.out chem.bin comp.out
EXES = chem.exe comp.exe
chem.exe: ckinterp.o
    $(LINK) chem.exe ckinterp.o
comp.exe: $(OBJS)
    $(LINK) comp.exe $(OBJS)
```

#### D.4 comp.f

```
C    Modeling of NO Removal From Various Gas Compositions Using A
C    Pulsed Streamer Corona Discharge Reactor.
C
C
C    Input : Pressure, Temperature, Initial Mole Fractions of
C            Different Species, Initial Time, Final Time and
C            Interval in a File Called comp.inp
C            : Set of Chemical Reactions Considered for the NOx Removal
C            in a File Called chem.inp
C    Output: Concentration Profile of Different Species till the
C            Final Time at Requested Intervals in a File Called Chem.out
C
C This Program calls the ODE solver to solve for the given input

C This program is for the mole fractions as its input ..
    PROGRAM CONP
C
C    Integration of adiabatic, constant pressure kinetics problems
C
C    VERSION 1.2:
C    1.  Implement new VODE solver
C
C*****precision > double
    IMPLICIT DOUBLE PRECISION (A-H,O-Z), INTEGER(I-N)
C*****END precision > double
C*****precision > single
```

```

C      IMPLICIT REAL (A-H,O-Z), INTEGER (I-N)
C*****END precision > single
C
      PARAMETER (LENIWK=4000, LENRWK=8000, LENCWK=500, NK=5, NLMAX=55,
1          LIN=5, LOUT=6, LINKCK=25, KMAX=50, ITOL=1, IOPT=0,
2          RTOL=1.0E-6, ITASK=1, ATOL=1.0E-20)
C
      DIMENSION IWORK(LENIWK), RWORK(LENRWK), X(KMAX), Z(KMAX)
      CHARACTER CWORK(LENCWK)*16, KSYM(KMAX)*16, LINE*80
      LOGICAL KERR, IERR
      EXTERNAL FUN
C
      COMMON /RCONS/ P, RU
      COMMON /ICONS/ KK, NWT, NH, NWDOT
C
      DATA KERR/.FALSE./, X/KMAX*0.0/, KSYM/KMAX*' '/

C      Initialize CHEMKIN
      OPEN(19, FILE="Conp.dat",STATUS="UNKNOWN")
      OPEN (22,FILE="CONP.DAT1",STATUS="UNKNOWN")
      OPEN (LINKCK, FORM='UNFORMATTED', STATUS='UNKNOWN',
1          FILE='chem.bin')
      CALL CKLEN (LINKCK, LOUT, LENI, LENR, LENC)
      CALL CKINIT (LENIWK, LENRWK, LENCWK, LINKCK, LOUT, IWORK,
1          RWORK, CWORK)
      CLOSE (LINKCK)
      CALL CKINDX (IWORK, RWORK, MM, KK, II, NFIT)

```

```

NEQ   = KK + 1
LRW   = 22 + 9*NEQ + 2*NEQ**2
NVODE = LENR + 1
NWT   = NVODE + LRW
NH     = NWT + KK
NWDOT = NH + KK
NTOT  = NWDOT+ KK - 1
LIW   = 30 + NEQ
IVODE = LENI + 1
ITOT  = IVODE + LIW - 1
IF (KK .GT. KMAX) THEN
    WRITE (LOUT, *)
1    ' Error...KMAX too small...must be at least ',KK
    KERR = .TRUE.
ENDIF
IF (LENRWK .LT. NTOT) THEN
    KERR = .TRUE.
    WRITE (LOUT, *)
1    ' Error...LENRWK too small...must be at least', NTOT
ENDIF
IF (LENIWK .LT. ITOT) THEN
    KERR = .TRUE.
    WRITE (LOUT, *)
1    ' Error...LENIWK too small...must be at least', ITOT
ENDIF
IF (KERR) STOP
CALL CKSYMS (CWORK, LOUT, KSYM, IERR)

```



```

      IF (IERR) KERR = .TRUE.
      CALL CKWT  (IWORK, RWORK, RWORK(NWT))
      CALL CKRP  (IWORK, RWORK, RU, RUC, PATM)
      READ  (LIN,    *) PA, T
      WRITE(19,*) PA, T
      P = PA*PATM
C      Initial non-zero moles
40  CONTINUE
      LINE = ' '
      READ  (LIN,  '(A)', END=45)  LINE
      ILEN = INDEX (LINE, '!')
      IF (ILEN .EQ. 1) GO TO 40
      ILEN = ILEN - 1
      IF (ILEN .LE. 0) ILEN = LEN(LINE)
      IF (INDEX(LINE(:ILEN), 'END') .EQ. 0) THEN
        IF (LINE(:ILEN) .NE. ' ') THEN
          CALL CKSNUM (LINE(:ILEN), 1, LOUT, KSYM, KK, KNUM,
1              NVAL, VAL, IERR)
          IF (IERR) THEN
            WRITE (LOUT,*) ' Error reading moles...'
            KERR = .TRUE.
          ELSE
            X(KNUM) = VAL
          ENDIF
        ENDIF
      GO TO 40
    ENDIF
  ENDIF

```

```

45 CONTINUE
C      Final time and print interval
      READ (LIN, *) TT1,T2, DT, III
      WRITE (22,7100) (KSYM(K), K=1,KK)
      IF (KERR) STOP
C      Initial conditions and mass fractions
      Z(1) = T
      CALL CKXTY (X, IWORK, RWORK, Z(2))
C      Integration control parameters for VODE
      TT2 = TT1
      MF = 22
      ISTATE= 1
      NLINES=NLMAX + 1
C      Integration loop
250 CONTINUE
      T = Z(1)
      CALL CKYTX (Z(2), IWORK, RWORK, X)
      CALL CKMMWY(Z(2), IWORK, RWORK, WW)
      WRITE (LOUT, 7105) TT1, T, (X(K), K=1,KK), WW
      IF (TT2 .GE. T2) THEN
        WRITE(19,7012)(KSYM(K),X(K), K=1,KK)
        WRITE(19,*)'END'
        JJJ=III/2
        QQQ=JJJ*2
        IF(QQQ.EQ.III) THEN
          XINT=1E-6
          T4=TT2

```

```

        TT1=T2
        T2=T2+XINT
        T3=XINT/10
        IF (MOD(III,120).EQ.0) THEN
WRITE(25,7105) TT2,T,(X(K), K= 1,KK), WW
        ENDIF
        ELSE
        XINT=16.667E-3
        TT1=T2
        T2=T2+XINT
        T3=XINT/10
        ENDIF
        III=III+1
        WRITE(19,*) TT1, T2,T3, III
        STOP
        ELSE
        TT2 = MIN(TT2 + DT, T2)
        ENDIF
C      Call the differential equation solver
        350 CONTINUE
C*****precision > single
C      CALL SVODE
C*****END precision > single
C*****precision > double
        CALL DVODE
C*****END precision > double
        *          (FUN, NEQ, Z, TT1, TT2, ITOL, RTOL, ATOL, ITASK,

```

```

1          ISTATE, IOPT, RWORK(NVODE), LRW, IWORK(IVODE),
2          LIW, JAC, MF, RWORK, IWORK)
      IF (ISTATE .LE. -2) THEN
        IF (ISTATE .EQ. -1) THEN
          ISTATE = 2
          GO TO 350
        ELSE
          WRITE (LOUT,*) ' ISTATE=',ISTATE
          STOP
        ENDIF
      ENDIF
      GO TO 250
C          FORMATS
      7003 FORMAT (1H1)
      7100 FORMAT (3X, 'T(SEC)', 9X, 'TMP(K)', 9X, 20(4X,A10))
      7105 FORMAT (50E16.8)
      7110 FORMAT (26X, 5(1X,A10))
      7115 FORMAT (22X, 10E11.3)
      7012 FORMAT ((1X,A10),4X,1E14.8)
      END
      SUBROUTINE FUN (N, TIME, Z, ZP, RPAR, IPAR)
C*****precision > double
      IMPLICIT DOUBLE PRECISION(A-H,O-Z), INTEGER(I-N)
C*****END precision > double
C*****precision > single
C      IMPLICIT REAL (A-H,O-Z), INTEGER(I-N)
C*****END precision > single

```

```

COMMON /RCONS/ P, RU
COMMON /ICONS/ KK, NWT, NH, NWDOT
DIMENSION Z(*), ZP(*), RPAR(*), IPAR(*)

C
C   Variables in Z are:  Z(1)   = T
C                       Z(K+1) = Y(K)
C
C   Call CHEMKIN subroutines
C
CALL CKRHOY (P, Z(1), Z(2), IPAR, RPAR, RHO)
CALL CKCPBS (Z(1), Z(2), IPAR, RPAR, CPB)
CALL CKWYP  (P, Z(1), Z(2), IPAR, RPAR, RPAR(NWDOT))
CALL CKHMS  (Z(1), IPAR, RPAR, RPAR(NH))

C
C   Form governing equation
C
SUM = 0.0
DO 100 K = 1, KK
    H    = RPAR(NH    + K - 1)
    WDOT = RPAR(NWDOT + K - 1)
    WT   = RPAR(NWT   + K - 1)
    ZP(K+1) = WDOT * WT / RHO
C    SUM = SUM + H * WDOT * WT
100 CONTINUE

RETURN

END

```

## D.5 comp.inp

1.0000000000000000	298.00000000000000
O2	0.2099
O	0.
N	0.
N2	0.79
NO	0.0001
O3	0.
NO2	0.
NO3	0.
N2O	0.
END	
0 1E-06 1E-07 1	